AIRESEARCH MANUFACTURING COMPANY
Los Angeles, California

HYPERSONIC RESEARCH ENGINE PROJECT - PHASE IIA
NASA CONTRACT NO. NAS1-6666
EXPERIMENTAL INVESTIGATION OF THE COOLING AND
STRUCTURAL PERFORMANCE FOR THE HRE COWL LEADING EDGE

Document No.   AP-69-5347   30 July 1969

CASE FILE COPY

Number of pages _____ 86 _____   Prepared by _____ Engineering Staff _____

Original date _____ 30 July 1969 _____   Edited by _____ L. F. Jilly _____

Approved by _Alfred G. Wolf_
for Henry J. Lopez
HRE Program Manager

ABSTRACT

Tests to determine the heat transfer and pressure drop performance
of the Hypersonic Research Engine (HRE) rectangular-offset, brazed
plate-fin cooling passage geometry are discussed. Two fin configurations
were used during the tests: (1) 20 fins per inch, 0.050 inch high, .006 inch
thick and (2) 28 fins per inch, .050 inch high and .006 inch thick. The
fins were formed from Hastelloy-X sheet material and brazed between .025
inch thick Hastelloy-X plates, using Palniro 1 braze alloy. The test minss
were approximately 6 inches wide by 6 inches long. The fin geometries
tested were different than previously tested by AiResearch, or others. Data
were taken at Reynold's numbers up to 55,000 (based on the fin passage
hydraulic diameter) or well beyond existing data for somewhat similar fin
geometries. These data indicate the measured pressure drop is as much as
25 percent below that predicted but the heat transfer coefficient correlates
well with the predicted values.

CONTENTS

ILLUSTRATIONS

ILLUSTRATIONS (Continued)

ILLUSTRATIONS (Continued)

TABLES

NOMENCLATURE

A — area, ft^2

C_p — specific heat at constant pressure, Btu/lb °R

G — coolant mass flux, lb/sec ft^2

H — hot gas enthalpy, Btu/lb

h — convective heat transfer coefficient, Btu/sec ft^2 °R

K — pressure loss coefficient

k — thermal conductivity, Btu/sec ft^2 °R

L — length, ft

Le — Lewis number

Nu — Nusselt number

P — pressure, psia

Pr — Prandtl number

Q, q — heat load, Btu/sec

R, r — radius, in.

Re — Reynolds number

St — Stanton number

T — temperature, °R

u — hot gas velocity, ft/sec

W — flow rate, lb/sec

x — axial location, in.

Δ — algebraic difference

θ — angle from leading edge tip stagnation line, deg

μ — hot gas or coolant absolute viscosity, lb/sec ft

ρ — hot gas or coolant density, lb/ft^3

NOMENCLATURE (Continued)

Subscripts

AW	adiabatic wall or recovery conditions
b	bulk coolant temperature conditions
c	coolant
E	energy of dissociation (Equations 5-3 and 5-4) expansion loss (Equations 4.3-3 and 4.3-4)
f	film temperature conditions
LE	leading edge
stag, s	stagnation point
T	freestream total conditions
W	wall conditions
W1, 1	inside leading edge wall conditions
W2, 2	outside leading edge wall conditions
∞	freestream static conditions

I. INTRODUCTION

This test report outlines the procedures and results of Category I tests on Hypersonic Research Engine (HRE) leading edge straight section test specimens to determine (1) thermal performance, (2) thermal cycling performance, and (3) coolant flow distribution.

I.I PURPOSE AND SCOPE

In order to reduce drag and insure inlet starting over a wide range of Mach numbers in the HRE, a cowl leading edge radius of 0.030 in. was selected as a practical minimum for cooling purposes. Larger radii are aerodynamically marginal for low-Mach-number starting with the inlet configuration now being used. Uncooled surfaces were rejected early in the leading edge design because (1) radiation equilibrium temperatures are at or above the melting temperatures of superalloys at flight Mach numbers of 6 or greater, and (2) the problems of thermal fatigue, attachment to cooled-structure, and oxidation resistance for 100-cycle and 10-hour design life would have made the use of refractory materials unacceptably developmental. The hydrogen-cooled leading edge selected for the design used 0.015-in.-thick Nickel-200 or Hastelloy X tips.

The physical characteristics which control the structural and cooling design of the cowl leading edge are closely related. Low cycle thermal fatigue limits the maximum temperature difference between leading edge stagnation line and adjacent structure. Creep-rupture strength limits maximum temperatures at high coolant pressures needed to obtain adequate cooling. In turn, high coolant pressures are necessary because flow passages must be small to provide high mass fluxes and/or small turning radii for high coolant heat transfer coefficients. The design of a leading edge that is compatible with these structural and cooling considerations was evaluated in a test program using two candidate designs.

The objectives of the test program were threefold:

(a) To evaluate the thermal performance of the two candidate leading edge tip coolant configurations shown in Figure I-I.

(b) To evaluate the low thermal cycle fatigue and creep rupture performance of the two leading edge coolant configurations.

(c) To evaluate the coolant flow distribution in configuration No. I with room temperature air under isothermal conditions and with hydrogen coolant under heat transfer conditions.

ALL HASTELLOY X
MATERIAL

B-14401

LEADING EDGE CONFIGURATION NO. 1

ALL HASTELLOY X MATERIAL EXCEPT
NICKEL-200 OUTER SHELL TIP

SIDE PLATE
COOLANT FLOW
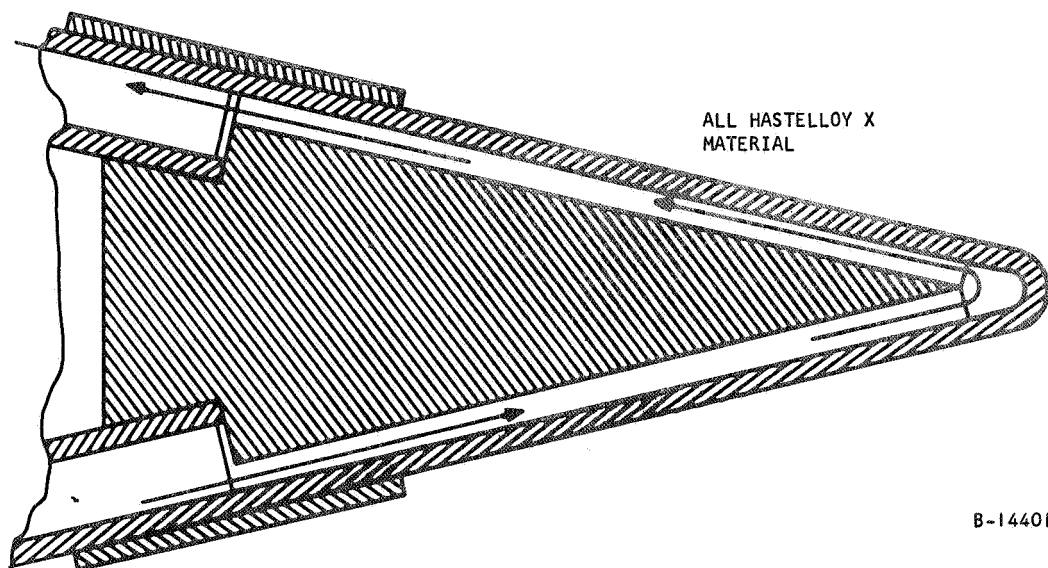
TIP COOLANT
FLOW

TIP COOLANT FLOW
PARALLEL TO TIP
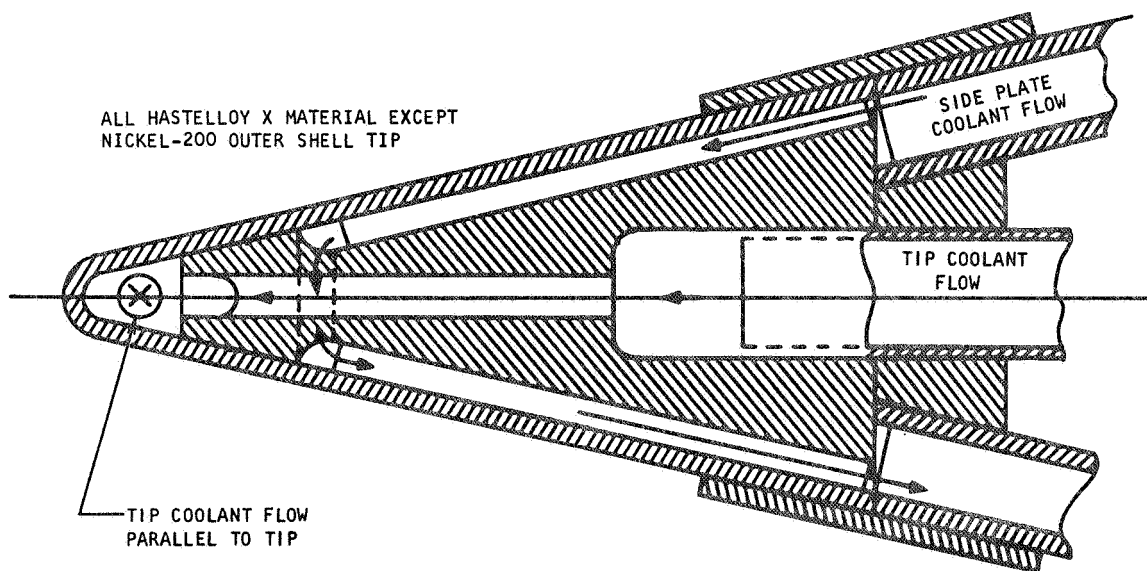
LEADING EDGE CONFIGURATION NO. 2

Figure 1-1.   Cowl Leading Edge Tip Configurations and Coolant Flow Paths

2. DESCRIPTION OF TEST SPECIMENS

The leading edge straight section test specimens are directly applicable to the flight engine axisymmetric outerbody leading edge. The use of a straight section, instead of a compound-curved section, greatly simplifies the fabrication and testing. The two types of specimens used in the test program predesignated configuration No. 1 and configuration No. 2, as shown in Figure 1-1. Both types have the same overall dimensions of an 8-in. span, a 4-in.,chord and a 26-deg wedge angle, as shown typically in Figure 2-1. The 8-in. length is approximately equal to 1/7 of the outerbody circumference at the leading edge tip. The features that distinguish the two types of specimens are described below.

2.1 CONFIGURATION NO. 1 (SK 51287-1)

Configuration No. 1 test specimens, as shown schematically in Figure 2-2, had leading edge tip-coolant flows perpendicular to the specimen stagnation line through a 154-deg turn. The tip-coolant also provides coolant to the sides of the specimen. All face sheets, fins, and structure are Hastelloy X. The tip, which is fabricated separately from the sides, has 20 R-.020-.004 plain rectangular fins brazed to the 1/2-in.-length arrowhead piece, and the 0.015-in. V-shaped surface sheet. The side subassemblies consist of 20R-.075-.100(0)-0.006 rectangular offset fins brazed between two 0.015-in.-thick sheets. The sides are brazed to the tip at the arrowhead piece and two outer skin joint covers. Coolant enters and exits from the specimen side fins through manifolds located at the base of the 26-deg wedge, as shown in Figure 2-1. The manifolding was selected to simulate the manifolding in the flight engine.

2.2 CONFIGURATION NO. 2 (SK 51428-1)

Configuration No. 2 test specimens had leading edge tip coolant flows parallel to the stagnation line and separate from the sides coolant flow. The construction details are similar to the configuration No. 1 specimen shown in Figure 2-2 except at the leading edge tip,where the construction detail shown in Figure 1-1 is used. All material is Hastelloy X except the tip outer sheet where Nickel-200 is used. Coolant enters and leaves the leading edge tip through the tubes shown in Figure 2-3. During radiant thermal performance tests, the two end tubes were used as inlets while the center tube was used as an outlet, and as outlets while the center tube was used as an inlet. Coolant in specimen sides bypassed the leading edge tip area by flowing through 10 slots (0.035 x 0.70 in.) along the 8-in. specimen length just in back of the tip.

INLET PLENUM

STATIC PRESSURE TAPS

OUTLET PLENUM
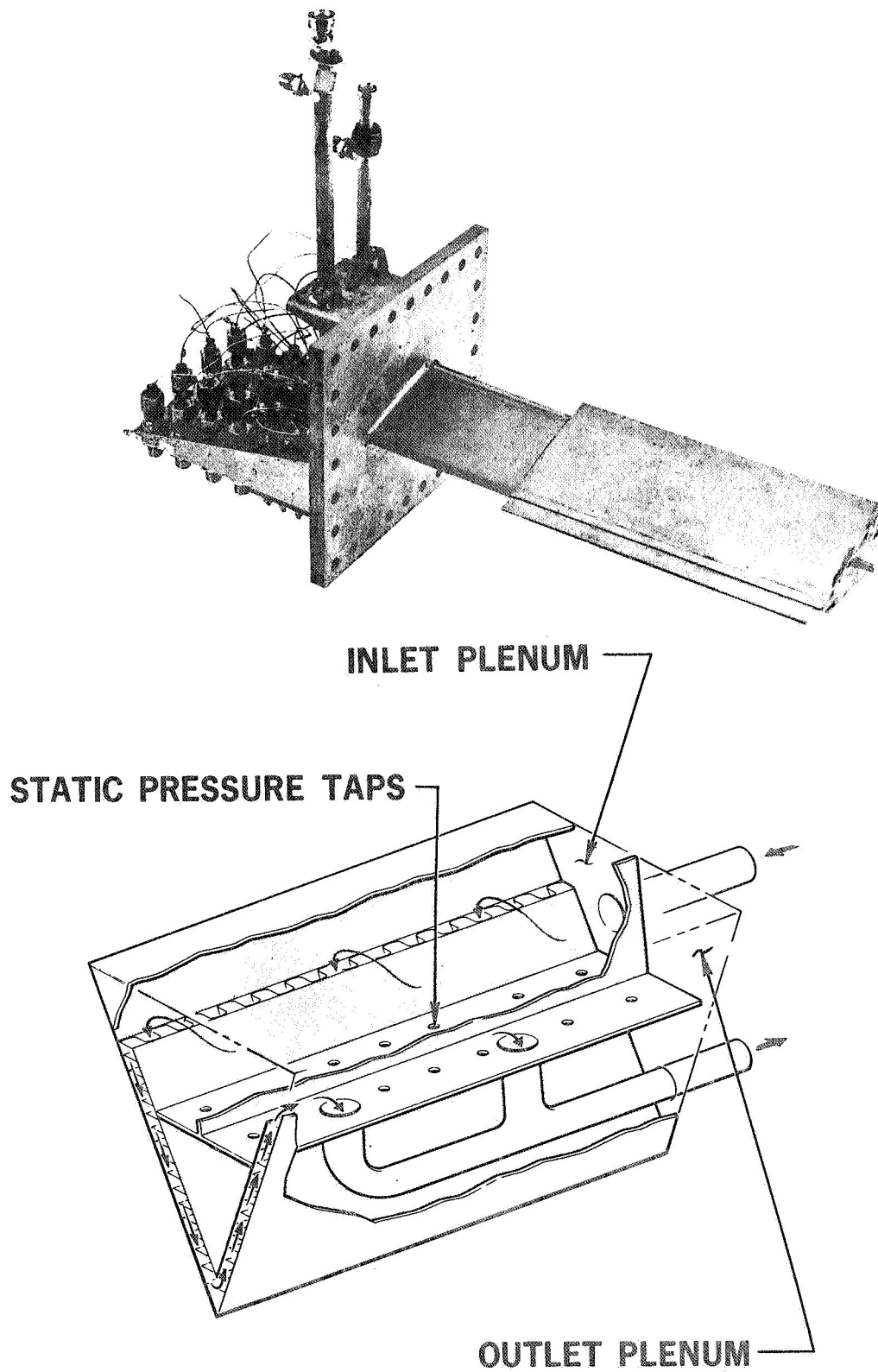
Figure 2-1.   Leading Edge Test Section

AIRESEARCH MANUFACTURING COMPANY
Los Angeles, California

69-5347
Page 2-2

COOLED AREA

BRAZE

4.2

3.3

BRAZE

SHIELD FOR
HOT GAS TESTING

0.030
RAD.

MANIFOLDING

1.9

BRAZE

0.015 FACE
SHEETS

0.020 HIGH
FIN, 20 PER INCH

0.075 FIN, 20
PER INCH

HEATED
STAGNATION
AREA

OUTER SKIN
JOINT COVER

BRAZED SUBASSEMBLIES

OUTER SKIN
JOINT COVER

A-30499-A
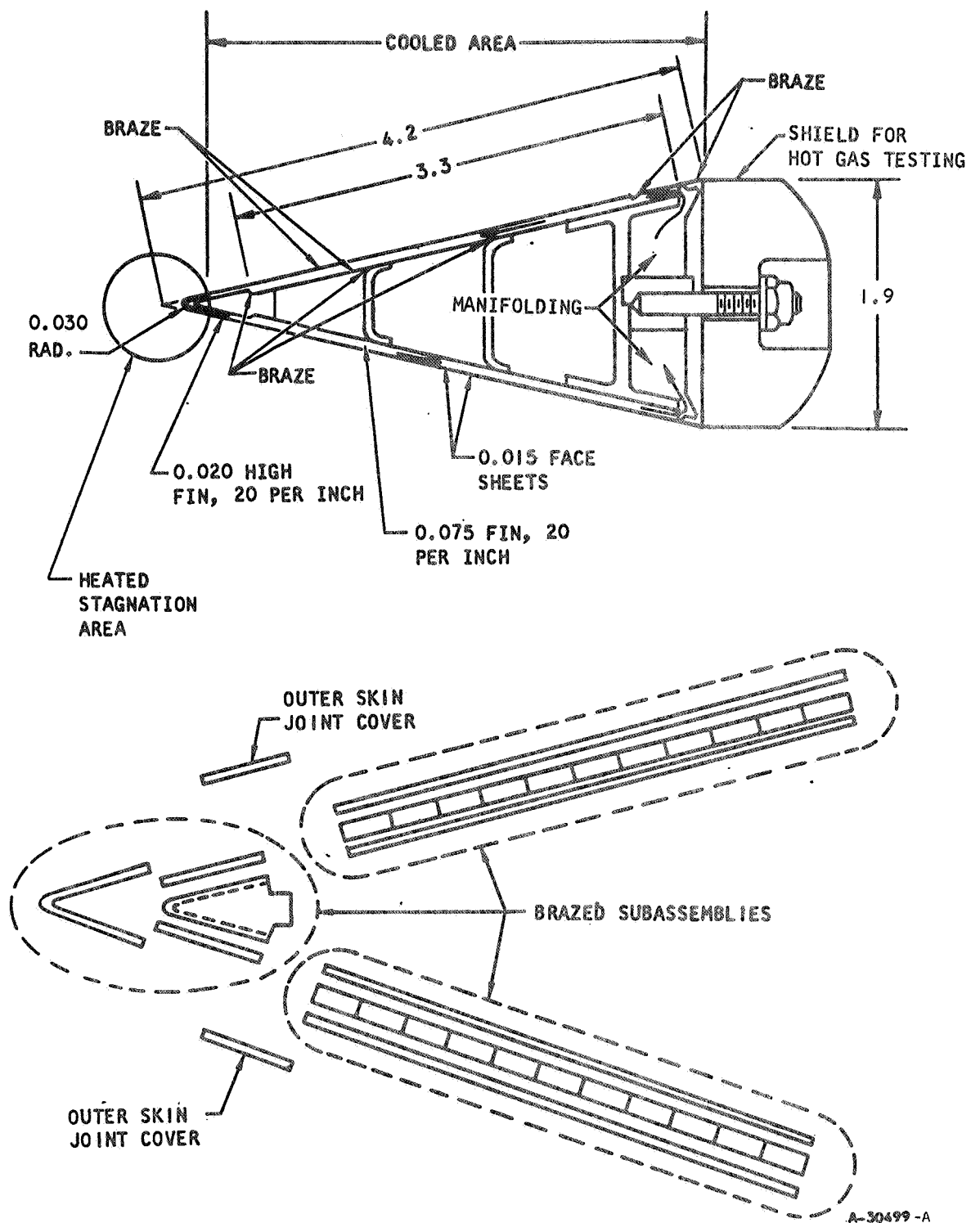
Figure 2-2. Leading Edge Straight Section, Configuration No. 1

63324-2
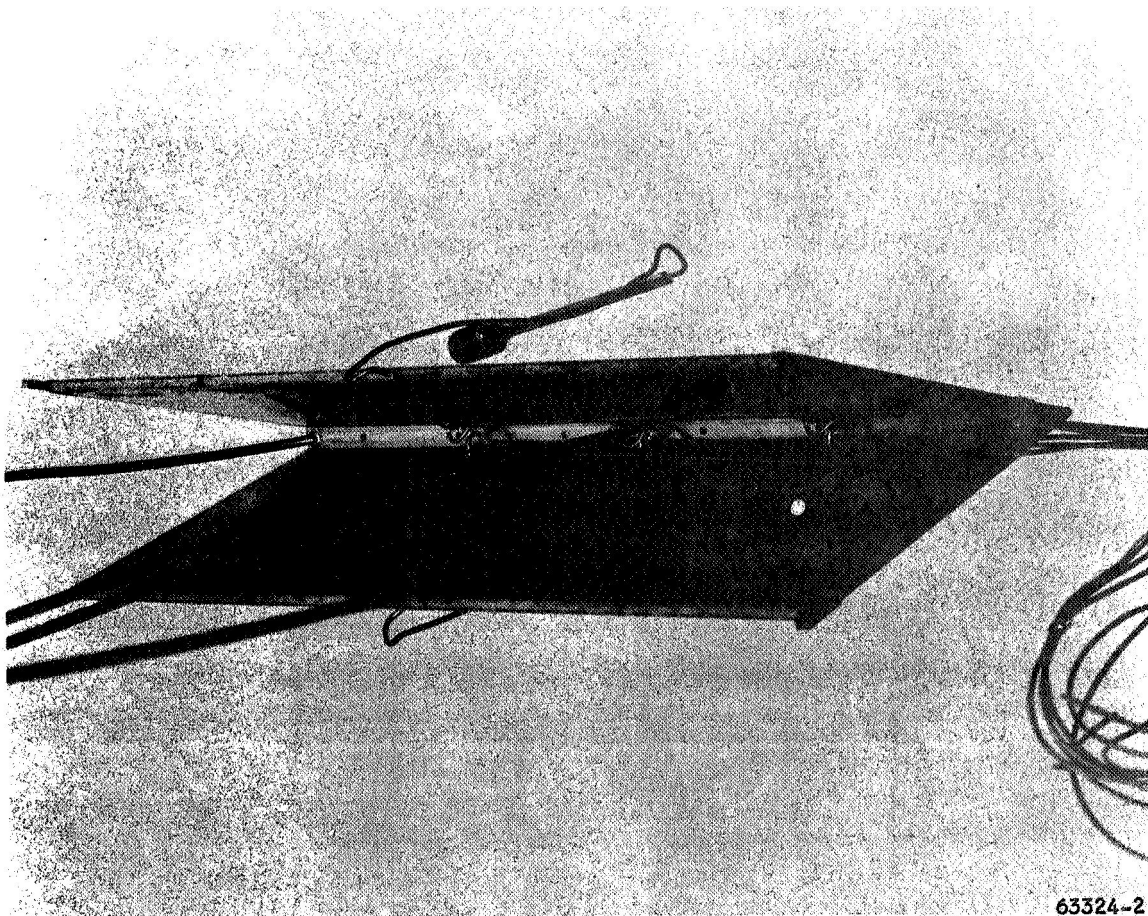
Figure 2-3.   Plate-Fin and Tip Assembly,Configuration No. 2

3. TEST SETUP

3.1 HOT GAS HEATING THERMAL PERFORMANCE

Hot gas thermal performance testing was conducted at the North American Rockwell (NAR) thermal laboratory on two of the configuration No. 1 leading edge straight section test specimens. The SN 2 test specimen is shown in Figure 3-1, in a typical installation in a test duct. The test duct (Figure 3-2), with hot gas inlet at the bottom, is attached to the exit of the air/hydrogen combustor, shown in Figure 3-3. A test setup schematic is shown in Figure 3-4 and a cross-section of the test duct is shown in Figure 3-5.

Subsonic air, heated by a hydrogen/oxygen combustor to temperatures between 2500° and $4000^\circ F$, was flowed over the test unit at rates between 2 lb/sec and 6.5 lb/sec. The test unit was cooled with gaseous hydrogen at inlet temperatures between 200° and $520^\circ F$, at inlet pressures between 400 psia and 700 psia, and at flow rates between 0.02 lb/sec and 0.12 lb/sec.

The test unit in Figure 3-6 has a mounting flange through which hydrogen coolant lines and instrumentation leads project. Figure 3-7 shows the zirconia shields on the top and back of the specimen and the zirconia filler block on the specimen bottom. After several hot gas tests the zirconia shields on the top and back of the specimen failed and were replaced with water-cooled metal shields, shown in Figure 3-8.

3.2 RADIANT HEATING THERMAL PERFORMANCE AND CYCLING

The radiant heating test setup shown schematically in Figures 3-9 and 3-10 is also shown in Figures 3-11 and 3-12. Both the water- and air-cooling lines are shown connected to the leading edge straight section (LESS) in Figure 3-10, but only one coolant is connected at any one time (air or water).

The radiant heat source is a single-element quartz lamp and elliptical-reflector combination which concentrates the 360-deg radiation about the lamp axis into a discrete focus 0.06- to 0.09-in. wide over the axial length of the lamp. The lamp was electrically controlled to maintain discrete power settings up to 6.5 kw. The lamp assembly was water-cooled, and the coolant ΔT, flow rate, and input electrical power were measured.

The sides of the test specimen were protected by a water-cooled aluminum fixture, which leaves only the leading edge stagnation area exposed. Cooling of the test specimens during test was accomplished with either ambient temperature air or water at 700 psia. The flow rates of the air and water were adjusted to yield the desired temperature differences between the external surfaces of the stagnation line and the internal structure.
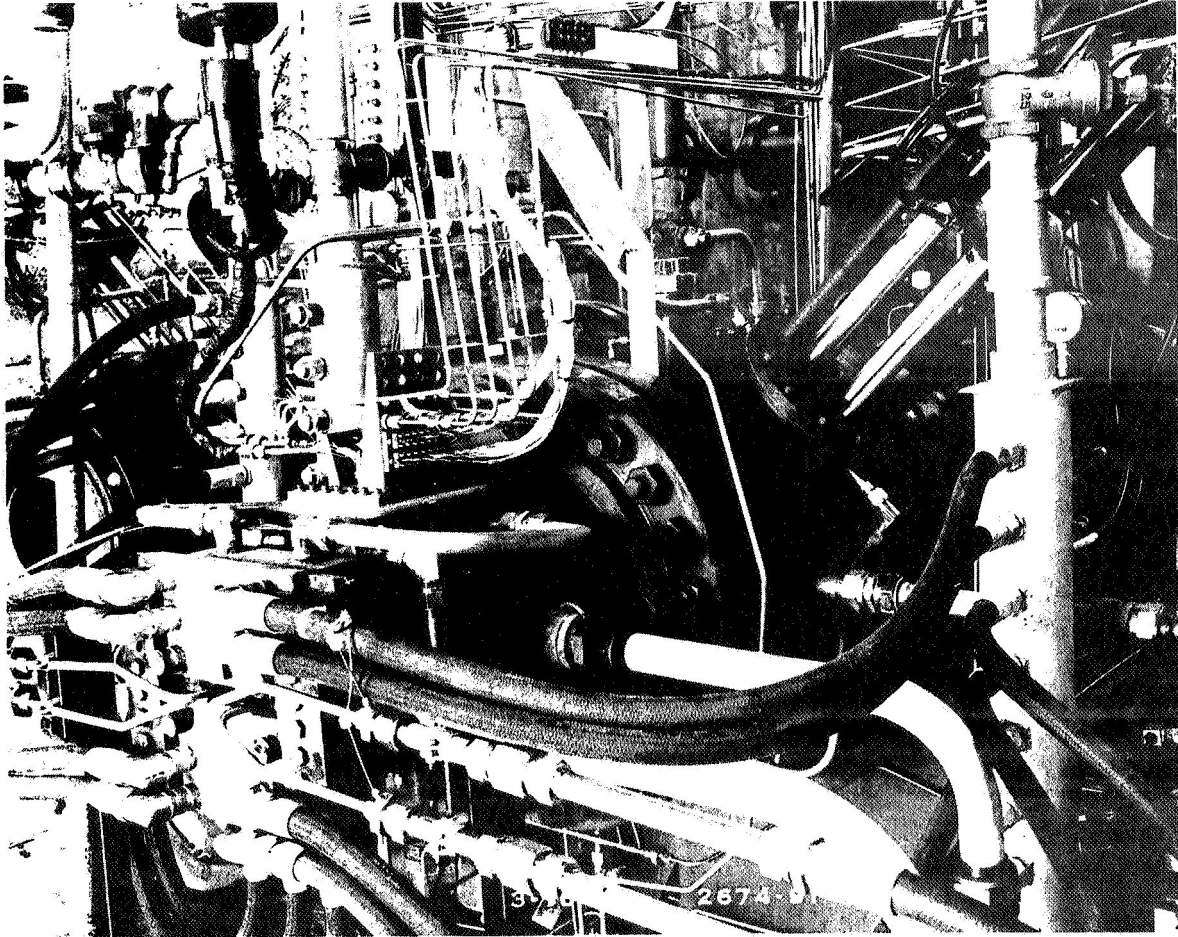
F-9424

Figure 3-1. Leading Edge Straight Section
Test Setup--Hot Gas Outlet
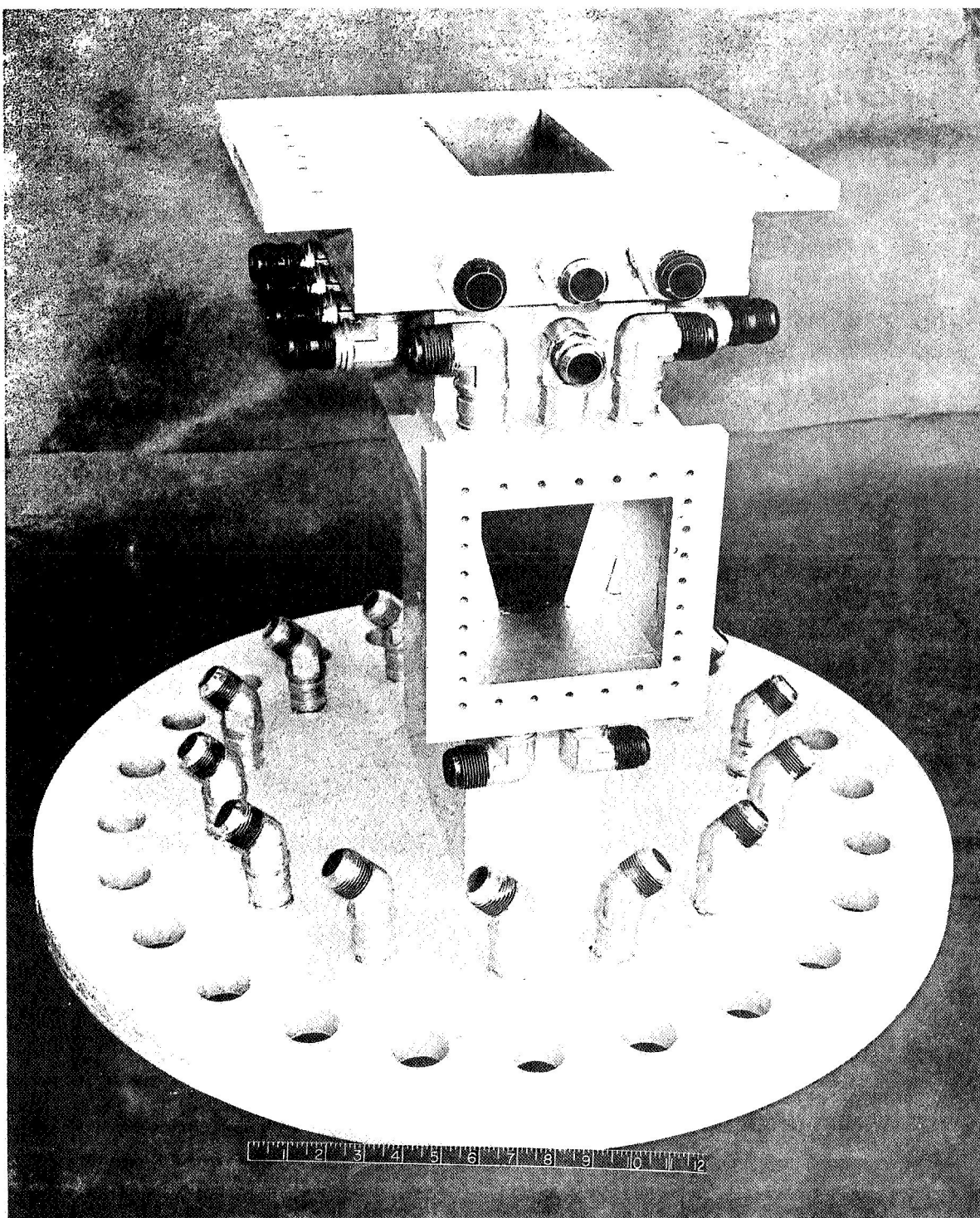
Figure 3-2. Water-Cooled Test Duct for Straight
Section Outerbody Leading Edge Test
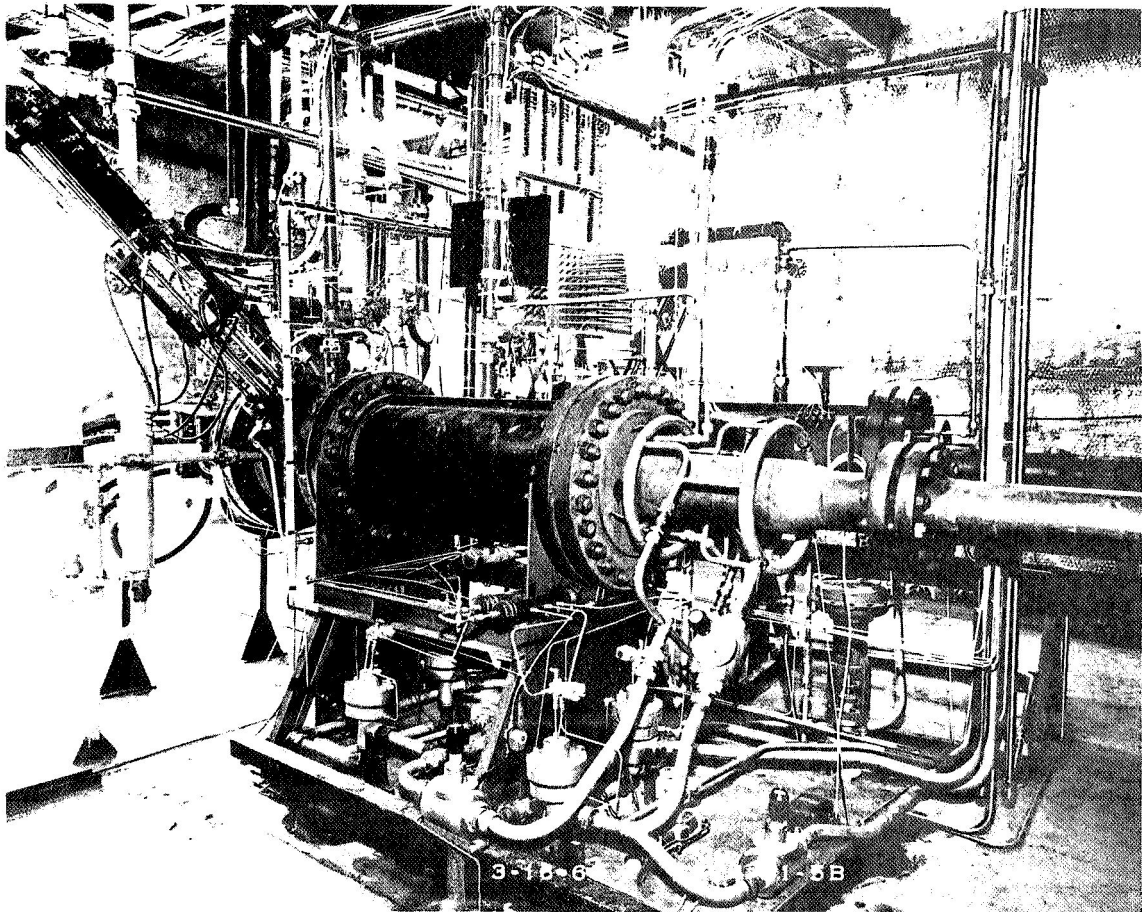
F-9423

Figure 3-3.   Burner for Test of Leading
Edge Straight Section
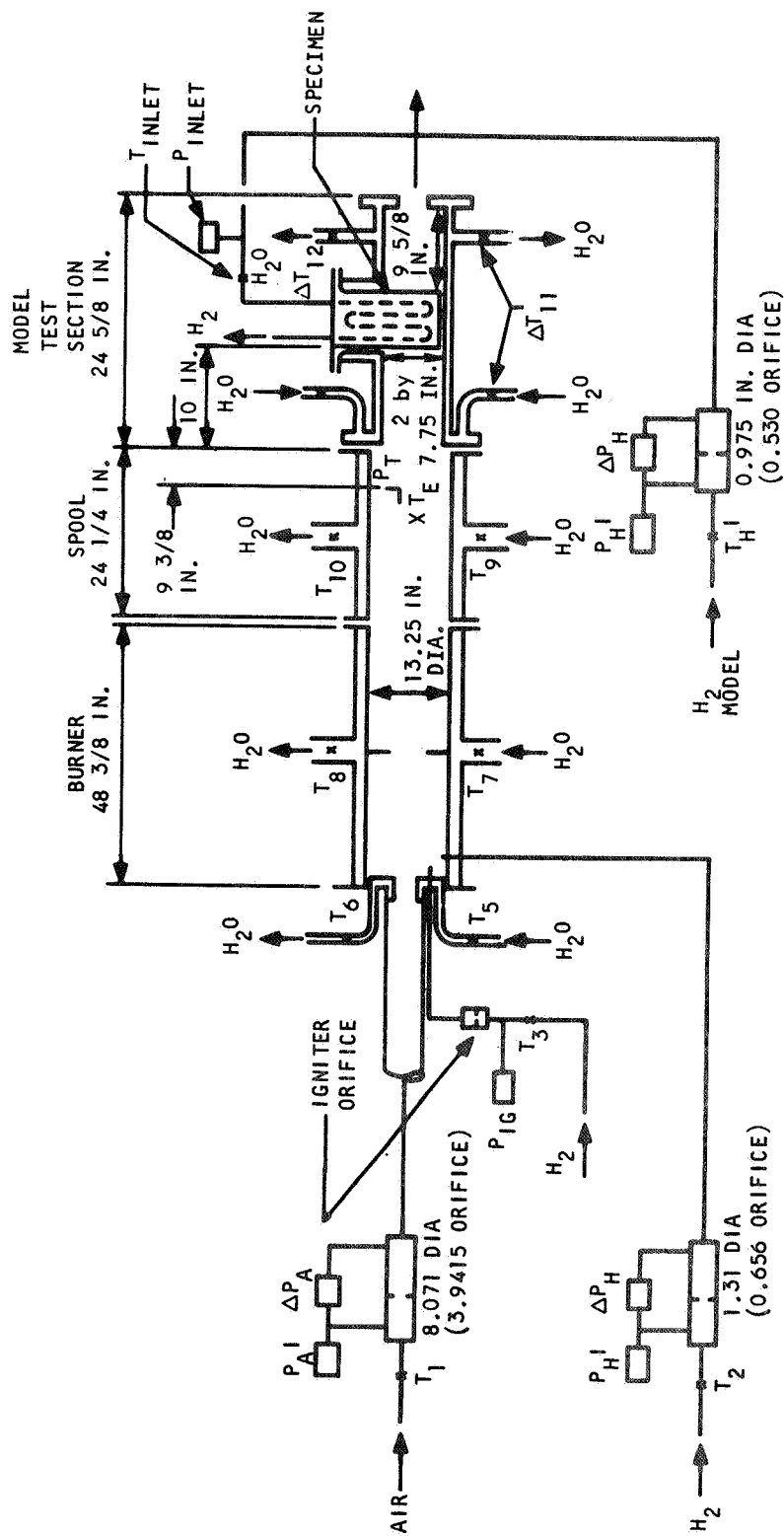
Figure 3-4. Leading Edge Straight Section Test Schematic

B-14167

NOTES:
1. SUBSCRIPT "A" = AIR, "H" = HYDROGEN, AND "E" = EXHAUST
2. "x" INDICATES THERMOCOUPLE LOCATION
3. THERMOCOUPLE T_4 IS CELL AMBIENT
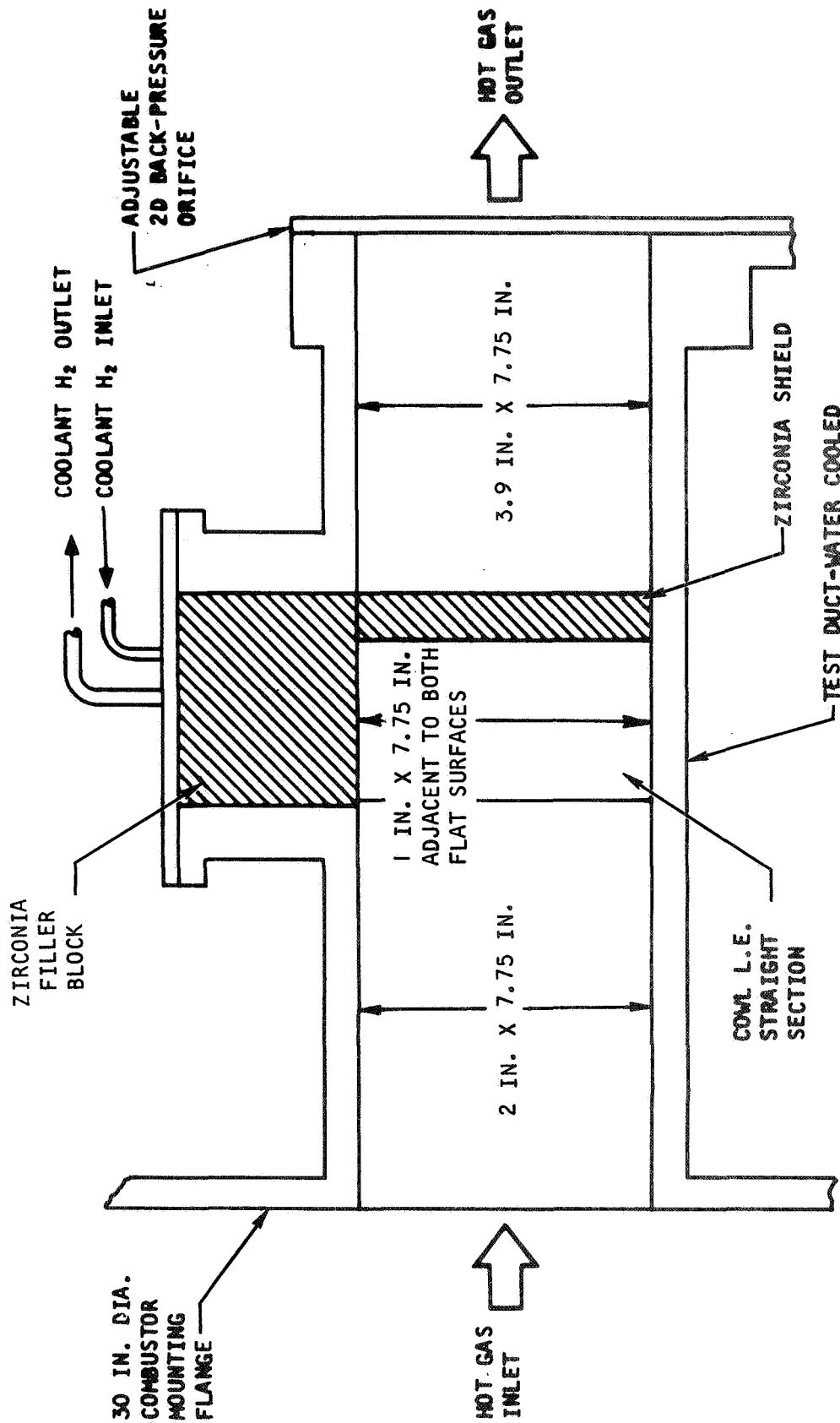
Figure 3-5. Straight Section Outerbody Leading Edge Test Setup
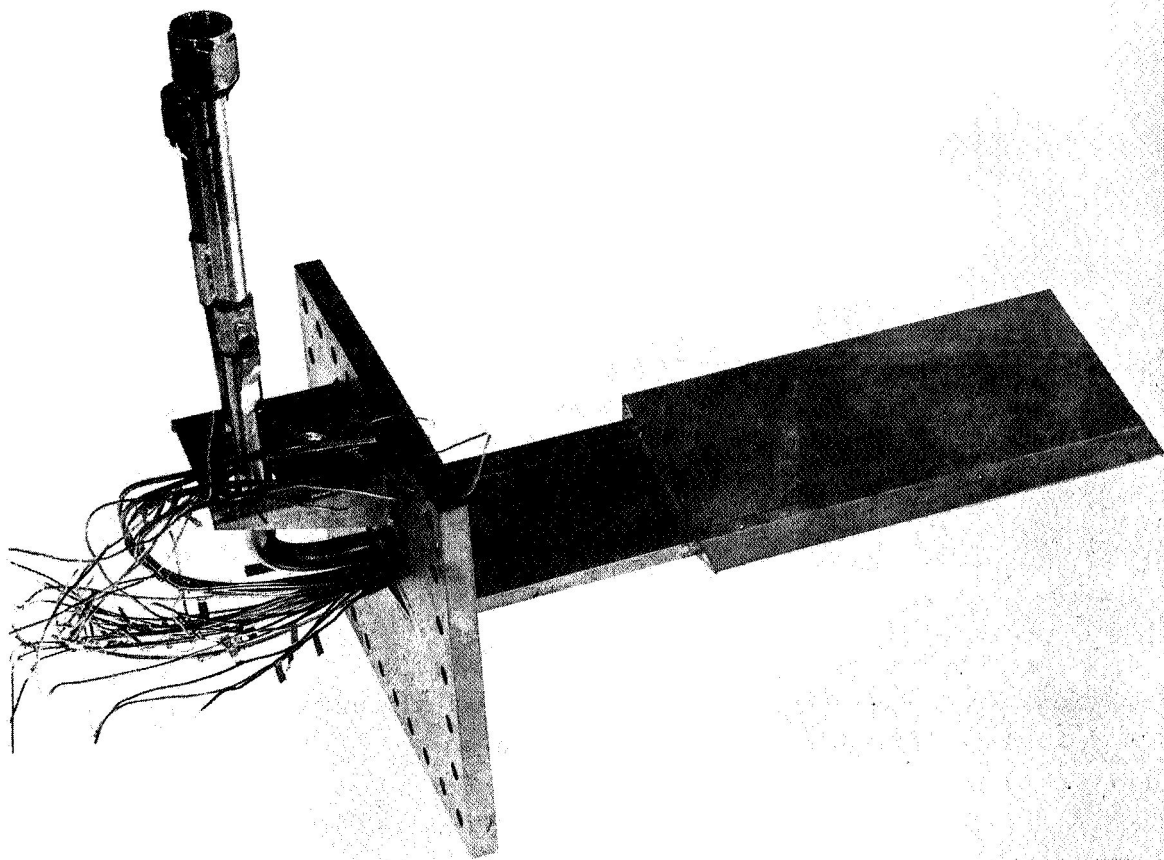
63382-1

Figure 3-6. Leading Edge Straight Section, SN 2
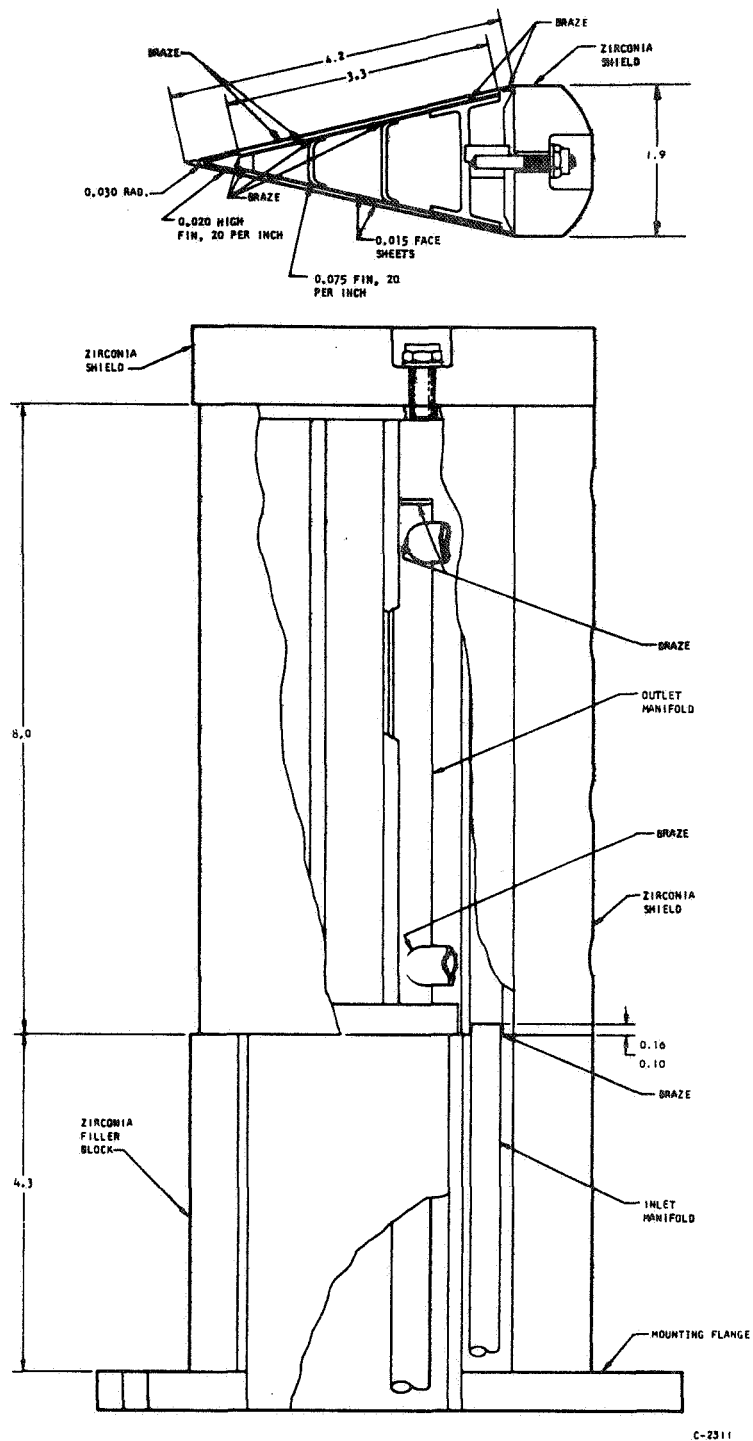
Figure 3-7. Outerbody Leading Edge Straight Section
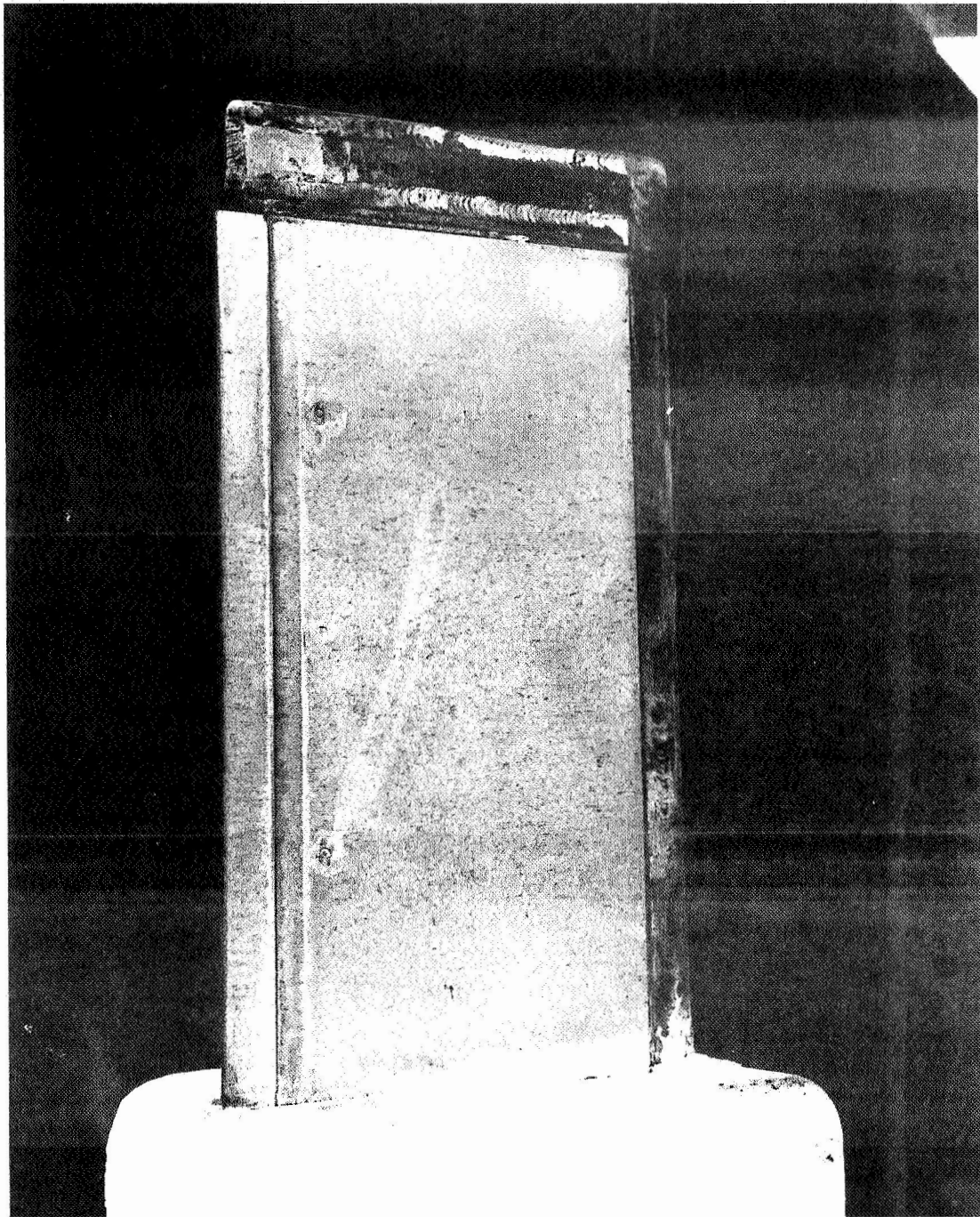
F-9426

Figure 3-8. Leading Edge Straight Section SN 4 with
Water-Cooled Trailing Edge and End-Shields

AIRESEARCH MANUFACTURING COMPANY
Los Angeles, California

NOTE: WATER COOLANT FLOW DIRECTION IS INDICATED BY →

END COOLING LOOP

FIXTURE COOLING LOOP

A

A

COWL LEADING EDGE STRAIGHT SECTION INSTALLED IN TEST FIXTURE   TOP VIEW

RADIANT HEATING LAMP ASSEMBLY

LEADING EDGE

TEST SPECIMEN

SECTION A-A

S-46985
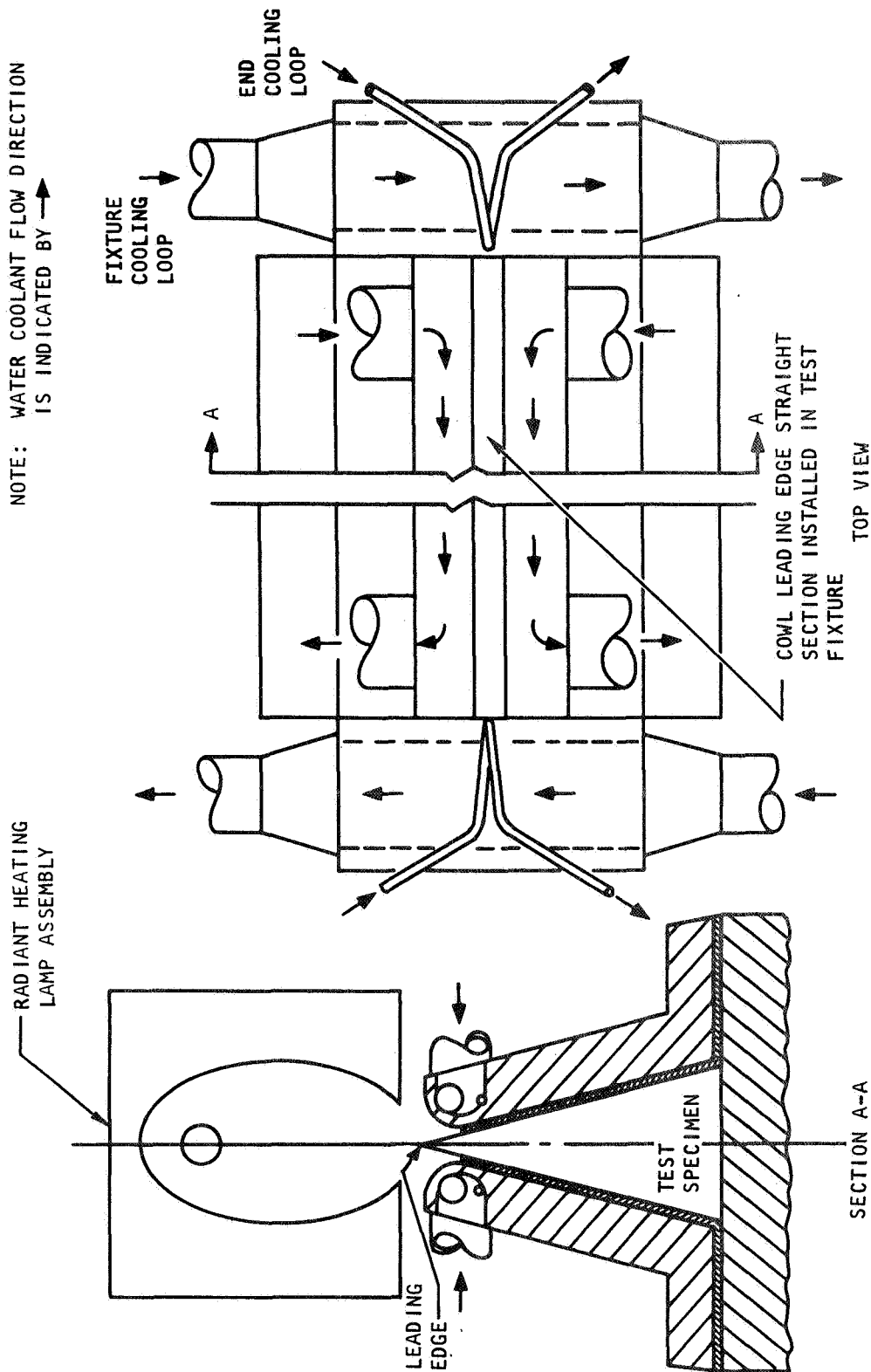
Figure 3-9. Leading Edge Straight Section, Radiant Heating Test Fixture Schematic
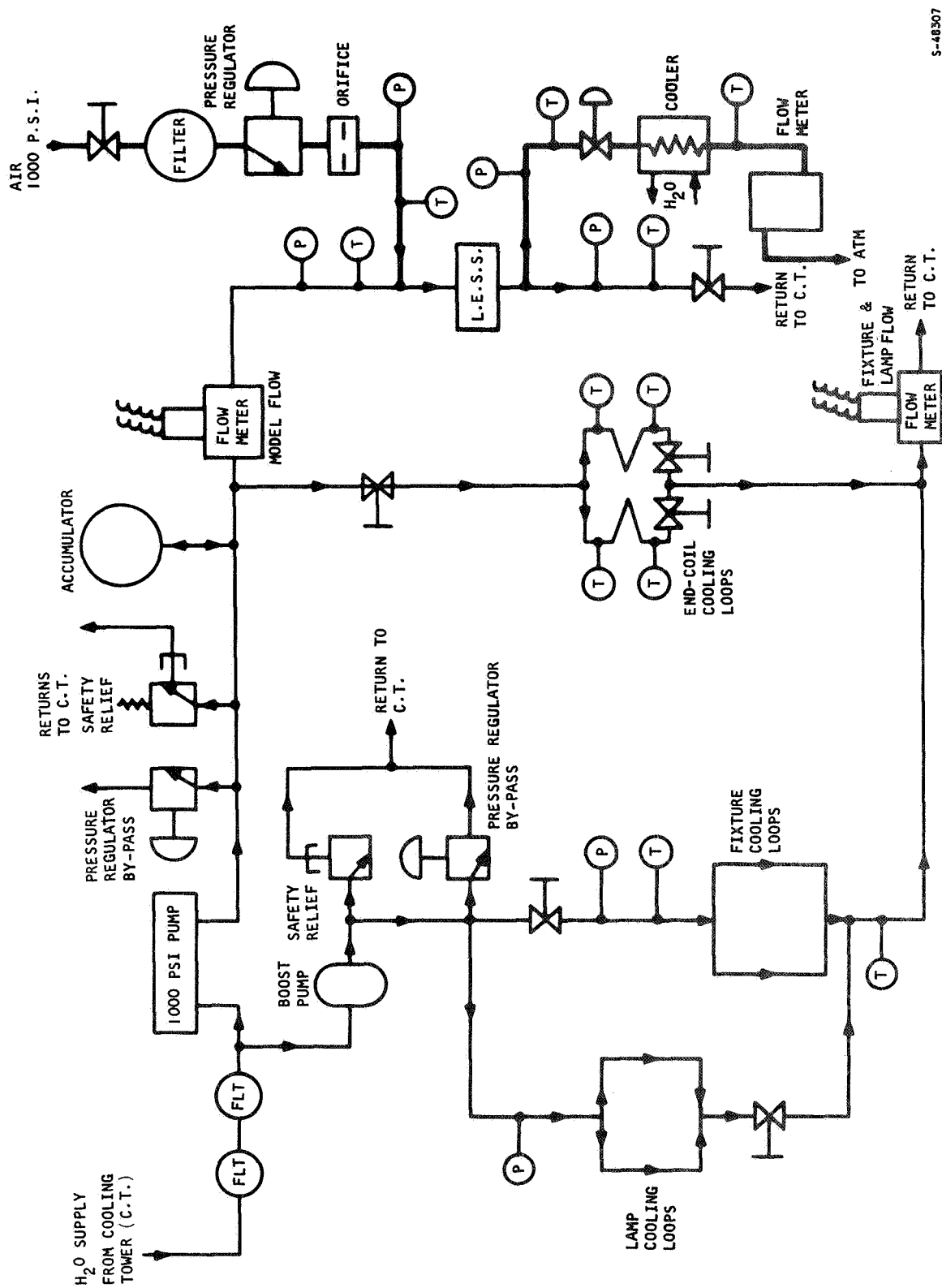
Figure 3-10. Schematic Water and Air Coolant Systems for Leading Edge Straight Section
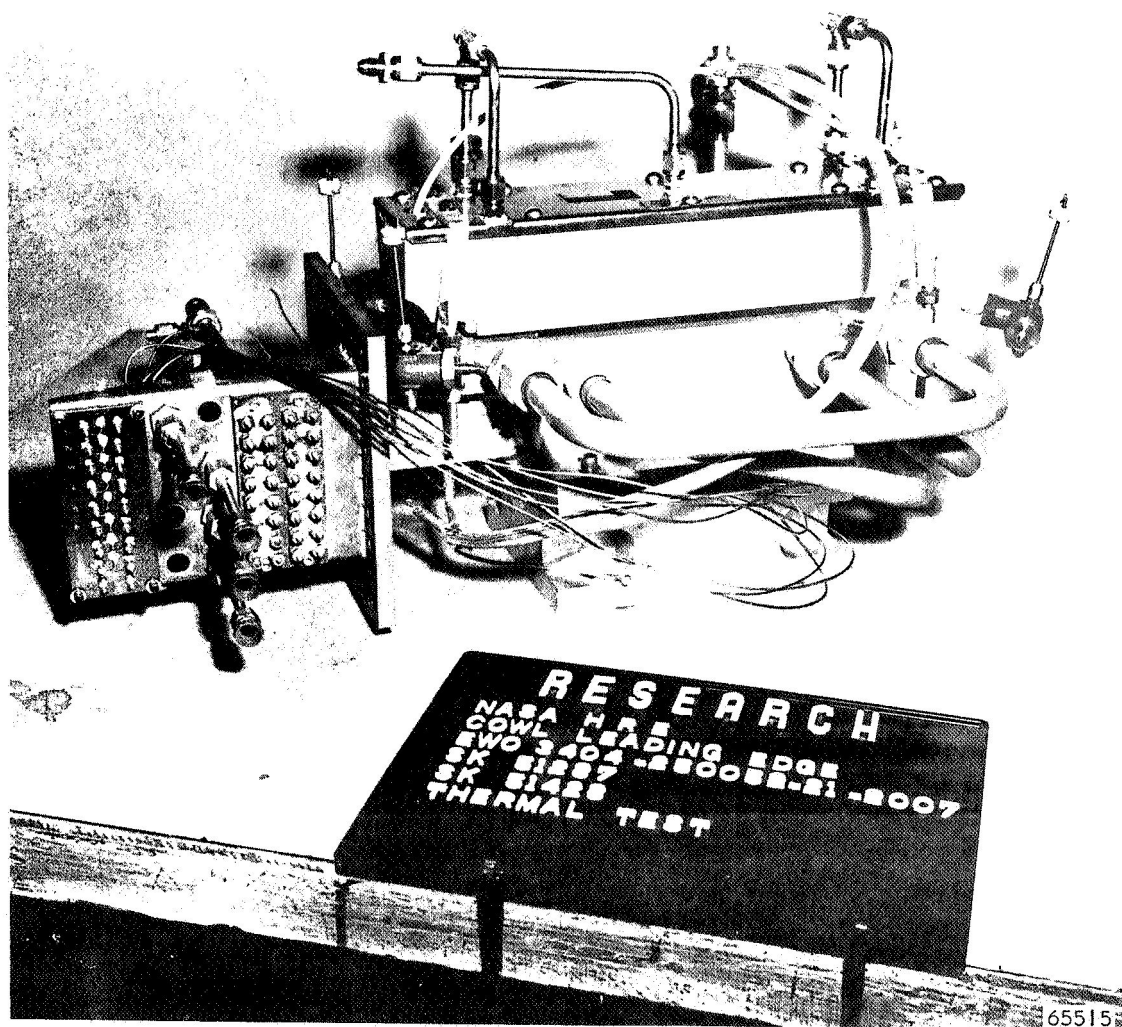
Figure 3-11. Leading Edge Straight Section
Test Setup with Lamp and Fixture
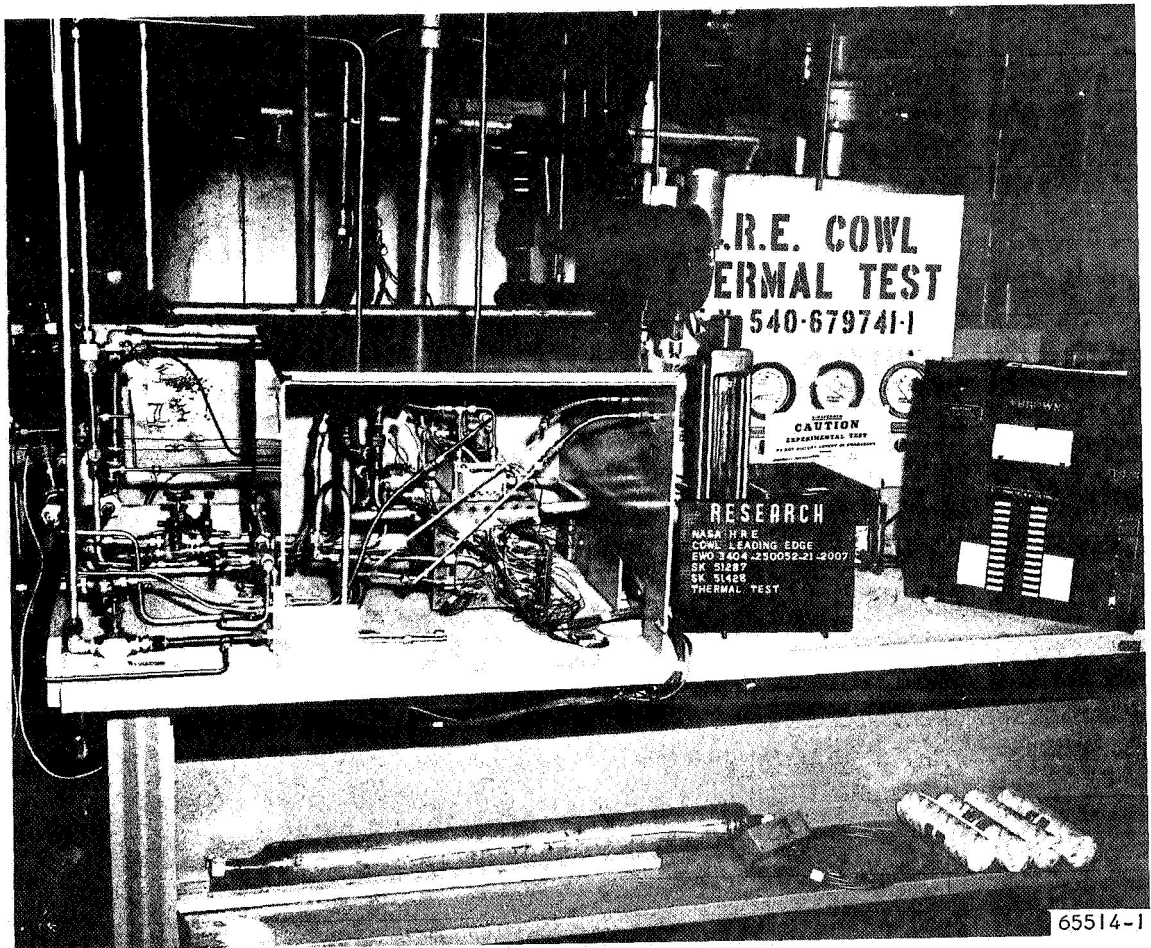
Figure 3-12.   Leading Edge Straight Section
in Radiant Heating Test Setup

The configuration No. 2 specimens were used for leading edge tip thermal performance testing and then for thermal cycle testing in the radiant heating test setup. The configuration No. 1 specimens were used for thermal cycle testing only. Thermal performance testing of configuration No. 1 was conducted in the hot gas tunnel facility described in Section 3.1. Water was used as the coolant during preliminary checkout tests for configuration No. 1 specimens, and air was used as the coolant for both configurations thereafter.

3.3 COOLANT FLOW DISTRIBUTION

Flow distribution tests were conducted on configuration No. 1. Tests were conducted using hydrogen coolant with heat transfer, and also isothermal air. Tests with hydrogen were conducted simultaneously with hot gas thermal performance tests. The hot gas test setup is described in Section 3.1. The test setup as shown in Figures 3-13 and 3-14 was used for isothermal airflow distribution tests. The important features of both test setups relative to flow distribution are measurement of total flow, inlet and outlet pressures and temperatures, and inlet and outlet manifold pressure distributions. In the isothermal air tests, six pressure taps were used in each manifold; in the hydrogen tests, three pressure taps were used in each manifold. The significant parameter of maximum-to-minimum flow ratio could be deduced from all sets of data, as the maximum and minimum manifold pressures were monitored continuously.
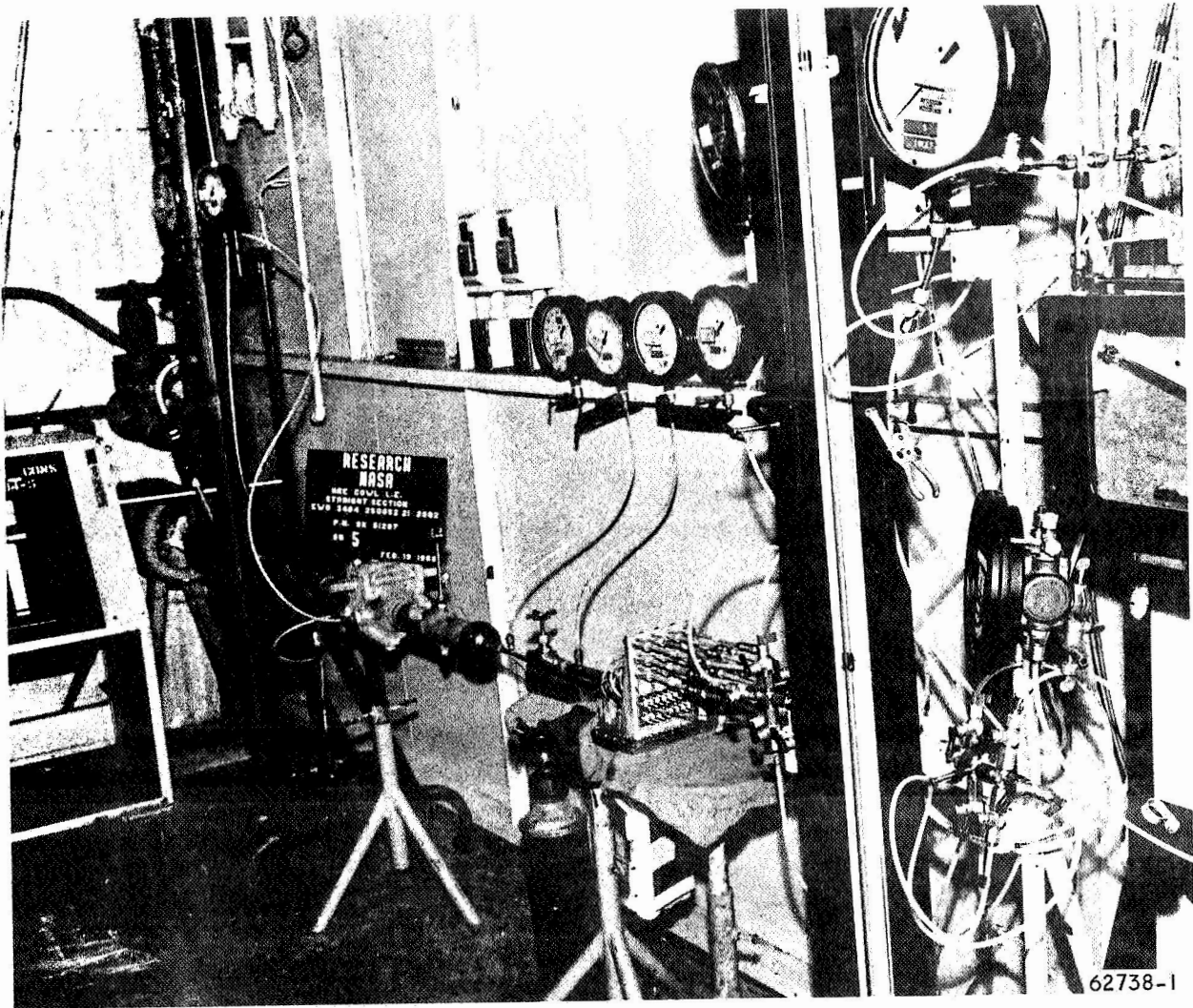
Figure 3-13.   Leading Edge Straight Section
Flow Distribution Test Setup
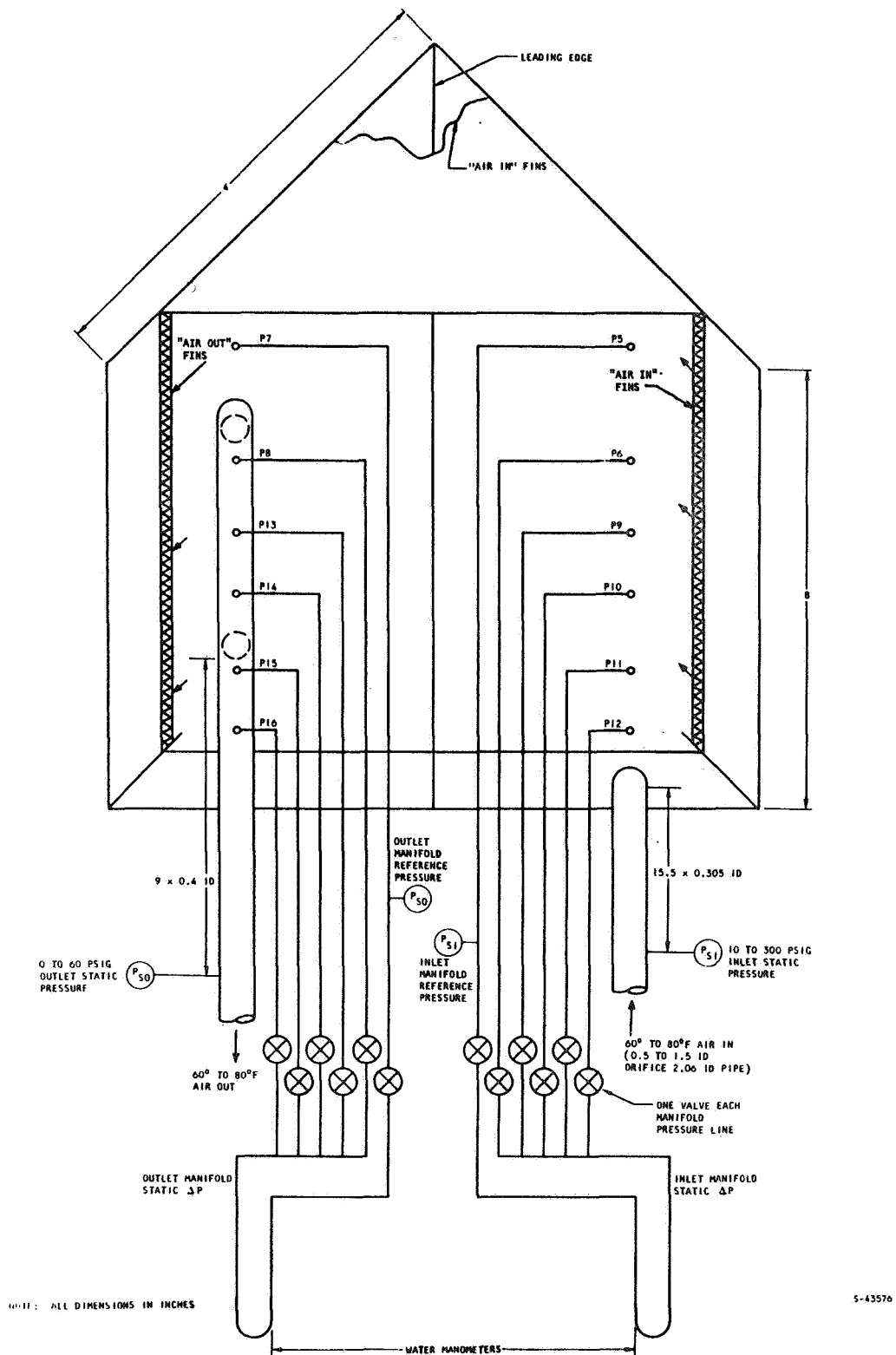
Figure 3-14. Leading Edge Straight Section Flow Distribution Test Schematic

4. TEST PROCEDURE

4.1 THERMAL PERFORMANCE TESTS

For configuration No. 1, the coolant fluid approaches perpendicular to the leading edge and then makes a sharp 154-deg turn. The sharp turn at the tip causes the flow to separate and makes knowledge of the effective flow uncertain. Thus, experimental evaluation of the stagnation region cooling design was necessary. A configuration No. 1 specimen made of Hastelloy X was subjected to a simulated flight-heating environment consisting of subsonic air, heated by a hydrogen/oxygen combustor, flowing over the test section. The test section was cooled with gaseous hydrogen. Hydrogen heat transfer coefficients on the inside surface of the stagnation region, and metal temperatures on the sides of the test specimen were calculated from experimental measurements and conditions. Configuration No. 2, which has leading edge coolant flow parallel to the stagnation line in a key-shaped passage, was subjected to a heating environment consisting of a radiant heat source (single-element quartz lamp and elliptical reflector) impinging on a discrete 0.06- to 0.09-in. width along the 8-in. length of the specimen stagnation line. The test section was cooled with room temperature inlet air. Air heat transfer coefficients on the inside surface of the stagnation line were calculated from experimental measurements and conditions. Configuration No. 2 is also made of Hastelloy X but has a 0.015-in.-thick Nickel-200 outer shell at the leading edge tip.

Although two stagnation-line cooling configurations were tested, configuration No. 1 had the greatest uncertainty in coolant heat transfer coefficient prediction. For configuration No. 2, with hydrogen flow parallel to the leading edge in a tube of complex cross-section, the coolant heat transfer coefficient could be predicted with greater confidence.

4.2 THERMAL CYCLING TESTS

The same radiant heat source that was used for thermal performance tests of the configuration No. 2 specimen was used for thermal cycling tests. With air-cooling in both configurations, radiant heat was applied to the leading edge tip so that the leading edge temperature was increased from room temperature to between 1400° and 1800°F and back to room temperature in a 5-min cycle. This cyclic heating pattern was continued until the specimens failed. Evaluation was based on examination of photomacrographs and photomicrographs of the crack locations.

4.3 COOLANT FLOW DISTRIBUTION TESTS

The inlet and outlet manifolding is similar to that on the flightweight engine. Several static pressure taps were located along the inlet and outlet

manifolds of the 8-in.-long specimen. The ratio of the local core-flow rate to the average core-flow rate along the length of the specimen was calculated from the measured pressure data.

5. TEST RESULTS

5.1 THERMAL PERFORMANCE TESTS

5.1.1 Hot Gas Heating Tests (Configuration No. 1)

5.1.1.1 Summary of Results

From the hot gas data for configuration No. 1, the internal cooling coefficient at the leading edge tip in terms of Nusselt number vs Reynolds number was calculated, based on stagnation line heat flux and the measured stagnation surface temperatures. The conversion of thermocouple readings to stagnation surface temperatures was based on a three-dimensional conduction model in the vicinity of the thermocouple junction. The leading edge heat flux was calculated by the theory of Reference 5-1 with the velocity gradient based on potential flow theory. Based on the data of Kestin (Reference 5-2), the heating coefficient was increased by 10 percent to account for turbulence. The experimentally determined coolant heat transfer coefficients at the stagnation line are equal to about four-times the heat transfer coefficient in the adjacent plain-fin passage. This increase in coolant coefficient is in fair agreement with the empirical relation of Reference 5-3 which predicts the heat transfer coefficient for multiple jets impinging on the inner surface of simulated turbine blade leading edges.

5.1.1.2 Test Data

The hot gas tests are divided into two parts. The first part consists of test runs 7 through 24 where reliance was placed on temperature-indicating paint in an attempt to measure leading edge tip temperatures and overall conditions. The second part consists of test runs 26a through 30b where thermocouples were attached to the leading edge tip and a screen mesh was inserted in the test tunnel upstream of the test section to reduce the flow turbulence to a low and calculable level. For both parts the test setup described in Section 3.1 was used.

An attempt was made to obtain quantitative temperature distribution patterns on the hot-surface leading edge of the SN 2 model. This model, which had some internal fin-plugging, was primarily intended for checking out and calibrating the facility. The hot surface was painted with "Thermindex" temperature-indicating paint and the model exposed to hot gas flow. The technique was unsuccessful, however, as the paint did not have sufficient adhesion to stick to the surface for the duration of the run. Consequently, the use of paint was abandoned after run 9A, Table 5-1, resulting in a lack of temperature data which limited the extent of data reduction possible in the stagnation area.

TABLE 5-1

LEADING EDGE STRAIGHT SECTION
TEST SPECIMEN DATA-POINT-RUN LOG

Run Number	Test Specimen Number	AiResearch Serial Number	Nominal Hot Gas Conditions			Nominal Hydrogen Coolant Conditions		
			Temperature, °R	Flow Rate, lb/sec	Pressure, psia	Temperature, °R	Flow Rate, lb/sec	Pressure, psia
7	1	SK51287-1 No. 2	2500	3	100	520	0.03	400
8			2500	6	100	520	0.03	400
9A			2500	6	100	520	0.02	400
10A			3000	6	100	200	0.086	400
11			2500	6	100	200	0.086	400
12			2500	6	100	200	0.120	400
13			3500	6	100	200	0.086	400
14			4000	2	100	200	0.086	400
15			4000	4	100	200	0.086	400
16			4000	6	100	200	0.086	400
17A	2	SK51287-1 No. 4	2500	6	100	400	0.086	400
18			3000	6	100	500	0.086	400
19			3000	6	100	200	0.060	700
20			3500	6	100	200	0.057	700
21			4000	2	56	200	0.086	700
22			4000	6	142	200	0.086	700
23			4000	4	97	200	0.086	700
24			4000	6	143	200	0.086	700

For run 9A, the zirconia end cap and trailing-edge blocks were replaced with a single-piece, water-cooled part which functioned satisfactorily on both the remainder of SN 2 test runs and SN 4 test runs. This replacement was necessitated by continued mechanical failure of the zirconia parts. It is shown installed on the SN 4 model in Figure 3-8.

SN 4 specimen, following calibration runs, showed no evidence of over-heating, indicating that the design was performing as anticipated.

During runs 26a through 30b the leading edge straight section, SN 4, was tested with stagnation line thermocouples. Also a 16 by 16-mesh-per-in. screen of 0.020-in.-diameter wire was used at a station 10-in. upstream of the leading edge at the entrance to the 2 by 7.75-in. duct, to reduce the flow turbulence to a low and calculable value.

Six chromel-alumel thermocouples, three each of 0.006-in. and 0.012-in. wire diameter, were resistance-welded to the cowl leading edge. One pair each of 0.006-in. and 0.012-in. diameter wires were attached to the cowl leading edge after the two wires were joined together to form a bead. Figure 5-1 shows the thermocouple installation.

These tests were conducted with subsonic flow (approximately Mach 0.28, 650 fps), of hydrogen-air combustion products at a constant pressure of 100 psia, and total temperature of 2400°R. The internal coolant flow rates were varied from 0.006 to 0.029 lb/sec to provide a range of Reynolds numbers. The coolant was normal hydrogen except for run No. 28, for which 75 percent para-hydrogen was used. The coolant inlet temperature was 520°R to 160°R to obtain a broader range of wall-to- bulk temperature ratios. The test data is reproduced in Table 5-2.

5.1.1.3 Data Analysis and Discussion

The test section total temperature was not measured directly. It has been plotted in Figure 5-2 against the percent of hydrogen inlet to the total gas flow. This curve is obtained using the theoretical combustion temperature and subtracting the experimental water jacket heat load.

The average enthalpy at the burner exit plane (BEP) is the theoretical combustion value (th) less the total burner water heat load per lb of hot gas flow.

$$H_{T_{BEP}} = H_{T_{th}} - \frac{(WC_p\Delta T)_{burner\ water\ jacket}}{W_{gas}} \qquad (5-1)$$

The average total enthalpy at the leading edge plane (LEP) is the enthalpy at the burner exit plane, less the total heat loss to the first 10 in. of test-section wall per lb of hot-gas flow. Assuming this loss is one-half of the total test-section heat load:

$$H_{T_{LEP}} = H_{T_{BEP}} - \frac{1/2(WC_p\Delta T)_{test\ section\ water\ jacket}}{W_{gas}} \qquad (5-2)$$
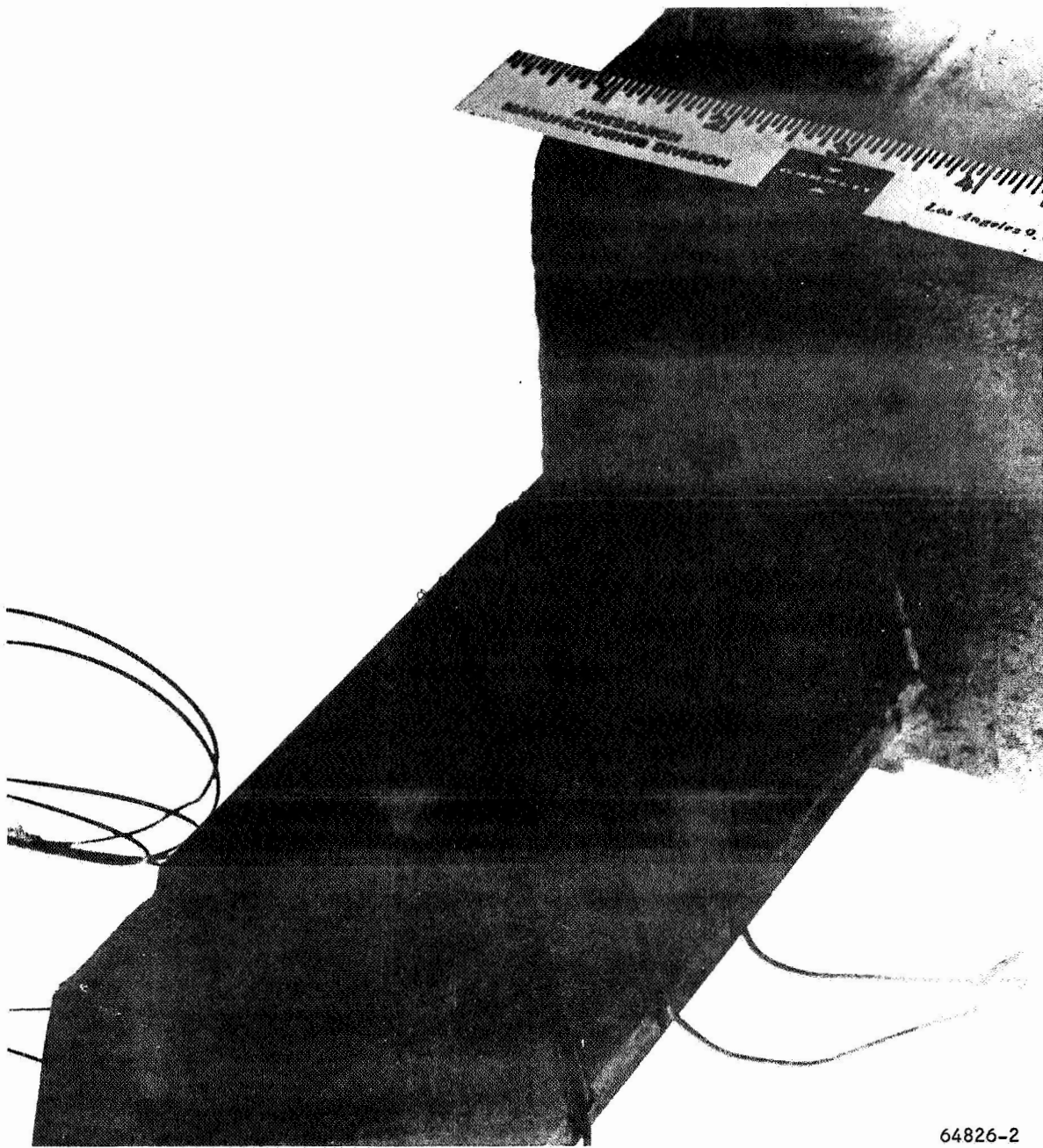
64826-2

Figure 5-1. Leading Edge Straight Section Coolant
Heat Transfer Test Configuration SN 4

TABLE 5-2

LEADING EDGE STRAIGHT SECTION TEST DATA

Hot gas conditions:

$P_T = 100$ psia
$T_T = 2400$ °R
$M = .28$
$U = 650$ pps

Burner:

$H_2 = .072$ lb/sec
AIR $= 5.9$ lb/sec

Run No.	Hydrogen Coolant					Thermocouple Readings		
						.006 in. dia		0.012 in. dia
	Flow Rate (W), lb/sec	Composition	Average Pressure, psia	Inlet Temp, (T_{ci}), °R	Outlet Temp, (T_{co}), °R	Single Wire, °R	Two Wires Joined, °R	Single Wire, °R
26 a	0.0274	Normal	470	547	906	1357	-	1485
26 b	0.0156	Normal	470	543	1118	1501	-	1614
27 a	0.0092	Normal	475	536	1330	1629	-	-
27 b	0.0072	Normal	480	536	1465	1706	-	-
28 a	0.0095	75% para	450	167	1128	1509	-	1629
28 b	0.0071	75% para	470	169	1308	1600	-	1700
28 c	0.0056	75% para	470	175	1460	1708	-	-
29 a	0.0189	Normal	490	163	791	1338	1549	1498
29 b	0.0151	Normal	495	165	918	1405	1577	1537
30 a	0.0076	Normal	470	169	1282	1604	1748	1732
30 b	0.0059	Normal	475	171	1429	1723	-	1822

Figure 5-2. Cowl Straight Section Test Tunnel Gas Total Temperature

TUNNEL NOMINAL FLOW RATE
(W) = 6 LB/SEC

CODE

I   THEORETICAL MAXIMUM TEM-
      PERATURE BASED ON FUEL
      AND AIR INITIAL TEMPERA-
      TURE OF 60°F AT A
      FINAL PRESSURE OF
      10 ATMOSPHERES

II   SAME AS CURVE I EXCEPT AT
      A FINAL PRESSURE OF
      1 ATMOSPHERE

III   CURVE I LESS ΔT, THE
      EQUIVALENT HEAT LOSS TO
      BURNER WATER JACKET

IV   CURVE I LESS ΔT, THE
      EQUIVALENT HEAT LOSS TO
      THE BURNER AND TEST
      SECTION WATER JACKETS

S-40141

The sudden contraction at the burner exit plane provides for good mixing of the hot gas flow, and the fluid properties at this point have been considered as uniform. This is not true in the leading-edge plane because the heat transferred to the wall between the burner exit and the leading edge comes primarily from within the boundary layer. Assuming the viscous layer and the thermal layer are of the same thickness, then, at the test station, (approximately 2-1/2-duct-hydraulic diameters from the test section entrance) the boundary layer is smaller than one-half of the duct height. Consequently, the properties at the leading edge are the properties of the core flow at the burner exit. This is confirmed by the results for test runs 19, 20, 22, and 24 in Table 5-3 which shows excellent agreement (within 0 to 6 percent) between the measured heat loads and the calculated heat loads using total-enthalpy values calculated with Equation (5-1) and turbulent flow starting at the leading edge.

Data analysis was performed for runs 17 through 24 in Table 5-1. These tests cover a range of total temperature of 2500° to $4000^{\circ}R$ with the corresponding enthalpy of 800 to 1400 Btu/lb. Runs 7 through 16 were not analyzed in detail because they were tests on specimen SN 2 which had internal coolant blockage and included no data points not available from the SN 4 model.

The highest heat flux on the stagnation zone during test was estimated to have ranged from 600 to 800 Btu/sec ft^2, while the corresponding average heat flux on the flat surface was 266 Btu/sec ft^2. Unsatisfactory performance of the temperature-indicating paint precluded the estimates of surface temperature at the leading edge tip required to more closely bracket this range.

The thermal data reduction procedure calculates the experimental heat loads and average heat fluxes for the sides of test specimen, SN 4, from coolant temperature rise. Surface temperature is calculated from fin ΔT and wall ΔT at these heat fluxes. The theoretical heat load is calculated by flat-plate equations, including the effect of water vapor condensation on the leading edge flat surfaces, as presented below, and hot gas total enthalpy presented by Equation (5-1).

Theoretical laminar:

$$q = 1.33 \int_{L=0}^{\text{Transition } L} \frac{0.344 \, \rho_f u \, (H_{AW} - H_W)}{(Re_f)^{1/2} (Pr_f)^{2/3}} \left[1 + (Le^{0.63} - 1) \frac{H_E}{H_T} \right] dL \quad (5\text{-}3)$$

Theoretical turbulent:

$$q = 1.33 \int_{\text{Transition } L}^{L=1/3 \text{ ft}} \frac{0.0296 \, \rho_f u \, (H_{AW} - H_W)}{(Re_f)^{0.2} (Pr_f)^{2/3}} \left[1 + (Le^{0.63} - 1) \right] dL \quad (5\text{-}4)$$

TABLE 5-3

COWL STRAIGHT SECTION EXPERIMENTAL RESULTS
AND COMPARISON WITH THEORIES

Item	Parameter	Run 19	Run 20	Run 22	Run 24
		Line 200	Line 512	Line 905	Line 602
Test section conditions	Hydrogen percentage	1.87	2.53	2.6	2.76
	Total temp $^\circ R$	2800	3440	3460	3600
	Tunnel flow, $\frac{lb}{sec}$	5.6	5.5	5.7	5.9
	Total pressure, psia	102	117	143	143
Hydrogen coolant	T_{in}, $^\circ R$	155	155	241	170
	T_{out}, $^\circ R$	508	624	587	553
	P_{in}, psig	650	680	690	665
	P_{out}, psig	628	665	660	622
	W_H, $\frac{lb}{sec}$	0.060	0.057	0.084	0.083
Heat transfer (q), Btu/sec	Measured	79	99	109	118
	Calculated using H_T from Eq (5-1) and transition Reynolds number of 200,000	67	88	94	107
	Percent error	15	11	14	10
	Calculated using H_T from Eq (5-1) and full turbulence	74	97	104	118
	Percent error	6	2	5	0
$\frac{q}{A}$, $\frac{Btu}{sec/ft^2}$	Test $(q/A)_{avg}$	178	222	246	266
	Test $(q/A)_{stag}$				600 to 800
Average wall temperature, $^\circ R$		800	940	920	940
Average fin ΔT, $^\circ R$		362	422	366	426

where 1.33 is two-times the leading edge height (both sides) of 8 inches,
expressed in units of feet,and "Transition L" is the length from the leading
edge tip,where laminar-to-turbulent transition takes place. Excellent agree-
ment between calculated theoretical heat load and measured test heat load
is obtained by assuming turbulent flow starts at the leading edge as shown
in Table 5-3. However, the calculated values are consistently 10 to 15 per-
cent low if a transition Reynolds number of 200,000 is assumed.

Boundary layer transition has also been evaluated by heat flux distribu-
tion. The relative heat flux distribution along the hydrogen flow path is
qualitatively indicated by the cold-wall temperature curves as shown in Figure
5-3. Within 10 or 20 degrees, the hydrogen bulk temperature is the same as
the cold-wall temperature. The rise in hydrogen temperature between any two
stations along the hydrogen flow path is directly proportional to the heat
absorbed between these stations. As shown in Figure 5-3, the cold-wall tempera-
ture rises abruptly near the leading edge between $X = 3.2$ and $X = 4.8$. $X = 0$
is the coolant entrance station of the test specimen, $X = 4$ is the leading
edge station,and $X = 8$ is the coolant exit station. The temperature rise
between $X = 3.2$ and $X = 4.8$ is 39 percent of the overall temperature change,
and occurs in only 20 percent of the flow length (surface area). For run 24,
the average heat flux for the tip section, within 0.8 in. from the leading
edge, is 510 Btu/sec ft^2,while the average heat flux for the remaining section
is 200 Btu/sec ft^2. This suggests that the flow is completely turbulent.

The primary purpose of test runs 26a through 30b (eleven runs total in
Table 5-2) using thermocouples on the leading edge tip surface was to establish
the coolant heat transfer coefficient at the 154-deg turn. The internal cool-
ing coefficient is determined following the procedures described below. This
method requires the external heat flux to be established first,from tunnel
flow properties and the external surface temperature. The internal leading
edge cooling coefficient is then computed with the stagnation heat flux and
the bulk temperature of the coolant. The stagnation line heat flux was
obtained from the Fay-Riddell equation (Reference 5-1). The Fay-Riddell equa-
tion is

$$\left(\frac{q}{A}\right)_{stag} = \frac{0.54}{Pr^{0.6}} \left(\frac{\rho_W \mu_W}{\rho_T \mu_T}\right)^{0.1} \sqrt{\rho_T \mu_T \left(\frac{du}{dx}\right)_T} (H_T - H_W) \qquad (5-5)$$

For this analysis, freestream turbulence effects and three-dimensional
conduction effects in the leading edge Hastelloy X tip were considered. Free-
stream turbulence has a marked influence on stagnation flow. A free-stream
with a turbulence level of 3 percent can increase the stagnation heating by
as much as 80 percent. For a freestream turbulence of 0.7 percent, the esti-
mated increase is 10 percent (Reference 5-2). The test section turbulence level
is estimated to be approximately 0.7 percent with the installation of a 16-
mesh screen 10 in. upstream of the test model (the level of turbulence behind
a screen is given on page 247 of Reference 5-4). Accordingly, the stagnation
line heat transfer coefficient has been raised by 10 percent above the nominal
turbulence-free solution to 0.283 Btu/sec°R ft^2 (variations in this coefficient
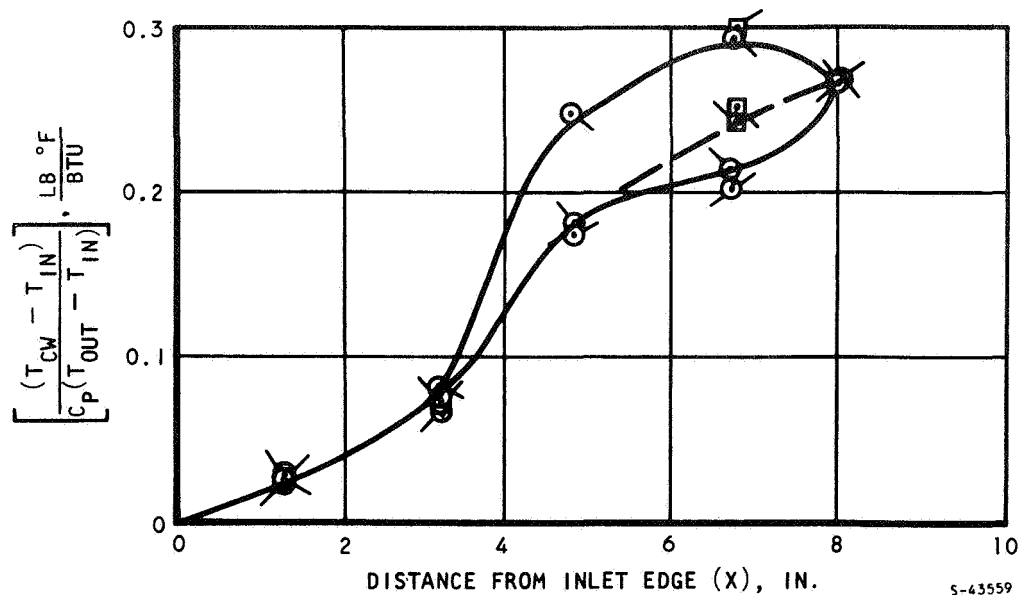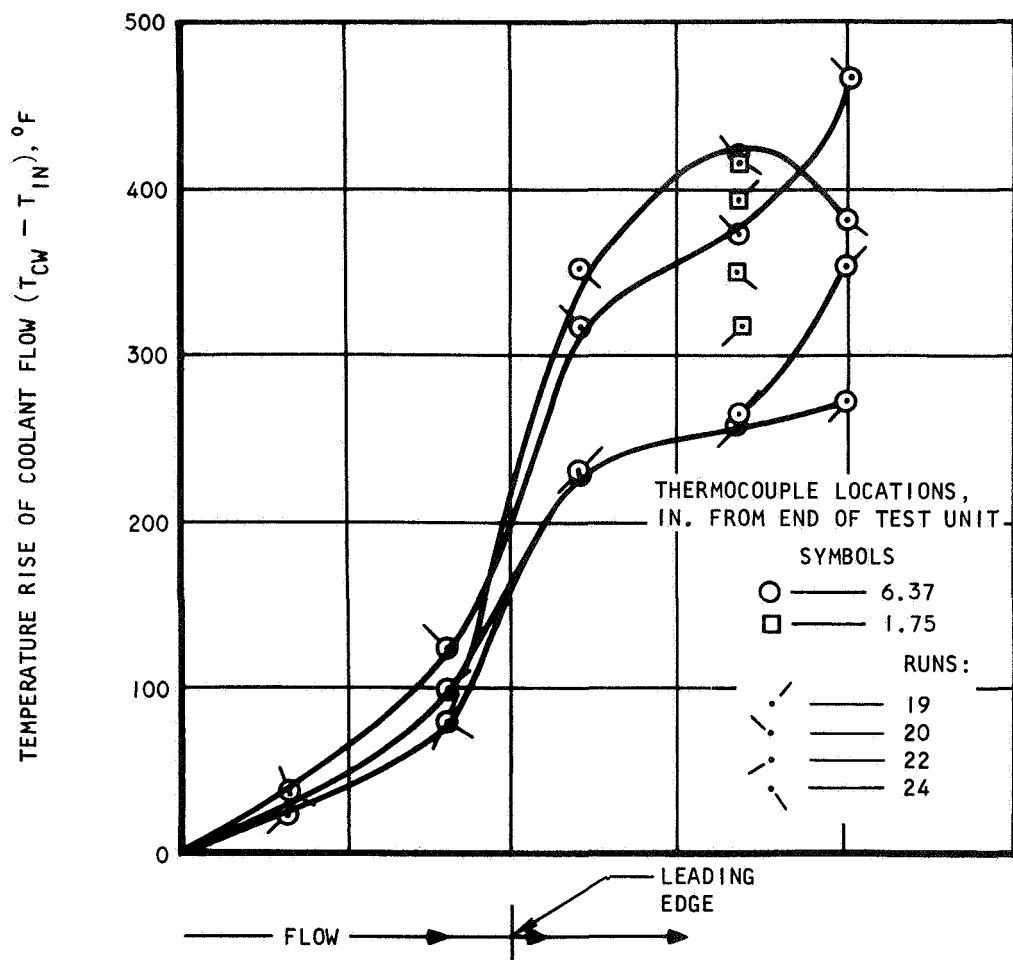were negligible).

Figure 5-3. Leading Edge Straight Section Cold Wall Temperature (Heat Flux) Variation

The conduction effects were analyzed to yield a thermocouple correction number, a constant coefficient for the ΔT across the leading edge wall, and a constant coefficient to relate the internal $(q/A)_1$ to external $(q/A)_2$ at the stagnation line. These two coefficients are defined below in Equations (5-6) and (5-7).

For metal ΔT:

$$\frac{(T_{w1} - T_{w2}) K}{(q/A_1)r_1 \ n \ r_1/r_2} = 0.88 \ (\text{constant}) \tag{5-6}$$

For the heat flux ratio

$$\frac{q/A_1}{q/A_2} = \frac{q/A \ \text{internal}}{q/A \ \text{external}} = 1.6 \ (\text{constant}) \tag{5-7}$$

Thermocouple correction number is defined as the difference between the thermocouple reading and the stagnation temperature without a thermocouple attached. Resulting values of N_{TC} are shown in Figure 5-4. The metal in the vicinity of the thermocouple was divided into small elements as shown in Figure 5-5. The thermal resistance between adjacent solid-solid or solid-fluid elements was used to obtain a heat balance and temperature at each element. Variation of metal thermal conductivity with temperature was automatically included in the calculations. Both the hot gas convective heating to the wire and the conduction between the wire and wall have been accounted for. The computed temperatures at nodes 30 and 505 in Figure 5-5 are the predicted thermocouple reading, and the stagnation temperature without a thermocouple, respectively.

The convective heat transfer coefficient for the bare wire is uncertain because of the small projection above the surface. When a wire is very small and is placed close to the leading edge surface, the heat transfer coefficient for the wire and the semicylindrical leading edge is approximately equal (the wire may be thought of as rough surface). As the wire diameter is increased, or as the wire is placed farther away from the surface, the influence of the leading edge on the flow field at the stagnation of the wire is diminished. At the extreme, the heat transfer to the wire is calculated assuming the wire as a cylinder subjected to crossflow. The former flow model, assuming the wire is a part of the leading edge surface, provides a lower limit for the thermocouple readings, and resulting coolant heat transfer coefficient while the latter, assuming the wire as an isolated cylinder, provides an upper limit for the thermocouple readings. The external surface temperatures, determined by subtracting the correction number N_{TC} from the measured thermocouple readings are presented in Table 5-4. To determine the correction number N_{TC}, convection to the wire = 1.0-, 1.3- and 2.25-times the stagnation heating were used for the singularly-attached 0.006-in. wire, singularly-attached 0.012-in. wire,
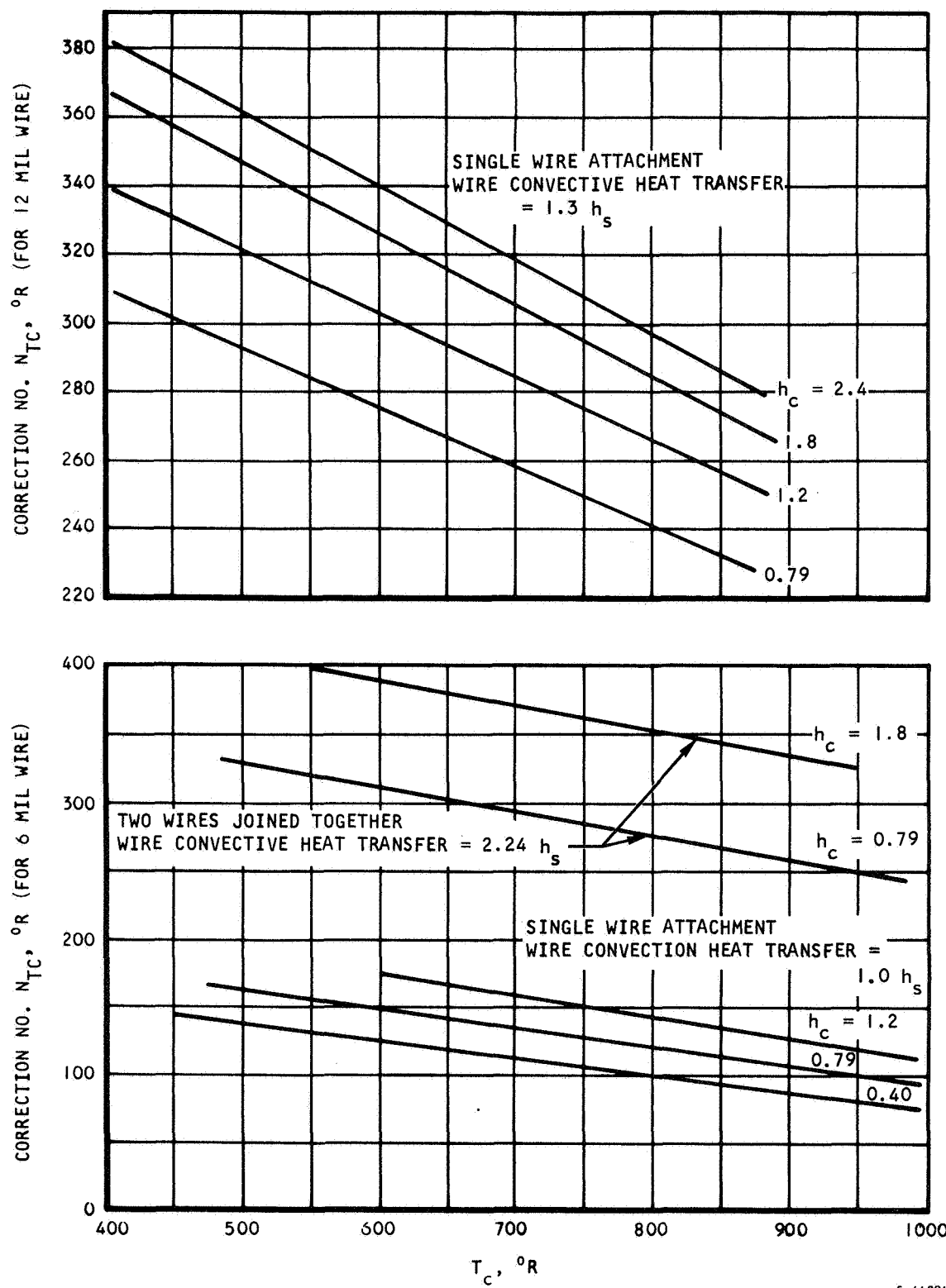
Figure 5-4. Theoretical Thermocouple Correction

ISOLATED SECTION

THERMOCOUPLE CORRECTION
NUMBER: $N_{TC} = T_{NODE\ 30} - T_{NODE\ 505}$

505

AERO HEATING

$$\frac{h}{h_s} = 1 - \left(\frac{\theta}{90}\right)^3$$

$h_s = 0.283$ BTU PER SEC-$^\circ$R-FT^2

$\theta \longleftarrow \ \longrightarrow \theta$

THERMOCOUPLE WIRE
5 NODES

30

COWL OUTER SKIN

INTERNAL
COOLING

0.015 IN.

0.030 IN.
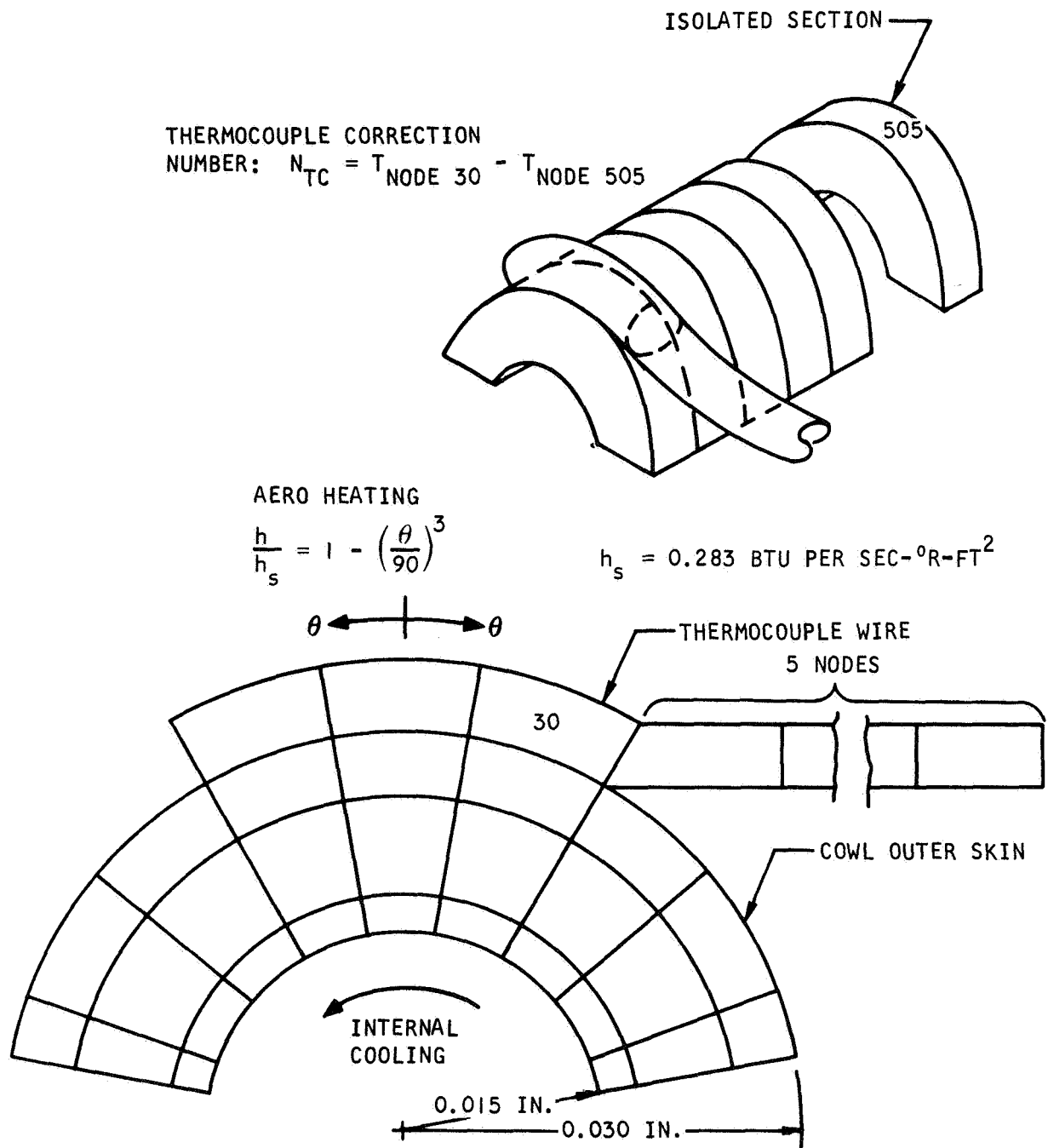
S-44888

Figure 5-5. Conduction Model for Thermocouple
Correction Number Analysis

and jointly-attached (bead) 0.006-in. wire, respectively. The smallest multiplier was used with the 0.006 wire because it projected less than 0.006 in. from the leading edge surface, and is being treated as part of the leading edge surface. The highest multiplier was used with the thermocouple bead formed from two wires of 0.006-in. diameter and with an effective radius of twice that of a single wire so that

$$\left(\frac{R_{cowl}}{R_{effective}}\right)^{0.5} = (0.03/0.006)^{0.5} = 2.24$$

TABLE 5-4

CALCULATED TEMPERATURE OF UNDISTURBED EXTERNAL SURFACE

Run No.	Single Wire 0.006 in., °R	Single Wire 0.012 in., °R	Two Wires Joined 0.006 in., °R
26a	1200	1190	
26b	1375	1360	
27a	1535		
27b	1620		
28a	1370	1364	
28b	1486	1470	
28c	1618		
29a	1152	1170	1180
29b	1235	1235	1225
30a	1490	1500	1484
30b	1630	1620	

After establishing the external surface temperature from the thermocouple readings with the correction number, the external heat flux $(q/A)_I$ and the internal wall temperature (T_{W2} in Equation 5-6) can be determined. The next step is to compute the cooling coefficient.

$$h_c = \frac{1.6(q/A)_I}{T_{W2} - T_{cs}} \tag{5-8}$$

where T_c = coolant temperature and the subscripts i, s, and o, designate inlet, stagnation zone and outlet, respectively.

The coolant temperature at the leading edge stagnation zone was calculated from the log mean differential temperatures:

$$T_T - T_{cs} = \frac{T_{co} - T_{ci}}{\ln \dfrac{T_T - T_{ci}}{T_T - T_{co}}} \qquad (5\text{-}9)$$

where T_T = hot gas total temperature

Hydrogen fluid properties were evaluated at bulk temperature, T_{cs}.

The range of hydrogen coolant Reynolds numbers tested was between 1700 and 10,000. The increase in heat transfer is in fair agreement with the empirical relation of Reference 5-3 which predicts the heat transfer rate for multiple jets impinging on the inner surface of simulated turbine blade leading edges. The test results and the predicted values by the duct-flow equation and the equation from Reference 5-3 are compared in Figure 5-6. Curve I of Figure 5-6 represents the average experimental values which can be expressed as:

$$Nu_b = 0.052 \, Re_b^{0.84}$$

where $\quad Nu_b = \dfrac{hD_h}{k_b} \quad$ and $\quad Re_b = \dfrac{\rho_b U D_h}{\mu_b} = \left(\dfrac{W}{A}\right)\dfrac{D_n}{\mu_b} \qquad (5\text{-}10)$

The parameters D_h, A, and U are the hydraulic diameter, free-flow area and coolant velocity, respectively, in the 20R-.020-.004 plain fin adjacent to the 154-deg turn. The subscript "b" refers to coolant property evaluation at bulk temperature conditions.

Curve II of Figure 5-6 is the cooling performance predicted with the empirical relation from Reference 5-3:

$$Nu_{stag} = 0.44 \, Re^{0.7} \left(\frac{d}{s}\right)^{0.8} e^{\left[-0.85 \frac{\ell}{d}\left(\frac{d}{D}\right)^{0.4}\right]}$$

For closely spaced jets, the distance between the centers of jets is one jet diameter and $\dfrac{d}{s} = 1$. Since $\dfrac{\ell}{d} = 1.5$ and $\dfrac{d}{D} = 0.6$ are the approximate values for the leading edge straight section, $Nu_{stag} = 0.156 \, Re^{0.7}$.

Curve III is the heat transfer of a fully developed turbulent duct flow.

TEST MODEL OF REF 5-3

$\ell = 0.035$ IN

$D_{INTERNAL} = 0.04$ IN

FIN

FIN
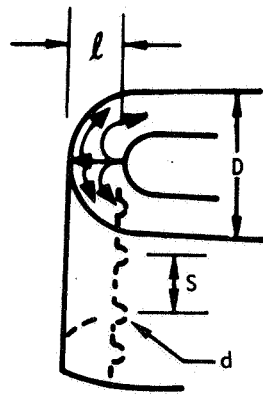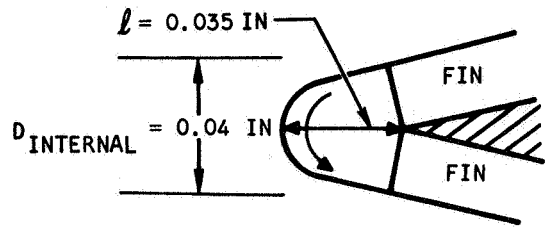
20R-0.020-0.500-0.004
HYDRAULIC DIA = 0.0237 IN.
LEADING EDGE

<u>CURVES</u>

I   EXPERIMENTAL AVERAGE $Nu_b = 0.053 \, Re_b^{0.84}$

II   FROM REF 5-3

$$Nu = 0.44 \, Re^{0.7} \left(\frac{d}{S}\right)^{0.8} e^{-0.85\frac{\ell}{d}\frac{d}{S}\left(\frac{d}{D}\right)^{0.4}}$$

$$\text{for } \frac{l}{d} \cong 1.5; \; \frac{d}{S} \cong 1; \; \frac{d}{D} \cong 0.6$$

III $Nu = 0.02 \, Re_b^{0.8}$

      for Pr = 0.72

      fin $Nu = 0.023 \, Re_b^{0.8} \, Pr_b^{0.4}$

○ NORMAL H_2
◖ 75 PERCENT PARA H_2

$Re_b \times 10^{-3}$

S-44892
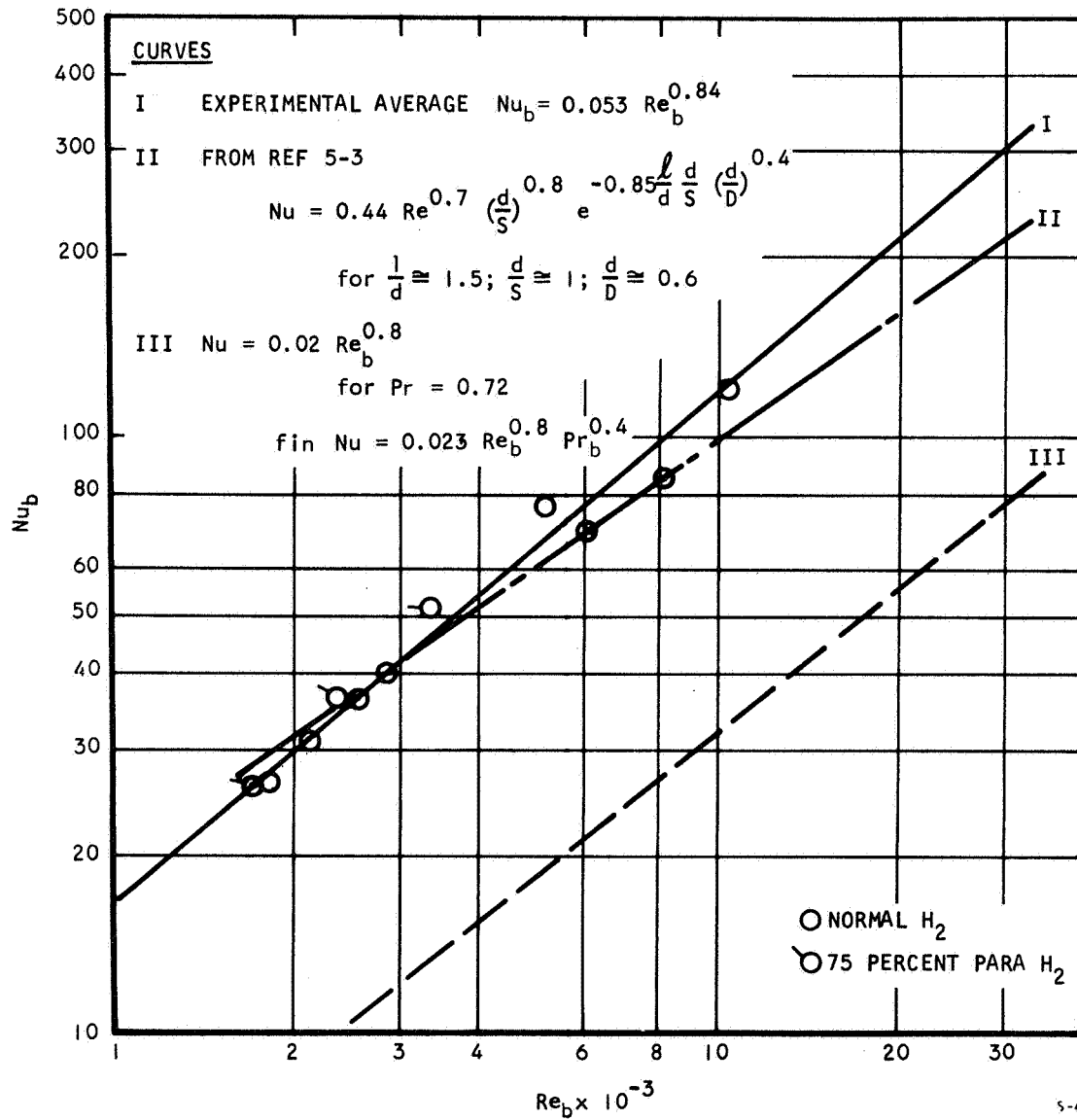
Figure 5-6.   Cowl Leading Edge Internal Cooling Nusselt Number

From the results in Figure 5-6, the internal coolant heat transfer coefficient at the leading edge tip is 3.9-times the straight-pipe coefficient at the design Reynold number of 30,000. A value of 1.94-times the straight-pipe coefficient at a Reynolds number of 30,000 was used for coolant analysis of the original flight engine leading edge.

5.1.2 Radiant Heating Tests (Configuration No. 2)

5.1.2.1 Summary of Results

On the radiant heating thermal performance tests, conducted on configuration No. 2 specimens, the internal cooling coefficient in the leading edge tip passage was calculated in terms of Stanton number vs Reynolds number from a heat balance on the air in the leading edge passage, and measured-metal temperatures in the stagnation region. The radiant heat input was assumed to occur in the 180-deg arc centered on the stagnation line. The remainder of the coolant passage was assumed to act as a fin which rejected heat to the air in the leading edge passage, and to the water-cooled aluminum test fixture. There was no airflow in the side fin passages just in back of the parallel-flow leading edge passage. Good agreement in coolant heat transfer was obtained between the average of the test data and the standard pipe-flow relation for plain rectangular tubes, when a suitable adjustment is made for unsymmetrical heating.

5.1.2.2 Test Data

Configuration No. 2 leading edge straight section SN 2 was tested for thermal performance in the radiant heating test setup described in Section 3.2. Leading edge temperatures were monitored using several thermocouples resistance-welded to the stagnation line as shown typically in Figure 5-7. Inlet and outlet temperatures on each of the fixture-cooling circuits, on the test section, and on the nitrogen used to purge the reflector cavity are measured, as are each of the flow rates. Energy balances obtained in this way are used to monitor the system operation, and support measurements of performance of the leading edge test section itself.

Performance test data for the Nickel-200 tip SN 2 leading edge with parallel flow is summarized in Table 5-5. Inlet and outlet temperature of the cooling air and the airflow rate were used to determine the heat transfer rate which is typically about 10 percent of the lamp-power input. The tabulated leading edge temperature was measured by a chromel-alumel thermocouple spot-welded to the stagnation region at 2 in. from the base end of the model. This location is half-way between the coolant inlet and outlet, since the air enters at both ends of the 8-in. span and exits at the center. For certain of the tests, the air was plumbed to enter at the center and exit at the ends.

5.1.2.3 Data Analysis and Discussion

The results of data analysis and the geometry used in this analysis are summarized in Figure 5-8. A standard pipe-flow relation for plain rectangular tubes, with and without an adjustment for unsymmetrical heating, is shown superimposed on the data.
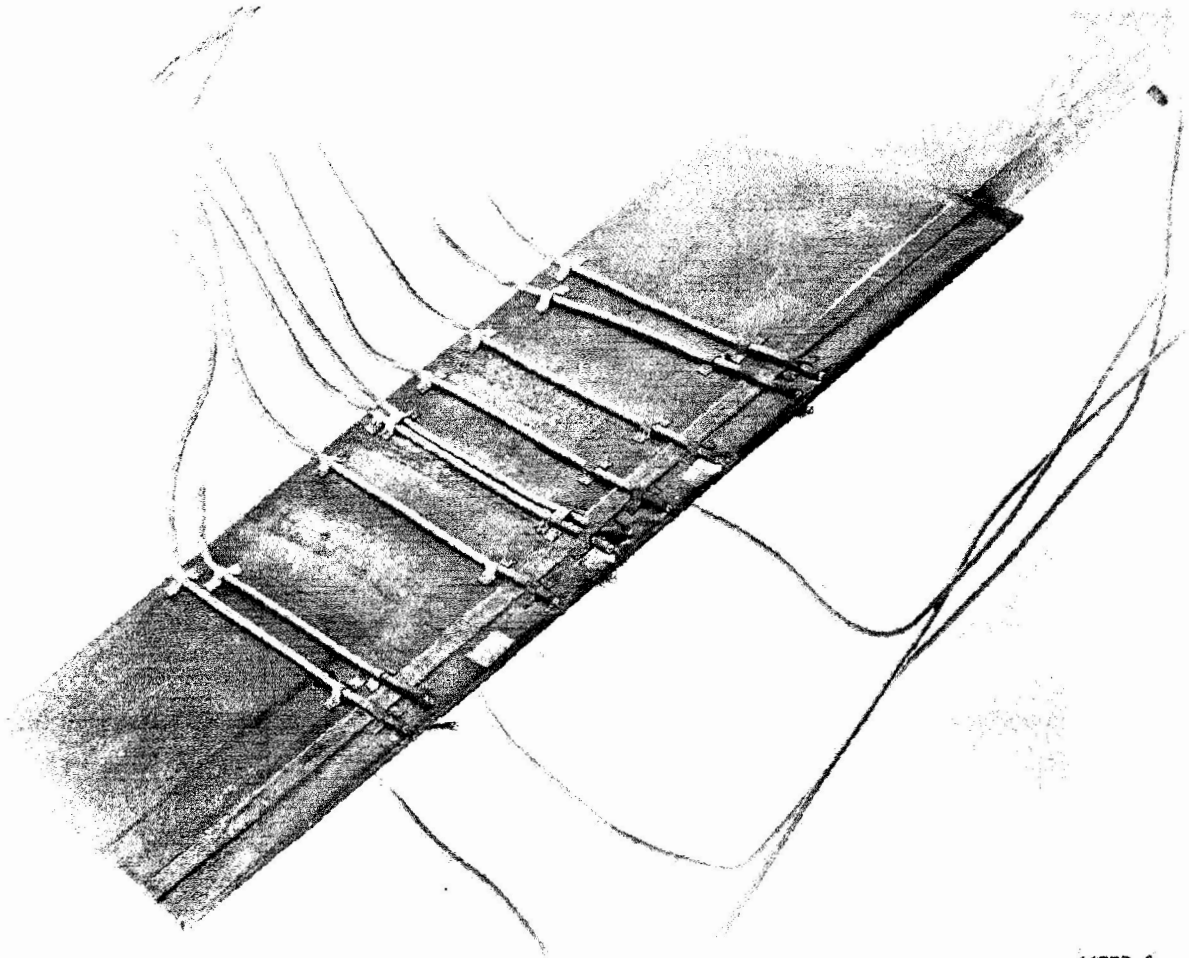
66333-2

Figure 5-7. Leading Edge Thermocouple Instrumentation
for Radiant Heating Tests

TABLE 5-5

AIR-COOLING DATA FOR RADIANT-HEATED PARALLEL-FLOW LEADING EDGE SN 2

Run	T_1, °F	T_2, °F	W, lb/min	Q, Btu/min	T_{LE}, °F	Flow Direction
1	68	181	1.2	32.6	1120	To center
2	76	216	1.0	33.6	1143	↑
3	72	328	0.477	29.3	1215	
4	80	468	0.255	23.8	1352	
5	81	572	0.127	15.0	1640	
6	76	240	1.19	46.9	1047	
7	74	276	1.0	48.4	1048	
8	78	434	0.473	40.4	1153	
9	77	567	0.25	29.4	1307	
10	92	606	0.137	16.9	1432	
11	90	542	0.138	15.0	1204	
12	88	469	0.138	12.6	1020	
13	85	378	0.137	9.65	796	
14	81	312	0.25	13.9	733	
15	80	226	0.472	16.6	673	
16	73	153	0.99	19.0	630	
17	72	126	1.2	15.6	610	↓
18	70	95	1.21	7.27	405	To center
19	70	204	1.05	33.8	1048	From center
20	70	216	0.99	34.7	1050	↑
21	76	326	0.473	28.4	1131	
22	81	434	0.249	20.8	1258	↓
23	88	436	0.137	11.4	1408	From center
24	82	415	0.138	11.0	1384	To center

$$st_{LE} = \frac{h}{GC_p} = \frac{(Q_{LE}/Q_{TOT})(WC_p)(T_2 - T_1)A_F}{A_{LE}(T_{LE} - 0.5T_1 - 0.5T_2(WC_p)}$$

$$st_{LE} = \frac{(Q_{LE}/Q_{TOT})(T_2 - T_1)(6.2 \times 10^{-5})}{4.36 \times 10^{-5}(T_{LE} - 0.5T_1 - 0.5T_2)}$$

$$\frac{A_{FIN}}{A} = 0.866$$

$$\frac{A_{LE}}{A} = 0.256$$

$$A = 0.00191 \; FT^2$$
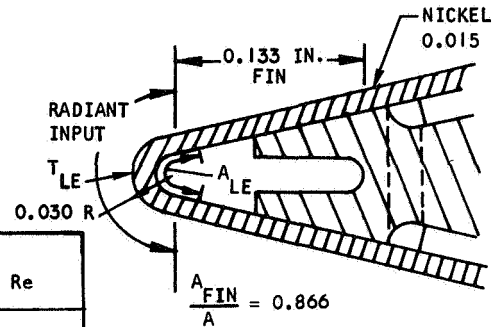
h_{AVG} BTU/SEC-$^\circ$R-FT^2	$\frac{Q_{LE}}{Q_{TOT}}$	$\frac{(q/A)_{LE}}{(q/A)_{AVG}} \simeq \frac{T_{LE} - 0.5T_1 - 0.5T_2}{T_{WAVG} - 0.5T_1 - 0.5T_2}$	Re
0.02	0.288	1.12	7,500
0.04	0.316	1.24	18,000
0.08	0.367	1.44	45,000
0.16	0.444	1.73	110,000

$$h_{AVG} = \frac{0.019 \, WC_p}{(Re)^{0.2}(Pr)^{2/3}(T_{WAVG}/(0.5 \, T_1 + 0.5T_2)^{0.37}}$$

$$\text{LINE A} = \frac{0.019}{Re^{0.2}Pr^{2/3}} \; \text{WHERE Pr} = 0.7$$

$$\text{LINE B} = \text{LINE A} \left(\frac{h_{UNSYM}}{h_{SYM}} \right)$$

$$Re = \frac{DW}{A_F \mu} = \frac{0.00422W}{6.5 \times 10^{-5} \mu}$$
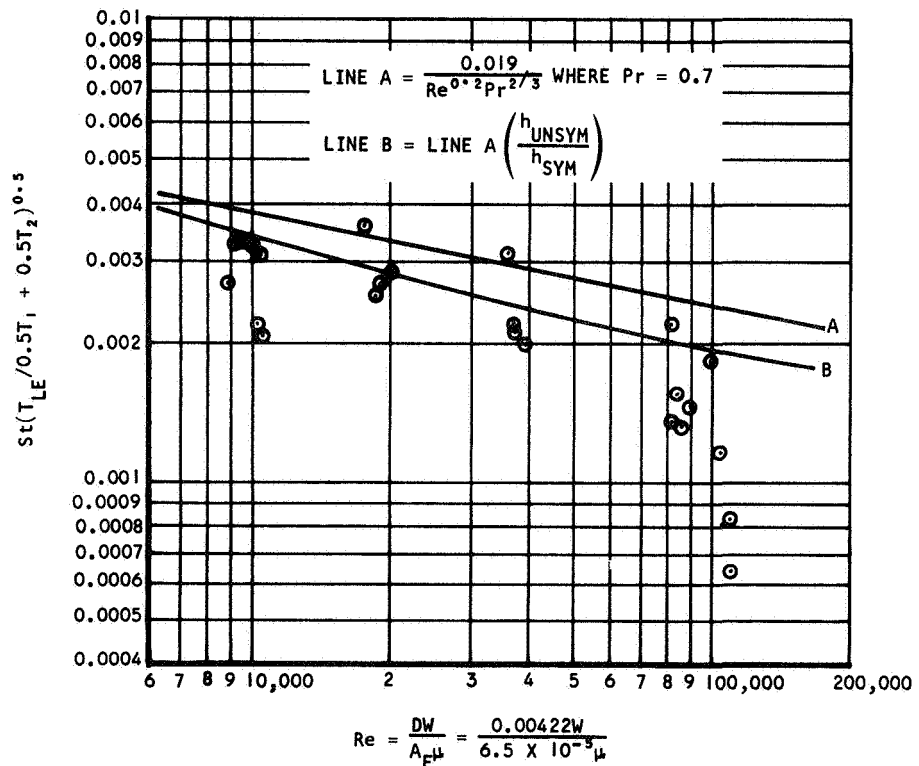
S-49816

Figure 5-8.   Cooling of Leading Edge With Parallel Flow

The radiant heat input was assumed to occur in the 180-deg arc centered on the stagnation line. The remainder of the coolant passage was assumed to act as a fin of 15-mil thickness and 133-mil length which rejected heat by convection to the air in the leading edge passage and by conduction and radiation to the water-cooled aluminum test fixture. There was no airflow in the fin passages, which are connected behind the leading edge passage, and where cooling is normally provided for the 4 by 8-in. flat surfaces of the wedge.

The test Stanton number, St_{LE}, was calculated by the equation in Figure 5-8 and multiplied by the square root of leading edge-to-coolant temperature ratio for plotting, as the circled points on Figure 5-8. Flagged points are for flow from the center toward the ends.

An average coolant heat transfer coefficient, h_{avg}, was calculated by the pipe-flow equation shown in Figure 5-8, where the coefficient 0.019 is for flow in a rectangular duct with aspect ratio of 5. The resulting Stanton number, for a Prandtl number of 0.7, is plotted as line "A". The ratio of leading edge to average heat transfer coefficient for the coolant is less than one, due to the effects of unsymmetrical heating. This effect is indicated as the difference between lines "A" and "B". The method of analysis used is that outlined in Reference 5-5 for a cosine heat flux variation in a round tube.

The average wall temperature was obtained by using a one-dimensional temperature distribution analysis of the coolant passage wall that was considered as a fin. The ratio of heat flux at the leading edge, to average heat flux was assumed equal to the ratio of temperature differences as tabulated in Figure 5-8. The ratio of leading edge heat load to total heat load, Q_{LE}/Q_{TOT}, was also obtained from the one-dimensional fin-temperature distribution analysis for a uniform heat transfer coefficient on the passage surfaces.

Line "B" is from 5 to 20 percent above the average of the data. No explanation for the data scatter has been found; however, the quoted Stanton numbers are minimum because the leading edge area, A_{LE}, was based on the full 8-in. length of the test section. Unblackened areas at the ends of the Hastelloy X units indicate reduced heat flux in these areas. No allowance was made for such a reduced flux because of the uncertainties involved. The effect of such a reduction would be to increase the test Stanton number.

5.2 THERMAL CYCLING TESTS

5.2.1 Summary of Results

Radiant heating thermal cycling tests conducted on configuration No. 1 specimens used room temperature inlet air coolant in the sides and perpendicular-flow leading edge tip passage; those conducted on configuration No. 2 specimens used room temperature inlet air coolant in the parallel-flow leading edge tip passage only. Radiant heat was applied to the leading edge tip so that the tip temperature was increased from room temperature to between 1400° and $1800^\circ F$ and back to room temperature in a 5-min cycle. This cyclic heating

pattern was continued until the specimens failed. Evaluation was based on examination of photomacrographs and photomicrographs of the crack locations. Configuration No. I specimens (Hastelloy X tip) failed at 110 and 200 cycles. Configuration No. 2 specimens (Nickel-200 tip) failed in the range of 40 to 260 cycles. Failure was defined as a large increase in pressure decay from an initial pressure of 700 psia during a one-minute period with the test unit isolated from the rest of the system.

5.2.2 Test Data

Thermal cycling tests were performed on both configuration No. I and configuration No. 2 leading edge test sections using the radiant heating test setup described in Section 3.2. The cycling of the power to the quartz lamp, and consequently of the leading edge temperature, is accomplished by an automatic controller. Cooling of the test specimens during test was accomplished with air at 700 psia. The flow rate of the air was adjusted to yield the desired temperature differences between the external surfaces of the stagnation line and the internal structure. Leading edge temperatures were monitored with thermocouples, as shown in Figure 5-7. The specimens were thermally cycled until failure.

Thermal cycle test data is summarized in Figure 5-9 where typical thermal cycles for two Hastelloy X units (SN's 4 and 5) and three Nickel-200 units (SN's I, 2 and 5) are shown. The plotted cycle for Hastelloy X units SN 4 and SN 5, and also for nickel unit SN I was just before failure was noted. Failure was defined as a large increase in pressure decay from an initial pressure of 700 psia during a one-minute period. The range of maximum temperatures during all cycles, and the average maximum temperature during all cycles is noted for each unit. Generally, the cracks occurred at the location of a thermocouple where heat input was maximum and where a local strain concentration occurs. In Nickel-200 units SN I and SN 5, this was not the case. The crack in SN I occurred in a hotter zone about one inch away from the thermocouple plotted. The dashed line indicates the average maximum at this crack of about 1630°F. Nickel-200 unit SN 5 survived 260 cycles, and the maximum temperature for various groups of cycles is listed (the test was terminated after 280 cycles).

5.2.3 Data Analysis and Discussion

5.2.3.1 Metallurgy

5.2.3.1.1 Nickel-200 Tip (SK 51428)

Three configuration No. 2 leading edge specimens with Nickel-200 tips were thermally cycled to failure. The specimens had all been proof-pressure tested to 1050 psig at room temperature, and accepted. Results of each test are discussed below:

(a) First Test, SN 2--Extensive creep damage was done as a result of cycles to 1800°F and 1600°F at 700 psi coolant pressure. Diagrams,
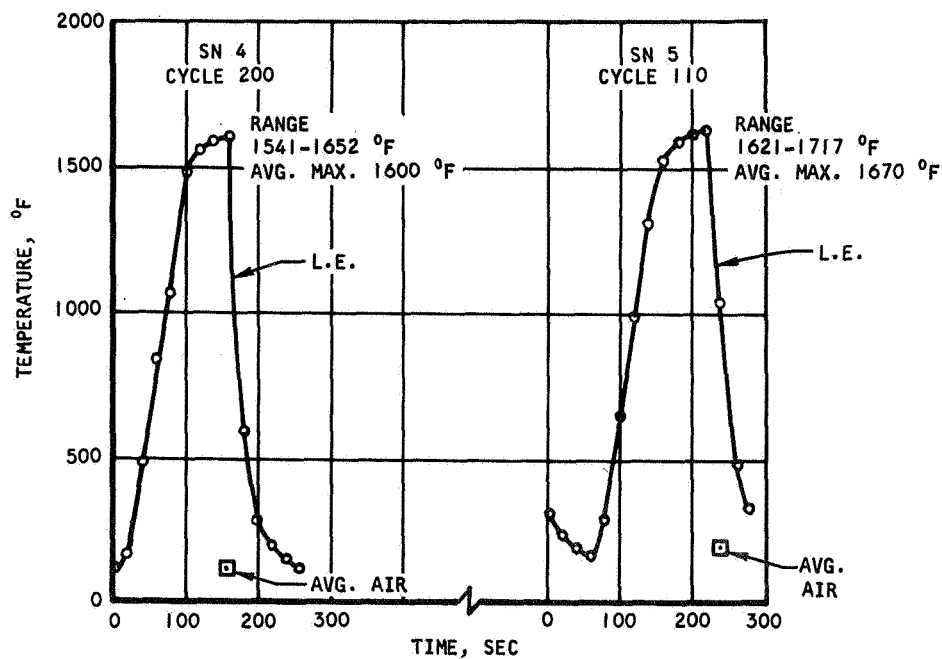
a. HASTELLOY X PERPENDICULAR FLOW SK 51287-1 (CONFIGURATION NO. 1)
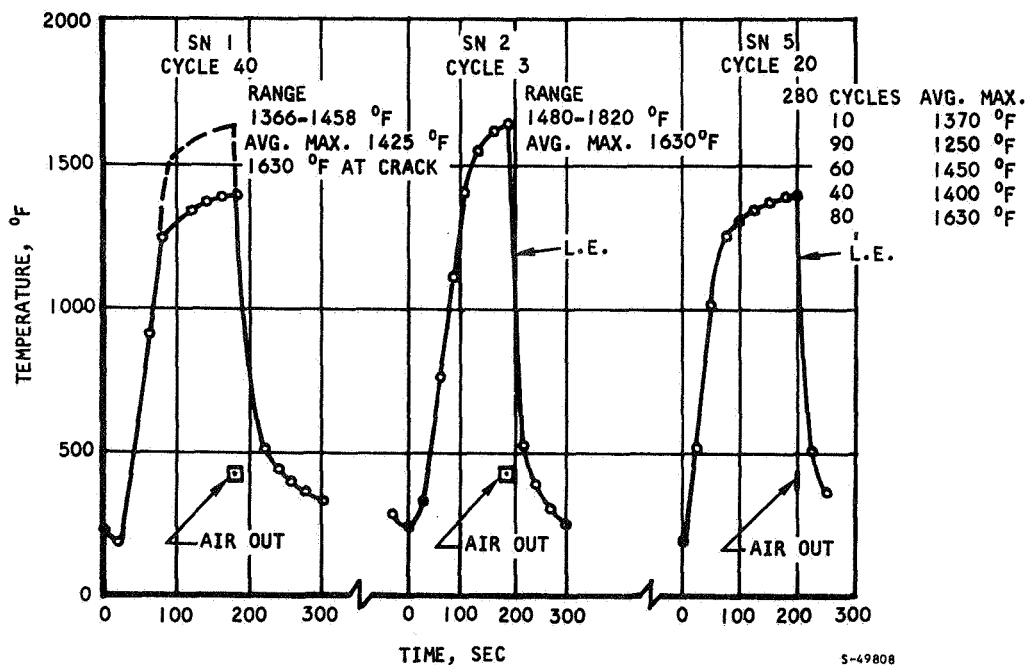
b. NICKEL-200 PARALLEL FLOW SK 51428-1 (CONFIGURATION NO. 2)

Figure 5-9.   Leading Edge Thermal Cycles

photomacrographs, and photomicrographs showing crack locations and general condition of leading edge after testing are presented in Figures 5-10 through 5-14.

Bulging of the Nickel-200 tip extended about 0.120 in. from the tip back to the brazed joint shown in Figure 5-13. The brazed joint was separated slightly due to incomplete brazing and apparently opened up, but did not crack. Cracks in the Nickel-200 tip were intergranular, typical for failure at high temperatures where grain boundaries are weaker than grains. The Nickel-200 grain size was large (about 0.010-in. grains) due to brazing at $2150^{\circ}F$.

(b) Second Test, SN 5--Thermal cycling tests to a nominal $1400^{\circ}F$ maximum tip temperature and 700 psig pressure produced failure after 260 to 270 cycles and in approximately 8-1/2-hr cumulative creep time.

A diagram of crack locations in the SN 5 cowl leading edge is shown in Figure 5-15a. A photomacrograph illustrating types of cracks is presented in Figure 5-15b. Almost all cracks were creep-type cracks at the side of the tip. The one crack which has the appearance of a low cycle fatigue crack may have initiated from a creep crack.

This leading edge was not sectioned for metallographic examination.

(c) Third Test, SN 1--A $1435^{\circ}F$ thermocouple calibration, using ASTM B260 BAg8 brazing alloy foil (a $1435^{\circ}F$-melting-point eutectic alloy composed of 72-percent-by-wt silver and 28-percent-by-wt copper) plated in three locations, resulted in failure at area A (Figure 5-16). The tube carrying coolant air to the inward side of the strut was plugged with brazing alloy, causing overheating and creep failure at point **A**. The outboard side, cooled by a different coolant tube, suffered no apparent damage. The leak was sealed with TIG-braze repair. The inboard side was then shielded with a water-cooled stainless steel tube while the outboard side was thermally cycled.

After approximately 40 thermal cycles, leaks developed in areas C and B. Photomacrographs of these cracks are shown in Figure 5-17. The cracks in both areas appear to be basically due to creep failure. Area C had been coated with brazing alloy foil and this may have contributed to failure by penetrating the Nickel-200 grain boundaries when melted at $1435^{\circ}F$ (Figure 5-18). Preferential oxidation during thermal cycling would accelerate creep failure. This type of intergranular attack in the lightly stressed area of Nickel-200 skin (Figure 5-18b) was not noted in a cross section at area B where no silver brazing alloy was present.

Exposure to 1435° to $1450^{\circ}F$ at 700 psig for 15 min during thermocouple calibration and possible hot spots on the tip (area C was darker and may have been a better heat absorber than adjacent areas) may also have contributed to fewer thermal cycles to failure for this leading edge than for SN 5 (40 cycles vs 260 cycles); however, scatter encountered in creep testing can account for a significant difference in cycles to failure.

Figure 5-10. Diagram of Leading Edge Showing Locations of Photomacrographs and Photomicrographs, SK51428-1, SN 2

ARROW → DENOTES VIEW IN PHOTOMICROGRAPH

AREA D

PHOTOMICROGRAPH SHOWS THIS FACE

AREA C

AREA B (OPPOSITE SIDE)

AREA A

NOTE: LEADING EDGE CRACKS WERE VERY NUMEROUS AND WERE CONCENTRATED IN THE REGION BETWEEN THE EXTREME LEFT AND EXTREME RIGHT THERMOCOUPLES.

S-49807
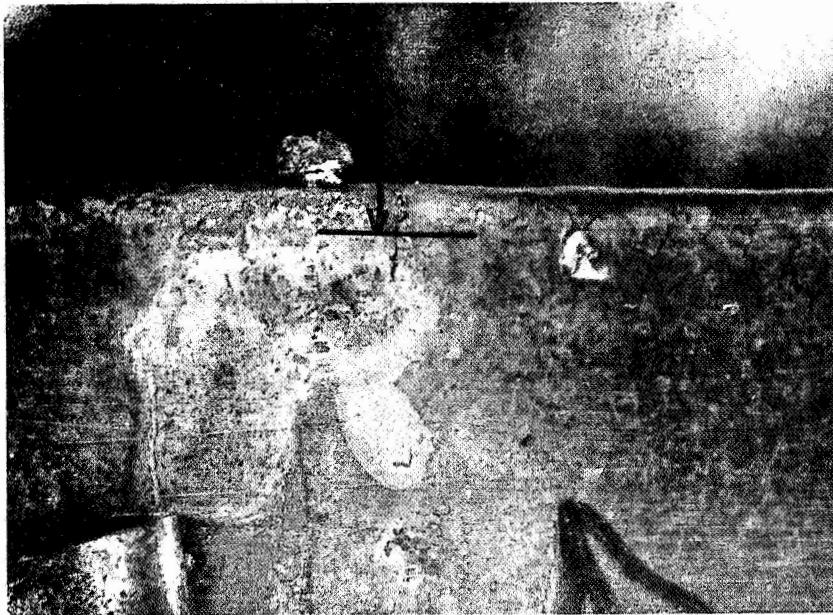
(a) CRACKS IN AREA A.
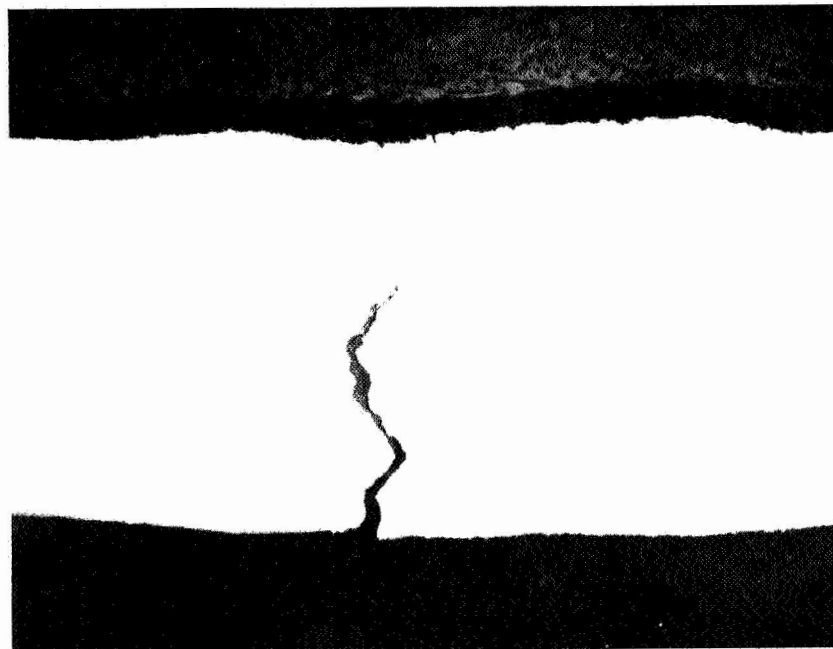
F-10994

(b) CROSS SECTION THROUGH CRACK SHOWN IN ABOVE PHOTO.
(MICRO NO. 16562 50X)

Figure 5-11.   Leading Edge Cracks, Area A,
Thermocouple Removed, SK 51428-1, SN 2

F-10992

NOTE: THESE CRACKS ARE TYPICAL OF CRACKS
FOUND ALONG ENTIRE LEADING EDGE.

Figure 5-12.   Leading Edge Cracks, Area B, SK 51428-1, SN 2

(a) CRACKS FOUND UNDER THERMOCOUPLE BEAD
AFTER T/C WAS REMOVED.
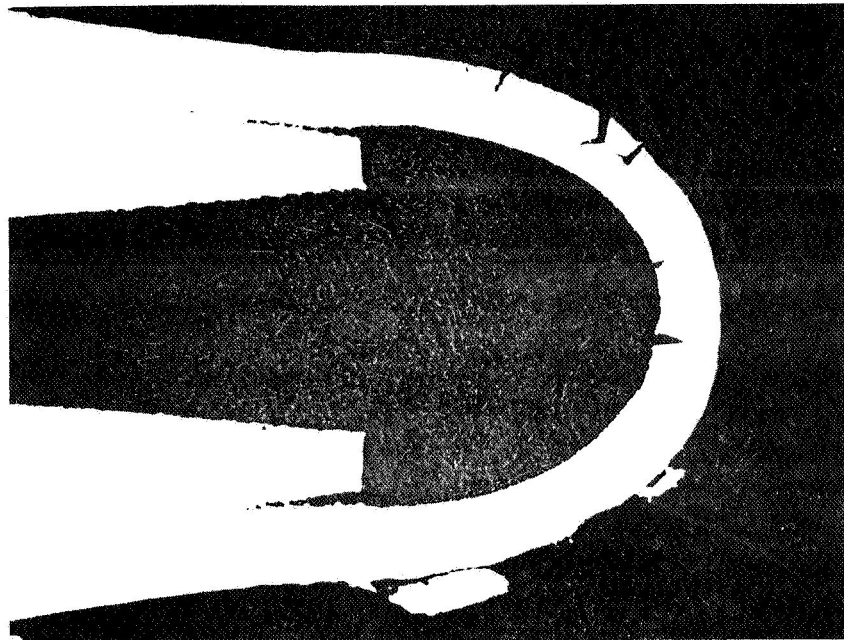
F-10991

(b) CROSS SECTION THROUGH LEADING EDGE WHERE CRACKS
OCCURRED UNDER T/C BEAD. NOTE CRACKS ON INSIDE
OF LEADING EDGE. (MICRO NO. 16563 25X)

Figure 5-13. Leading Edge Cracks, Area C, SK 51428-1, SN 2

(a) CRACKS OCCURRED IN AREA WHERE NICKEL SHEET BULGED AWAY FROM INTERNAL BRAZED JOINT.
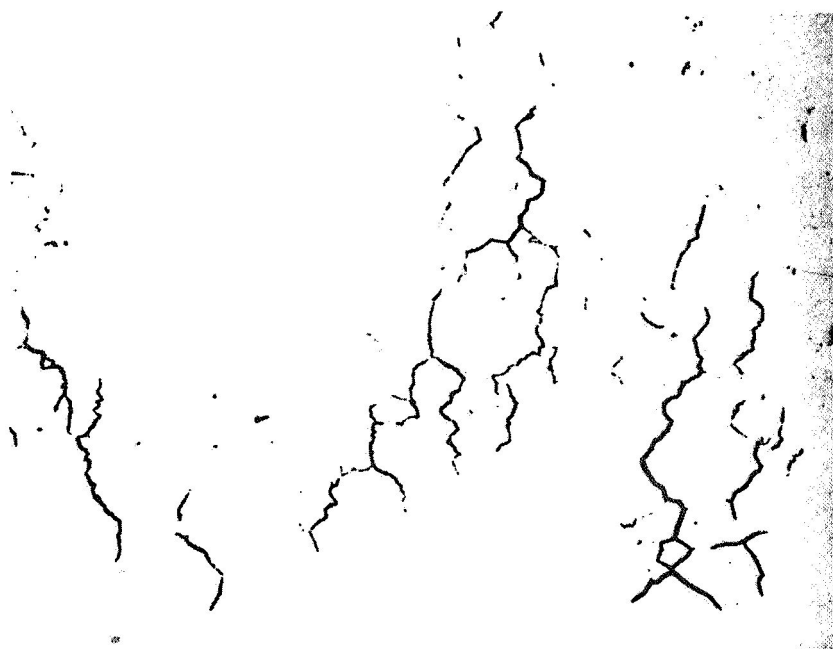
F-10993

(b) FACE OF AREA SHOWN IN PHOTO ABOVE, ABOUT 0.003 IN. BELOW SURFACE. (MICRO NO. 16564 50X)

Figure 5-14. Leading Edge Cracks, Area D, SK 51428-1, SN 2
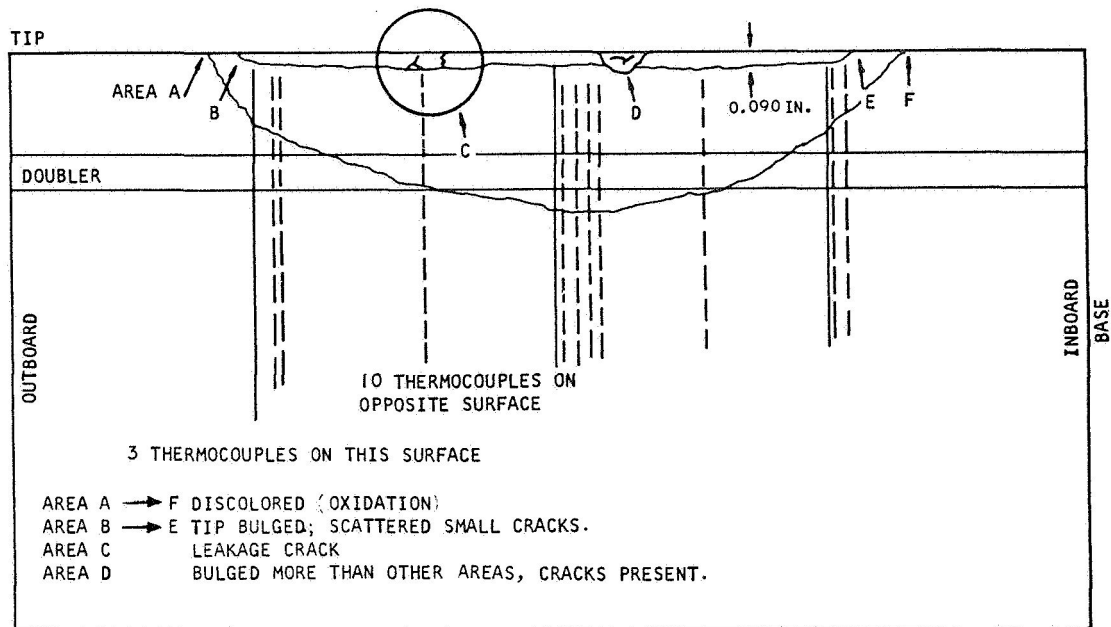
(a) SKETCH ILLUSTRATING LOCATION OF CRACKS, BULGES, THERMOCOUPLES AND
GENERAL CONDITION OF SPECIMEN AFTER TESTING.
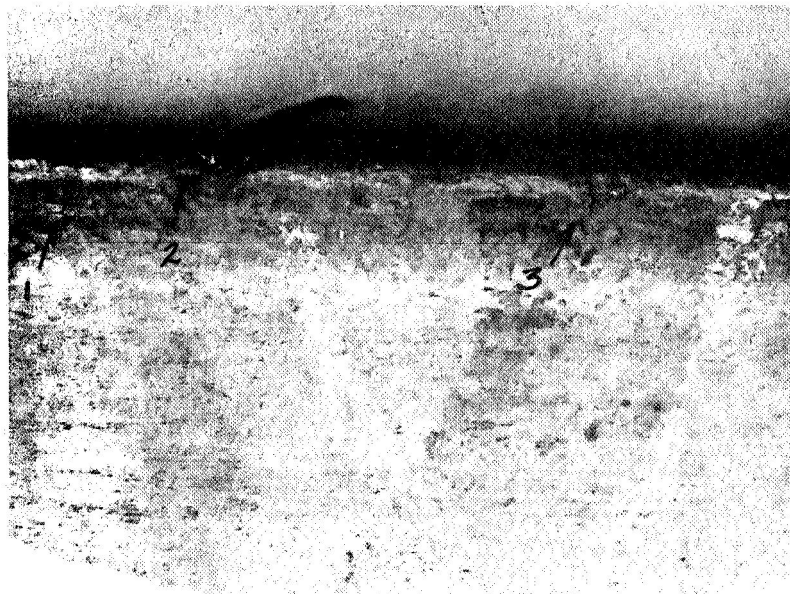
(b) PHOTOMACROGRAPH OF AREA C ABOVE SHOWING (1) CREEP TYPE CRACK ,
(2) LEAKAGE CRACK NEXT TO T.C., AND (3) LOW CYCLE FATIGUE-TYPE
CRACK.(MAG. 8X)

F-10997

Figure 5-15. Diagram and Photomacrograph of Cowl Leading
Edge with Nickel-200 Tip (SK 51428, SN 5)
That Failed After 260 Thermal Cycles

AREA A — LEAKED IN T.C. CALIBRATION TEST BECAUSE OF PLUGGED AIR LINE
AREAS B AND C — "C" LEAKED FIRST, THEN B, AFTER 40 THERMAL CYCLES (SEE PHOTOMICROGRAPHS).

▨ = SILVER BRAZING ALLOY FOIL FOR CALLIBRATING THERMOCOUPLES (72 SILVER-28 COPPER, 1435 °F M. P.), COVERED TIP.
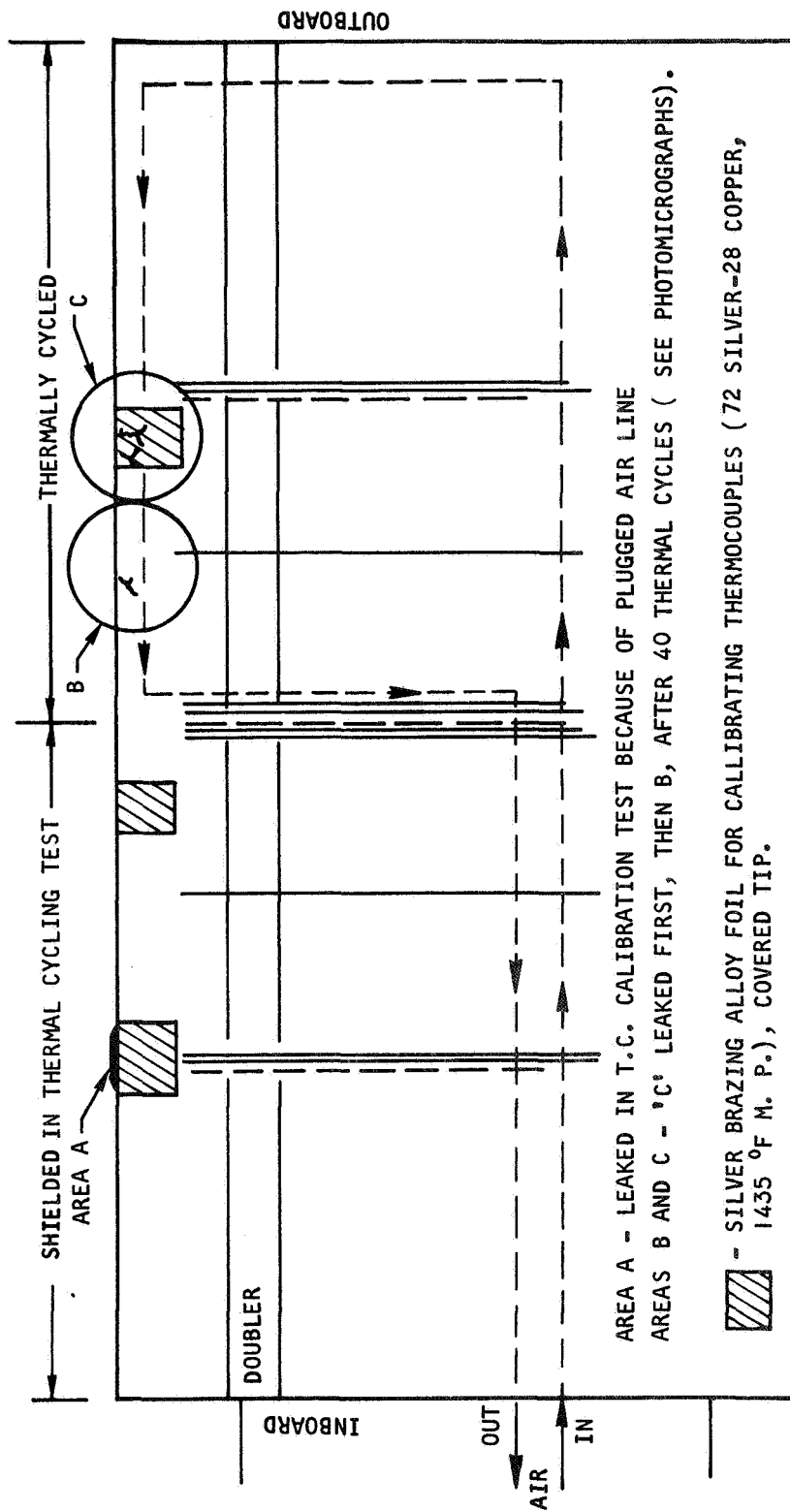
S-49803

Figure 5-16. Sketch Illustrating Locations of Cracks, Thermocouples, and Brazing Alloy Coupons (for T.C. Calibration) in Cowl Leading Edge with Nickel-200 Tip (SK 51428, SN 1) That Failed After 40 Thermal Cycles
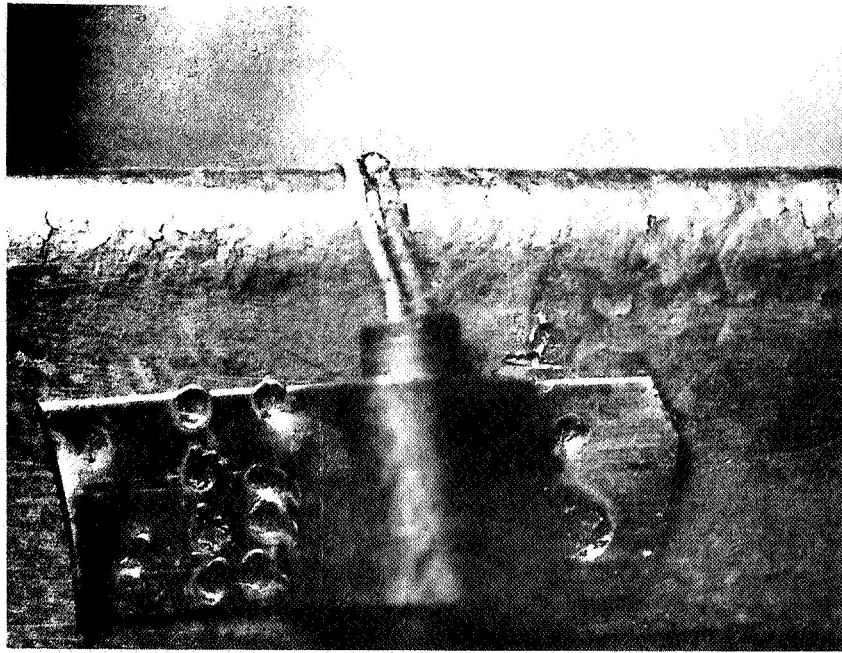
(a) CRACKS AT AREA B IN FIGURE 8.1-10 (MAG. 8X)
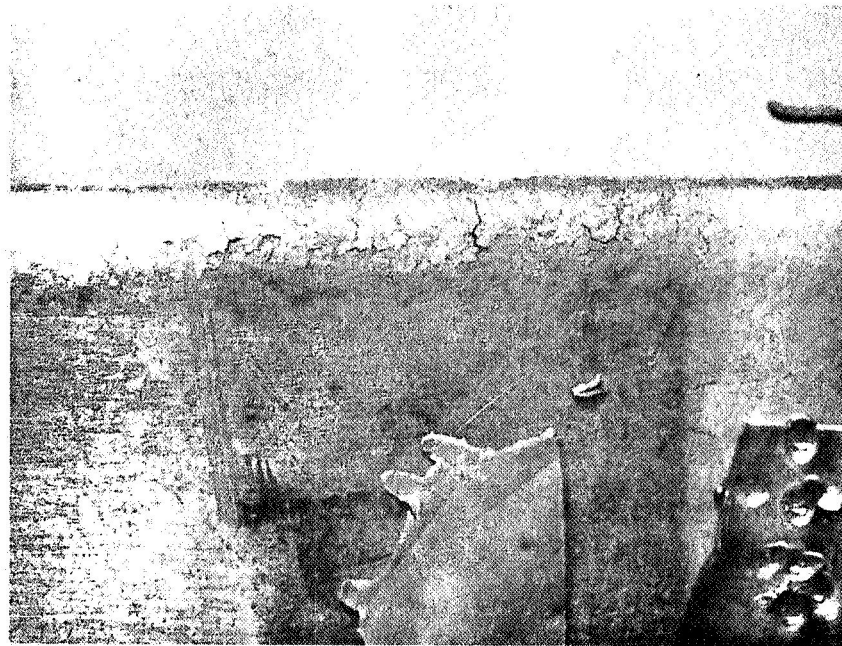
(b) CRACKS AT AREA C IN FIGURE 8.1-10. FAILURE INITIATED HERE WHERE SILVER   F-10989
     BRAZING ALLOY WAS PLACED. (MAG. 8X)

Figure 5-17. Photomacrographs of Cracks in Areas B and C of Figure
              5-16 (Cowl Leading Edge, Nickel-200 Tip, SN 1)
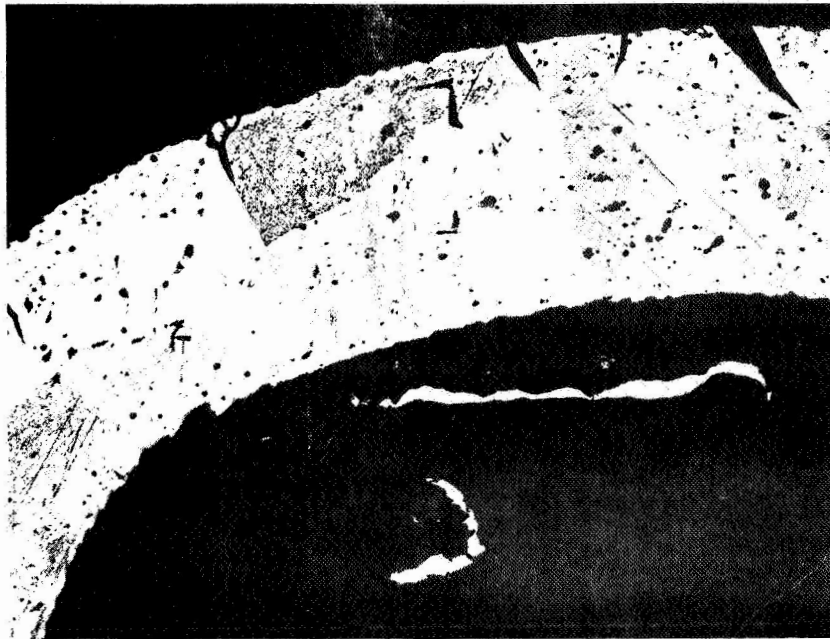
(a) EXAMPLE OF CRACKS IN Ni-200 TIP THAT LED TO FAILURE. CRACKS ARE INTERGRANULAR; GRAINS IN Ni-200 ARE LARGE (ALMOST THICKNESS OF TIP, 0.015 IN.). FAILED IN 40 THERMAL CYCLES. KALLING'S ETCHANT. (MAG. 100X)
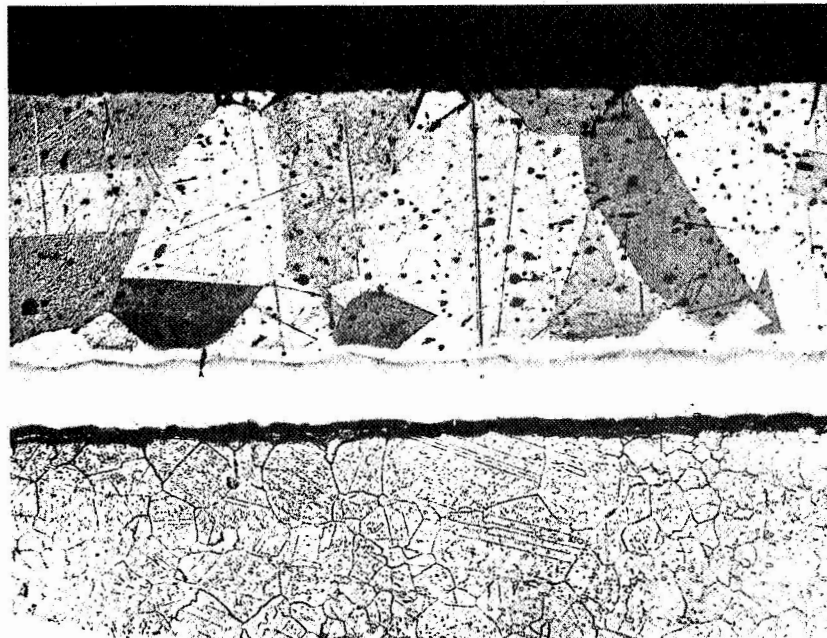
(b) INTERGRANULAR ATTACK AND OXIDATION OF Ni-200 WHERE SILVER BRAZING ALLOY WAS ALLOYED (TOP SURFACE). SIMILAR ATTACK AT TIP MAY HAVE CONTRIBUTED TO EARLY FAILURE. KALLING'S ETCHANT. (MAG. 100X)

F-10996

Figure 5-18. Photomicrographs of Area C in Figure 5-17 Showing Creep-Type Cracks in Nickel-200 Tip (SN 1) and Possible Cause for Early Failure

5.2.3.1.2 Hastelloy X Tip (SK 51287-1)

Two configuration No. 1 Hastelloy X specimens were thermally cycled to 1600°F maximum tip temperature while internally pressurized to 700 psig. Failures occurred after 110 cycles and 200 cycles. Because Hastelloy X creep strength was high at 1600°F, relative to design requirements, cumulative creep strain was a very small factor in the cause of failure; low-cycle fatigue, however, was the probable cause.

A sketch of the failure location in SN 5 specimen after 110 cycles, and a cross-section of the failure are shown in Figure 5-19. The crack was at the very tip of the leading edge and parallel to coolant flow direction--an excellent example of a low-cycle fatigue failure. A close-up of this crack is shown in Figure 5-20a. The Hastelloy X surface was coated on one side with Palniro-1 brazing alloy from the doubler. The other side was coated with a ceramic cement for insulating thermocouples. Neither of these may have affected low-cycle fatigue life. The Palniro-1 alloy is ductile and the cement was not applied at the very tip of the leading edge but off to one side.

The Hastelloy X microstructure was satisfactory. Grain boundaries were fine and did not contain excessive carbide precipitation. Grain size was not large either. All brazed joints examined in the area shown in Figure 5-19 were good.

The failure crack was transgranular rather than intergranular as in Nickel-200. This indicates Hastelloy X is still relatively strong at this temperature and failure was most likely due to low-cycle fatigue rather than creep.

A cross section at a thermocouple spot-weld is shown in Figure 5-20b. Very little damage of the Hastelloy X was noted in this area.

Test unit SN 4 was not sectioned. It had the same general appearance as SN 5 following the test.

5.2.3.2 Stress

The data reduction for the three configuration No. 2 Nickel-200 test specimens required the utilization of fatigue test results on solid nickel bars and plate-fin test bars that have been performed during the course of this program. The test results of the two configuration No. 1 Hastelloy X leading edge test units were analyzed by employing test data from a low-cycle fatigue experimental program carried out under NASA Contract No. NAS1-5002.

For the three configuration No. 2 Nickel-200 specimens, the coolant flow passes through the leading edge only and is parallel to the leading edge. Coolant does not flow through the portion of the test piece away from the leading edge, but this region is shielded from heating by an external, water-cooled shroud. The bulk of the structure, therefore, essentially remains at room temperature during the course of the test. As a result, the locally heated stagnation area of the leading edge test piece will be fully constrained from free thermal expansion. The fact that heavy end-plates are employed in the test piece further restricts the heated leading edge from free expansion.

VIEW IN MICRO BELOW

TIP

CRACK ON TIP

9 T. C. ON "A" SIDE, 3 T. C. ON "B" SIDE (DOTTED)
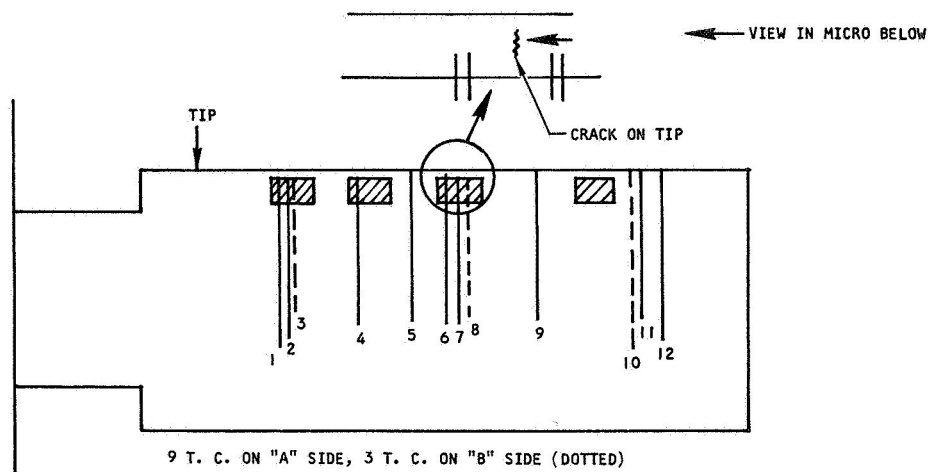
CEMENT INSULATOR FOR THERMOCOUPLES APPLIED TO SIDES.

(a) LOCATION OF LOW CYCLE FATIGUE CRACK AT TIP BETWEEN
THERMOCOUPLES 6 AND 7.
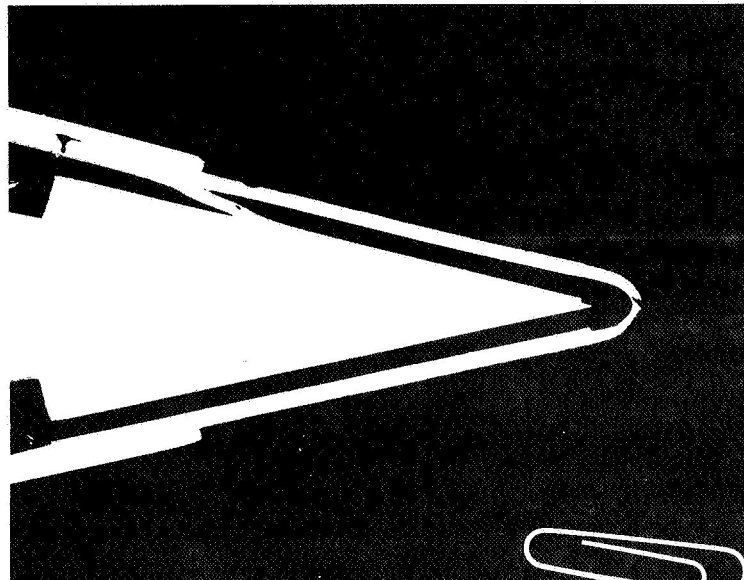
(b) CROSS SECTION AT CRACK. (MAG. 5X)

F-10998

Figure 5-19. Illustration of Crack Location in Hastelloy X
Cowl Leading Edge (SK 51287, SN 5) After
Thermal Cycling Test
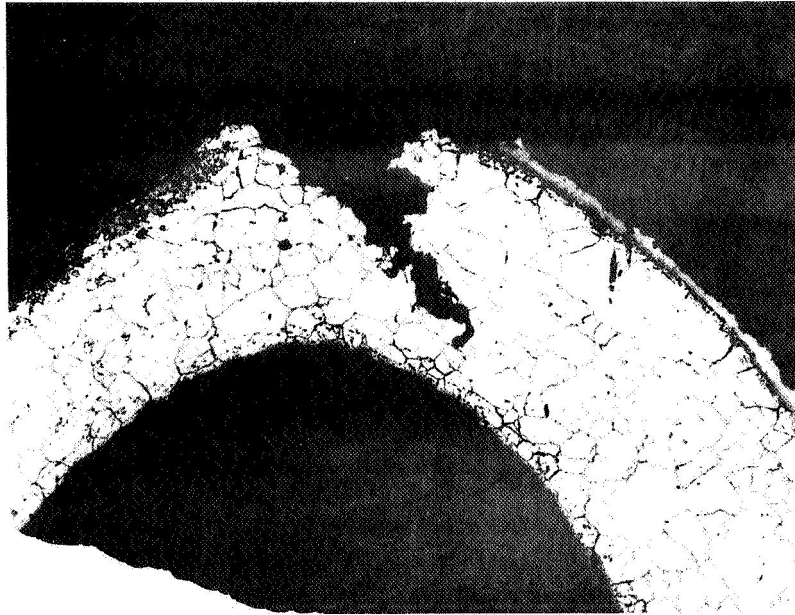
(a) CLOSEUP OF CRACK AT TIP. BRAZING ALLOY FROM DOUBLER IS
ON RIGHT SIDE. CERAMIC CEMENT, USED FOR THERMOCOUPLE
INSULATION REACTED WITH HASTELLOY X TO A DEPTH OF 0.0015
ON LEFT SIDE. ETCHANT: KALLING'S ETCH (MAG. 100X)
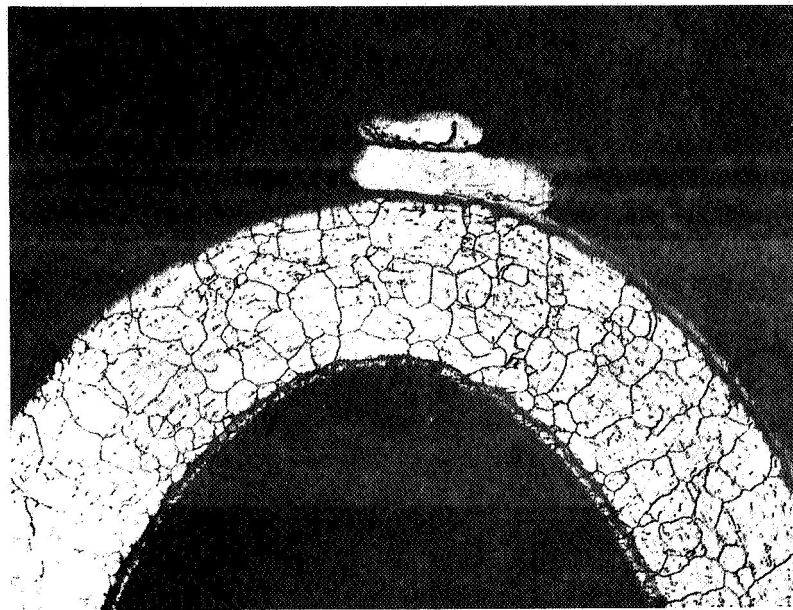
F-10990

(b) THERMOCOUPLE WELD, ADJACENT TO CRACK, SPOTWELDED TO BRAZING
ALLOY. NO APPARENT DAMAGE FROM SPOTWELD. ETCHANT: KALLING'S ETCH
(MAG. 100X)

Figure 5-20. Photomicrographs of Cowl Leading Edge
Tip (SK 51287, SN 5) at Failed Areas

The two configuration No. I Hastelloy X test pieces utilize a coolant-flow direction perpendicular to the leading edge stagnation line. The coolant is introduced along one lengthwise edge at the rear of the test unit and exhausts along the other lengthwise edge. The major part of the test piece away from the stagnation line area will be at an average temperature between the coolant inlet and outlet temperatures. Similar to the configuration No. 2 nickel leading edge test specimens, this bulk of material does not change in temperature appreciably during the thermal cycling and it will prevent any free thermal expansion of the heated stagnation area.

5.2.3.2.1 Nickel-200 Test Data Reduction

(a) First Test, SN 2--This unit was cooled with ambient air at 700 psia pressure to approximate operating pressures, and therefore, actual containment conditions. The flow rate was adjusted to produce the test temperature differences between the most highly heated metal area at the stagnation line and the remainder of the total structure.

Prior to the initiation of the thermal-cycling sequence, the unit was subjected to a number of performance cycles. Since these cycles contributed to both thermal fatigue and creep rupture damage of the test piece, this data has been included in the test data reduction of life performance. A total of 25 cycles occurred, and the temperature history data is given in Table 5-6. While the bulk of metal remained at a virtually stationary temperature, the leading edge stagnation area cycled between the high temperature actual value indicated in the table, to the low temperature value. It is this variation in temperature that produced the repetitive cycle plastic-flow that contributed towards low-cycle fatigue damage. The creep- and fatigue-damage effects during each cycle were computed, and these results are given in Table 5-7. The creep-damage figures are based upon extrapolated Nickel-200 creep rupture data.

Of the 25 total test runs carried out, peak stagnation line temperatures ranged from 250° to 1820°F and cyclic ΔT's ranged from 130° to 1610°F. The test unit was held at these temperatures for 10 min during each cycle. During seven cycles, the maximum metal temperature was less than 1000°F and the ΔT's were less than 770°F. The cumulative creep and low cycle fatigue damage fractions were found to be negligible for these cycles. Of the remaining 18 cycles, the maximum metal temperature fell within the range from 1480° to 1630°F, with ΔT's ranging from 1260° to 1410°F in 13 of the cycles. The estimated creep damage fraction for these 13 cycles was less than 0.200, while the cyclic fatigue damage fraction was less than 0.025. In the remaining five cycles, the peak temperatures were 1675°F, 1690°F, 1710°F, 1785°F, and 1825°F respectively. The ΔT's ranged from 1450° to 1610°F. The low cycle fatigue damage fraction was less than 0.010 for these five cycles, but the creep damage fraction was approximately 0.895. The cumulative sum of the damages from these 25 test cycles was actually in excess of 1.0, which means that the test unit failure was largely attributable to this sequence of tests with the bulk of the damage being due to creep effects.

TABLE 5-6

CONFIGURATION NO. 2, SN 2, THERMAL CYCLE RUN CONDITIONS

Cycle No.	Test Run No.	Highest Cycle Temp, °F	Lowest Cycle Temp, °F	Test Cycle ΔT, °F
1	101	1486	210	1276
2	102	1502	220	1282
3	103	1571	220	1351
4	104	1674	220	1454
5	105	1588	220	1368
6	201	1615	220	1395
7	202	1624	220	1404
8	203	1710	220	1490
9	204	1826	220	1606
10	205	1484	220	1264
11	206	1629	220	1409
12	207	1580	220	1360
13	208	983	220	763
14	301	890	220	670
15	302	805	220	585
16	303	751	220	531
17	304	725	220	505
18	305	463	220	243
19	306	251	220	31
20	401	1571	220	1351
21	402	1550	220	1330
22	403	1611	220	1391
23	404	1690	220	1470
24	405	1784	220	1564
25	501	1570	220	1350

NOTE: Test time at highest cycle temperature was approximately 10 min for each cycle.

TABLE 5-7

CONFIGURATION NO. 2, SN 2 CREEP AND FATIGUE DAMAGE SUMMARY

Cycle No.	Estimated Creep Life at Highest Temp,hr	Thermal Expansion Range, $\alpha\Delta T$	Plastic Strain Range, ϵ_p	Low Cycle Fatigue Life	Creep Damage Fraction
1	100	0.00116	0.00106	660	0.0017
2	60	0.00116	0.00106	660	0.0028
3	15	0.00125	0.00115	576	0.0111
4	2.5	0.00136	0.00126	485	0.0667
5	11	0.00126	0.00116	567	0.0151
6	6	0.00132	0.00122	515	0.0278
7	5	0.00132	0.00122	515	0.0333
8	1.4	0.00141	0.00131	450	0.120
9	0.40	0.00153	0.00143	385	0.417
10	100	0.00116	0.00106	660	0.0017
11	5	0.00132	0.00132	515	0.0338
12	12	0.00125	0.00115	516	0.0139
13	>1000	0.00066	0.00056	>1000	0.0
14	>1000	0.00059	0.00049	>1000	0.0
15	>1000	0.00048	0.00038	>1000	0.0
16	>1000	0.00055	0.00045	>1000	0.0
17	>1000	0.00054	0.00044	>1000	0.0
18	>1000	0.00033	0.00023	>1000	0.0
19	>1000	0.0	0.0	>1000	0.0
20	12	0.00125	0.00115	576	0.0139
21	20	0.00123	0.00113	590	0.0083
22	10	0.00132	0.00122	515	0.0167
23	2	0.00137	0.00127	480	0.0833
24	0.80	0.00150	0.00140	460	0.208
25	15	0.00124	0.00114	585	0.0111

TOTAL LIFE FRACTION DAMAGE $\approx$ 0.033 $\approx$ 1.09

Following the performance runs, ten additional checkout cycles were imposed upon the test unit of approximately two minutes duration, each with a maximum metal temperature of 1550°F and a cyclic ΔT of 1330°F. The combined creep and cycle fatigue damage fraction was computed to be approximately 0.06 for these cycles.

Finally, the unit was subjected to a total of 40 rapid thermal fatigue cycles. The maximum metal temperature in these cycles was 1550° to 1600°F and the test time at peak temperature was one minute. Actual unit failure at the time of increased leakage occurred after 20 cycles. The accumulated creep damage fraction was 0.042 and the low cycle fatigue damage fraction was 0.035 for these 20 cycles. Hence, these cycles contributed a damage fraction of less than 0.080 towards the failure life of the test unit.

The high metal temperatures during the performance runs were responsible for the relatively short cycle life of the test unit. Once creep was taken into account, as indicated above, the correlation between life of the leading edge unit and the analysis results cited are in good agreement.

(b) **Second Test, SN 5**--The second test unit survived a total of 260 cycles at the various conditions noted in Figure 5-9. The mean lowest cycle temperature for this sequence of tests was approximately 300°F. The ΔT's were, therefore, the maximum cycle temperature minus 300°F.

The thermal conditions for this test run are summarized in Table 5-8a and the creep and fatigue damage summary is provided in Table 5-8b. The total damage fraction of 0.87 indicates a reasonable correlation between the test panel fatigue results and the leading edge test. Approximately one-third of the total damage was apparently due to plastic-flow-induced low cycle fatigue. The remaining two-thirds of the damage was due to creep, with most of the creep taking place in the final sixty test cycles. Considering that the temperatures could have varied by as much as 50°F from these tabulated, the test results represent a good substantiation of leading edge fatigue performance. It can be observed that the first two hundred cycles which are representative of operating engine ΔT's, but at higher test temperatures than operating temperatures by at least 200°F, only produced a total life damage fraction of 0.37, indicating a life in excess of 550 cycles even for these test conditions.

(c) **Third Test, SN 1**--The third test unit survived 40 total thermal cycles with estimated temperatures of 1630°F at the cracked area away from the silver braze zone. This test condition was almost identical to that used for the last 60 cycles on SN 5. Referring to Table 5-8b, the creep and fatigue damage fractions for 40 such cycles would have been 0.267 and 0.071, respectively, or a total of 0.34. The indicated temperature uncertainty on this test could be as much as 100°F, as a result of loss of thermocouple instrumentation. For example, an increase in temperature from 1630° to 1700°F would

TABLE 5-8

CONFIGURATION NO. 2, SN 5 DATA REDUCTION

(a) THERMAL CONDITIONS

Cycle No.	Total No. of Test Cycles	Highest Cycle Temp, °F	Lowest Cycle Temp, °F	Test Cycle ΔT, °F
0-10	10	1370	300	1070
11-100	90	1250	300	950
101-160	60	1450	300	1150
161-200	40	1400	300	1100
201-260	60	1630	300	1330

(b) CREEP AND FATIGUE DAMAGE SUMMARY

Cycle No.	Estimated Creep Life at Highest Temp, hr	Thermal Expansion Range, $\alpha\Delta T$	Plastic Strain Range, ϵp	Low Cycle Fatigue Life	Fatigue Damage Fraction	Creep Damage Fraction
0-10	800	0.0097	0.0090	800	0.0125	0.0004
11-100	>1000	0.0085	0.0078	1000	0.0900	0.0
101-160	175	0.0105	0.0096	700	0.0860	0.114
161-200	500	0.0100	0.0092	750	0.0530	0.013
201-260	5	0.0126	0.0116	567	0.1058	0.400
TOTAL LIFE FRACTION DAMAGE					0.347	0.527

Σ FATIGUE + CREEP = 0.87

cause a reduction in creep life to 1.67 hr from 5.0 hr and a corresponding increase in creep damage fraction to 0.800 as well as an increase in fatigue fraction from 0.071 to 0.080. This would increase the test total damage fraction to 0.88, with almost all of the damage being due to creep.

Some variation in life can also be due to the scatter effects for the variation in creep-rupture performance between different test specimens. Although not a conclusive fatigue life test, the results are consistent with the data from SN 2 and SN 5.

5.2.3.2.2 Hastelloy X Test Data Reduction

(a) First Test, SN 5--This unit survived 110 cycles of thermal fatigue testing with estimated maximum cycle temperatures ranging from 1620^0 to 1717^0F, and an average maximum of 1670^0F. With an average cooling air temperature of 200^0F, the average value of thermal expansion cyclic range was an $\alpha\Delta T$ of 0.0140 in./in. Based on the tests of solid Hastelloy X test specimens, the fatigue life with this applied total strain range was estimated as 190 cycles.

The test pressure of 700 psi caused a containment stress of approximately 1000 psi. Based upon a Hastelloy X stress rupture life at this temperature of well in excess of 1000 hr, the creep damage fraction was not of any consequence. The test panel work was performed on Hastelloy X bars in the as-received condition. The material in the leading edge test piece had been exposed to brazing temperature and alloying. These effects could well have accounted for the reduced test life as compared to the computed life.

(b) Second Test, SN 4--This unit was subjected to a total of 200 thermal fatigue cycles, with a maximum cycle temperature ranging from 1541^0 to 1652^0F, and an average maximum value of approximately 1600^0F. As in SN 5, the effects of creep damage were negligible. The lowered maximum temperature would have led to a computed life of 220 cycles, or a figure that is in excellent agreement with the previous solid-bar fatigue test work.

5.3 COOLANT FLOW DISTRIBUTION TESTS

5.3.1 Summary of Results

Flow distribution tests were conducted on two configuration No. 1 specimens using isothermal air and hydrogen with heat transfer. Extrapolation of test results to full-scale leading edge geometry and hydrogen conditions indicated an acceptable range of maximum-to-minimum flow ratio of 1.01 to 1.03.

5.3.2 Test Data

The results of the flow distribution tests on configuration No. 1 leading edge straight sections are reported here, along with an extrapolation of the data to the conditions for the full-scale flightweight leading edge. The test

results summarized in Figure 5-21 are for air in SN 4 and 5 and hydrogen in SN 4. The test setup is described in Section 3.3.

The inlet and outlet manifold pressure distributions were used to obtain flow distribution. Typical pressure distributions are shown in Figure 5-22. The resulting flow distributions are shown in Figure 5-23. The difference between the shape of air and hydrogen flow distribution curves is explained later. Figure 5-22 includes views of both the test and full-scale leading edge manifolds, both in cross-section and looking from the back of the manifold toward the leading edge. The range of test conditions is indicated in Table 5-9 for tests with isothermal air and hydrogen with heat transfer.

TABLE 5-9

FLOW DISTRIBUTION TEST CONDITIONS IN LEADING
EDGE STRAIGHT SECTION

Gas	Air	Hydrogen
Inlet total pressure, psia	22 - 340	649 - 705
Outlet total pressure, psia	15 - 122	630 - 676
Inlet temperature, ^{0}R	520 - 535	160 - 200
Outlet temperature, ^{0}F	520 - 535	270 - 630
Flow rate, lb/min	0.8 - 22	3.4 - 5.4
Reynolds number in core fins	1400 - 39000	11000 - 36000
Mach number in core fins	0.03 - 0.1	0.008 - 0.025
Inlet duct Mach number	0.23 - 0.4	0.06 - 0.1
Outlet duct Mach number	0.2 - 0.8	0.07 - 0.11

5.3.3 Data Analysis and Discussion

In Figure 5-21, the ratios of core ΔP to overall ΔP, and inlet manifold ΔP to core ΔP are plotted vs maximum W/minimum W. The local flow-rate ratio is considered the dependent variable. The test pressure-drop ratios are defined by Equations (5-10) and (5-11).

$$\frac{\text{core } \Delta P}{\text{overall } \Delta P} = \frac{\text{inlet manifold average } P_S - \text{outlet manifold average } P_S}{\text{unit inlet } P_T - \text{unit outlet } P_T}$$
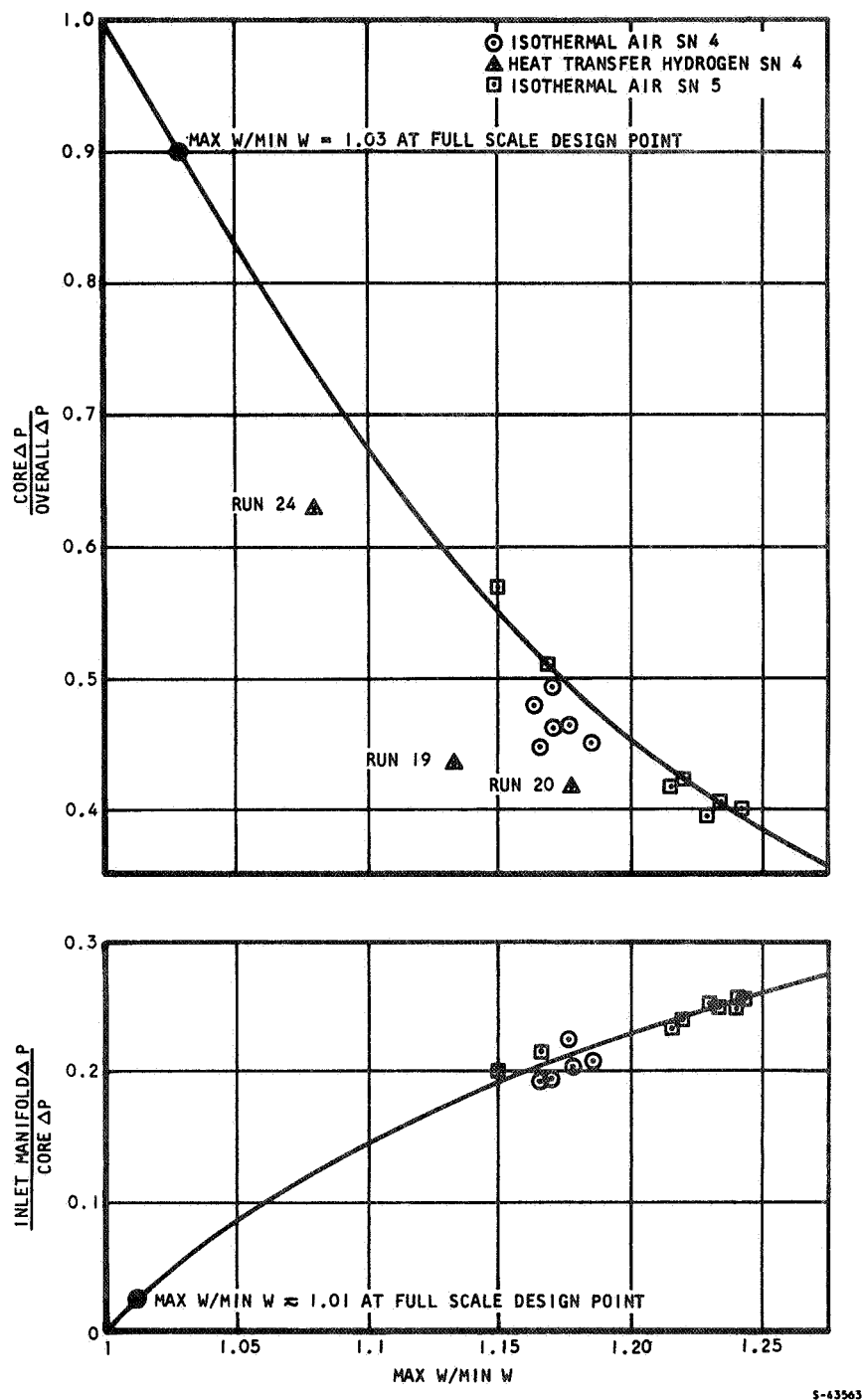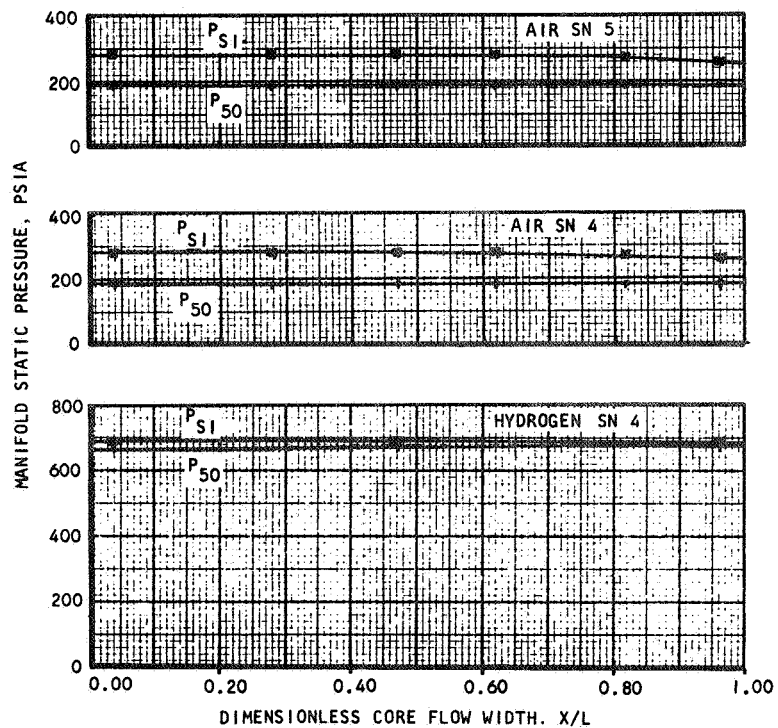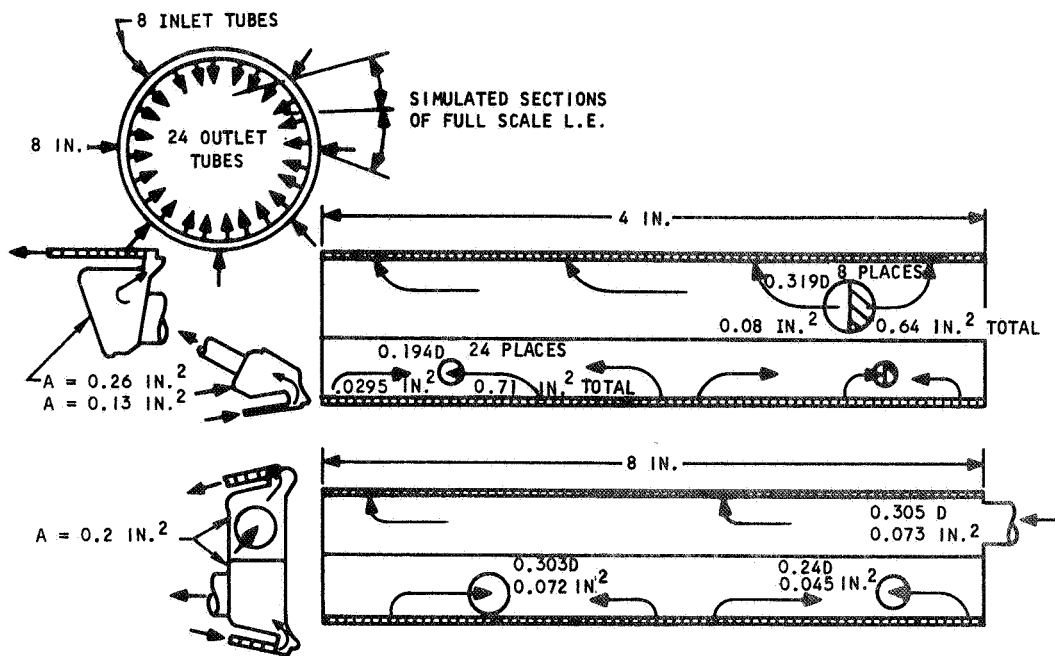
$$(5-10)$$

Figure 5-21.   Leading Edge Straight Section Flow Ratio

Figure 5-22. Typical Manifold Pressure Distributions and Manifold Schematic for Leading Edge Straight Section

S-43573
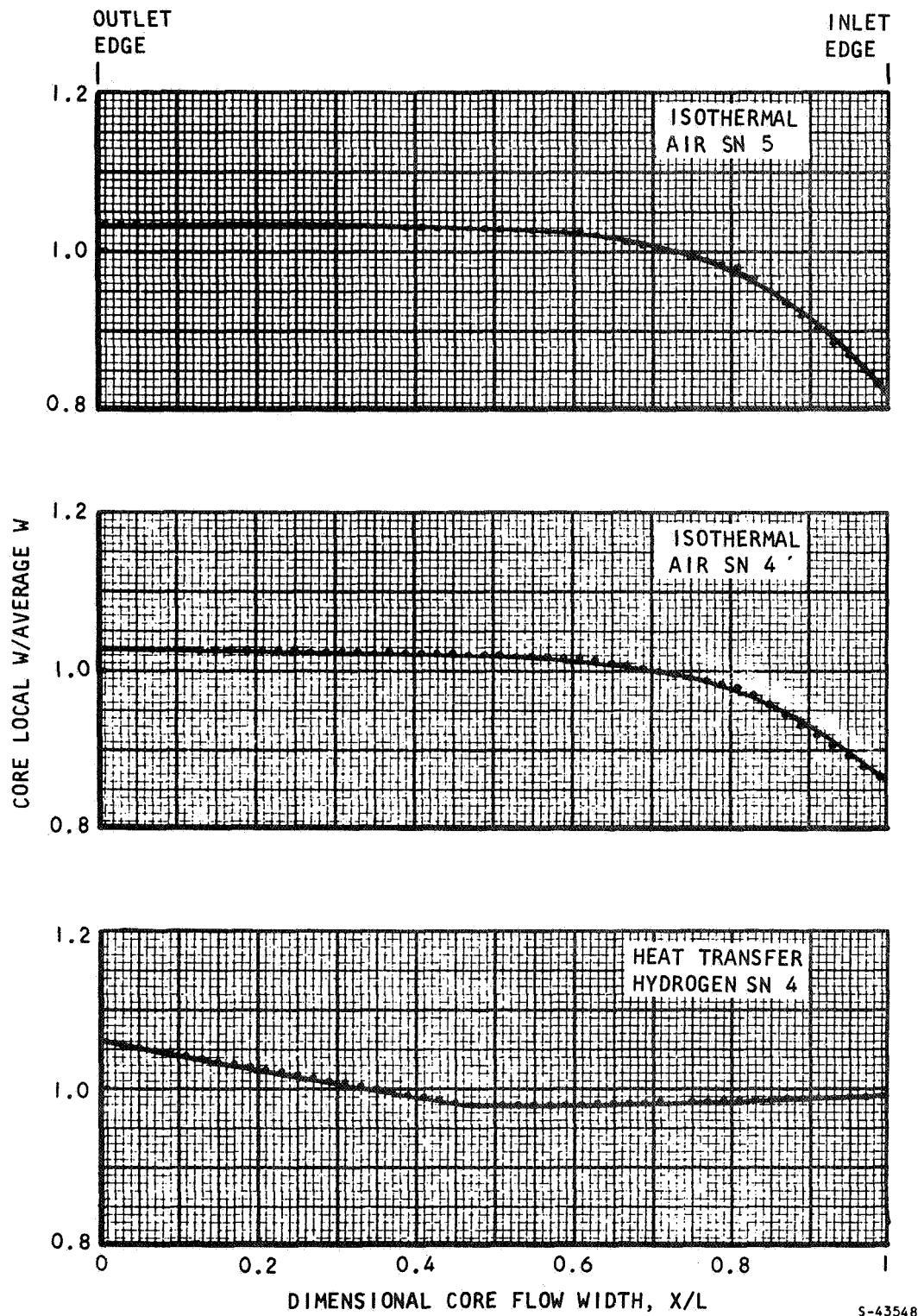
Figure 5-23. Typical Flow Distributions for Leading
Edge Straight Sections

S-43548

$$\frac{\text{inlet manifold } \Delta P}{\text{core } \Delta P} =$$

<div align="right">(5-11)</div>

$$\frac{\text{manifold } P_S \text{ max} - \text{manifold } P_S \text{ min}}{\text{inlet manifold average } P_S - \text{outlet manifold average } P_S}$$

where subscripts S and T are static and total, respectively.

The flow will be uniform (max W/min W = 1) for core ΔP/overall ΔP = 1 and inlet manifold ΔP/core ΔP = 0. The air data for SN 4 and 5 are in good agreement, showing repeatable test unit geometry and use of the test setup. The three hydrogen data points for SN 4 are averages of five points each. The data scatter was large because three local hydrogen pressures were measured separately in each manifold whereas, for air tests, the difference between one reference manifold pressure and the other five were measured in each manifold. Good agreement (as expected) was obtained between hydrogen and air tests because the tests are all in the Reynolds number regime above 1400 based on the 20R-0.075-0.100-0.004 Hastelloy X fin hydraulic radius of 0.01396 in. and most of the pressure drop is due to turns and area changes.

The data was interpreted relative to the full-scale leading edge configuration by use of the geometry shown in Figure 5-22. The test unit port geometry simulates approximately 1/16 of the full scale leading edge core, primarily because of fin height. The core ΔP and overall ΔP presented below are for the full-scale leading edge. At a hydrogen flow rate of 0.87 lb/sec, inlet temperature of 100°R and outlet temperature of 406°R,

$$\text{core } \Delta P = 792.7 - 727.1 = 65.6 \text{ psi}$$

$$\text{overall } \Delta P = (799.4-2/3(6.7)) - 727.1-15,4/3 = 75 \text{ psi}$$

Using Equation (5-10), core ΔP/overall ΔP = 0.9 and from Figure 5-21 the full-scale leading edge maximum-to-minimum flow ratio is expected to be about 1.03.

Another estimate of full-scale leading edge flow ratio was made using inlet manifold ΔP test data. It was observed that the outlet manifold static pressure profile is practically uniform and the flow is nonuniform, primarily because the inlet static pressure is nonuniform. Inlet static pressure is nonuniform because of a partial conversion of the inlet duct velocity head to static pressure in the inlet manifold. The fraction of the velocity head converted to static pressure is a function of the expansion loss at the inlet manifold inlet port. The experimental values for the expansion loss coefficient in the leading edge straight section are $0.32^{+0.05}_{-0.12}$ and $0.26^{+0.17}_{-0.13}$ for SN 4 and SN 5, respectively. The calculated value is

$$K_E = (1 - A_1 A_2)^2 = (1 - 0.073/0.2)^2 = 0.4 \tag{5-12}$$

where A_1 = inlet tube area, in.^{2}

A_2 = manifold cross-sectional area, in.^{2}

The experimental values were determined from

$$K_E = \frac{q_{0.073} - \left(P_{S\ max} - P_{S\ min}\right)}{q_{0.073}} \tag{5-13}$$

where $q_{0.073}$ = velocity head in the inlet tube

$P_{S\ max}$ and $P_{S\ min}$ = maximum and minimum static pressures in the inlet manifold

The area ratio is larger in the full-scale leading edge so that loss coefficient is larger. The calculated value is reduced by the ratio of test-to-calculated loss coefficients for the leading edge straight section, so that

$$\text{full-scale } K_E = \left(1 - \frac{0.08}{2(0.26)}\right)^2 \left(\frac{0.26}{0.4}\right) = 0.46$$

The actual loss coefficient should increase about 0.46 because of the 90-deg turn required in the full-scale inlet manifold. Equation (5-13) was used in the following form to obtain

$$P_{S\ max} - P_{S\ min} = q_{0.08} - K_E\ q_{0.08} = 2 - 0.46(2) = 1.08 \text{ psi}$$

Using Equation (5-11)

$$\frac{\text{inlet manifold } \Delta P}{\text{core } \Delta P} = \frac{1.08}{65.6} = 0.0165$$

and from Figure 5-21, the full-scale leading edge maximum-to-minimum flow ratio is expected to be about 1.01.

6. CONCLUSIONS

Two leading edge straight section configurations were designed and tested to determine the feasibility for flight engine leading edge cooling, coolant flow distribution, and low cycle thermal fatigue and creep rupture performance. Based on test results presented in Section 5.0, the following conclusions were drawn.

6.1 THERMAL PERFORMANCE

The cooling coefficient for coolant flow perpendicular to leading edge stagnation line (configuration No. 1) is 3.9-times that for a straight duct at the Mach 8 local design Reynolds number of 30,000. This is twice the value of 1.94-times the straight-duct coefficient at a Reynolds number of 30,000 used for the original flight engine leading edge cooling analysis.

The cooling coefficient for coolant flow parallel to the leading edge stagnation line (configuration No. 2) is in reasonable agreement with predicted coefficients for plain rectangular tubes when a suitable adjustment is made for unsymmetrical heating.

6.2 THERMAL CYCLING

Once the creep effects of high temperature are distinguished in Nickel-200 tests, it is evident that even for the same ΔT magnitude, the fatigue life of Nickel-200 is better than that obtainable with Hastelloy X for this leading edge application. For the Nickel-200 configuration, the Mach 8 operating conditions would lead to the following temperatures:

Temp at L.E. Stagnation Line = $1620^{\circ}R$ ($1160^{\circ}F$)

Coolant Temp = $160^{\circ}R$ ($-300^{\circ}F$)

$\alpha\Delta T = 0.01160$

Thermal fatigue failure, based upon the Nickel-200 data, would occur after approximately 690 cycles of operation. Creep effects would have a moderate influence on total life. Containment of 700 psi coolant at $1160^{\circ}F$ would cause creep rupture of the leading edge in 60 hr. By using the total damage fraction analysis, the creep life fraction for 10 hr of sustained usage would exhaust a damage fraction of 0.167, leaving a life fraction of 0.833 for low-cycle fatigue. This would produce a reduction from 690 to 575 cycles.

This prediction is consistent with the test results for SN 5, which indicated a cycle life in excess of 550 cycles for similar ΔT's, but higher temperatures and somewhat longer time exposure to containment (18 hr). Also, it can

be concluded that the Hastelloy X unit showed a lower cycle life (110 to 200 cycles), and that Nickel-200 is the better design choice for this application in terms of low-cycle fatigue life.

6.3 COOLANT FLOW DISTRIBUTION

The conclusions of flow distribution tests performed on configuration No. 1 leading edge straight sections are:

(a) The flow is always highest at the end of the core farthest from the inlet because the inlet manifold static pressure increases with distance from the inlet port, and the outlet manifold static pressure is almost uniform.

(b) Hydrogen and air data, as well as data for different units of the same geometry, are in good agreement.

(c) Extrapolation of test results to full-scale leading edge geometry and hydrogen-conditions indicates an acceptable range of maximum-to-minimum flow ratio of about 1.01 to 1.03.

## 6.4 APPLICATION TO HRE FLIGHTWEIGHT ENGINE

A Nickel-200 leading edge tip with coolant flowing perpendicular to the stagnation line was selected for the flightweight engine leading edge design. This design was selected because test results indicated that coolant flow distribution was acceptable and the internal coefficient in the 154-deg turn was acceptable for cooling, even when high shock-impingement heat flows on the leading edge tip are considered. In addition, coolant flow is perpendicular to the stagnation line is preferred because fabrication and flow routing are greatly simplified and coolant pressures required for equal metal temperatures are lower. Nickel-200 was selected for its greater low cycle fatigue life.

Results of a thermal analysis performed to determine the internal and external surface temperatures of the selected leading edge design at the 88,000-ft altitude, freestream Mach 8 design point are presented in Figure 6-1. Coolant hydrogen heat transfer coefficients were calculated with the correlation for the 154-deg turn reported in Section 5. A 70 node, two-dimensional steady-state thermal analysis of the 15-mil-thick nickel wall with 30-mil outside leading edge radius was conducted. Curves labeled "no shock" are the inside and outside surface temperature distributions, assuming the spike shock falls outside of the leading edge. Curves labeled "shock" are the inside and outside surface temperatures, assuming the spike shock impinges on the leading edge. The heat transfer coefficient for a shock impinging on a leading edge was calculated on the basis of data from Reference 6-1 to be 15.4-times the value for the shock located inside of the leading edge. This area with high heat transfer has a width of 4 mils and extends around the entire 56.7-in. circumference of the leading edge. Although the maximum local heat flux for the Mach 8 design increases from 2050 to 10,200 $\frac{BTU}{sec\ ft^2}$ when shock impingement
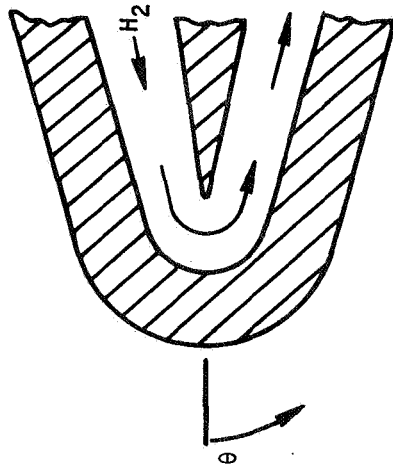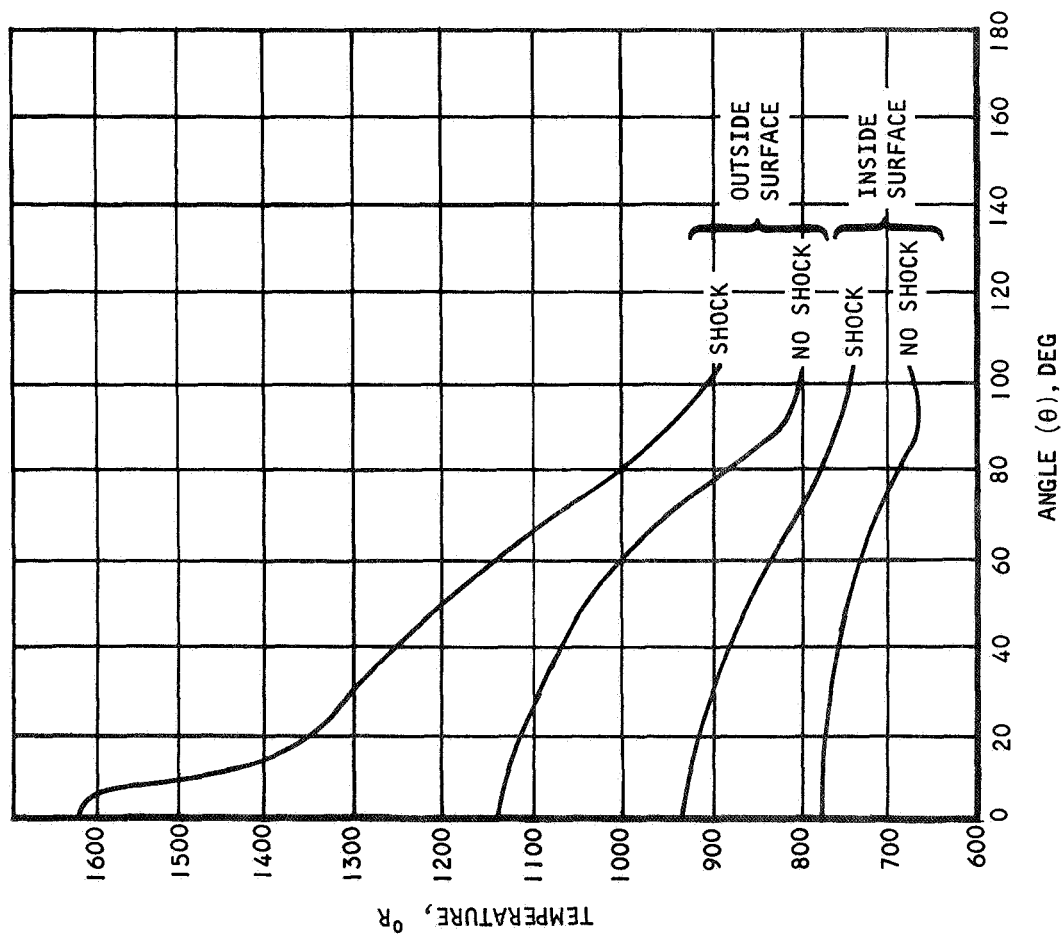
Figure 6-1. Leading Edge Design Thermal Performance

S-50772

is assumed, conduction in the nickel wall permits a maximum metal temperature increase of only 470°R and an acceptable overall temperature difference increase from 990° to 1460°R.

REFERENCES

5-1   Fay, J. A., and F. R. Riddell, "Theory of Stagnation Point Heat Transfer in Dissociated Air," <u>Journal of the Aeronautical Sciences</u>, Volume 25, No. 2, February 1958.

5-2   Kestin, J., "The Effect of Freestream Turbulence on Heat Transfer Rates," Rates," <u>Advances in Heat Transfer</u>, Chapter I, by T. F. Irvine and J. P. Hartnett, Academic Press, 1966.

5-3   Chupp, R. E., H. E. Helms, P. W. McFadden, and T. R. Brown, "Evaluation of Internal Heat Transfer Coefficients for Impingement Cooled Turbine Airfoils," AIAA 4th Propulsion Joint Specialist Conference Paper No. 68-564, June 1968.

5-4   Kuethe and Schetzer, <u>Foundations of Aerodynamics</u>, Wiley, 1950.

5-5   Kays, W. M., <u>Convective Heat and Mass Transfer</u>, McGraw Hill, 1966.

6-1   Edney, R. E., "Effects of Shock Impingement on Heat Transfer Around Blunt Bodies," <u>AIAA Journal</u>, Vol. 6, No. 1, January 1968.